Departamento de Física

Laboratorio de Óptica

CALIDAD OPTICA EN OJOS PSEUDOFAQUICOS: MEDIDAS EXPERIMENTALES, MODELADO Y APLICACIONES

Trabajo presentado en la Facultad de Química
de la Universidad de Murcia por:

Carmen Cánovas Vidal

para aspirar al grado de Doctor por la Universidad de Murcia.

Laboratorio de Óptica. Departamento de Física. Universidad de Murcia.
Murcia, 11 de Julio de 2012

D. Pablo Artal Soriano, Catedrático de Universidad del Área de Óptica en el Departamento de Física, AUTORIZA:

La presentación de la tesis doctoral titulada “CALIDAD OPTICA EN OJOS PSEUDOFAQUICOS: MEDIDAS EXPERIMENTALES, MODELADO Y APLICACIONES”, realizada por D. Carmen Cánovas Vidal bajo mi inmediata dirección y supervisión, en el Departamento de Física, y que presenta para la obtención del grado de Doctor por la Universidad de Murcia.

Murcia, 11 de Julio de 2012

Índice

RESUMEN

La cirugía de catarata es la operación ambulatoria más común, con casi 4 millones de intervenciones en 2010 en Europa. Consiste en sustituir el cristalino natural opacificado por una lente artificial, denominada lente intraocular (LIO), que restituye la calidad de imagen en la retina del paciente. En un principio, ese era el único objetivo de la LIO, pero con los avances de las técnicas quirúrgicas, los diseños de lente también han evolucionado, siendo capaces de mejorar otros aspectos ópticos y permitir así que el paciente sea independiente de cualquier otro tipo de corrección oftálmica. Así pues, hay actualmente LIOs disponibles que incorporan diversos diseños multifocales, evitando así la necesidad de gafas para enfocar objetos cercanos. Existen también otros tipos de lentes intraoculares, como las lentes tóricas que corrigen el astigmatismo corneal, o las lentes asféricas, con aberración esférica negativa, imitando al cristalino joven que compensa la aberración esférica positiva de la cornea. El éxito de todas estas mejoras en el diseño de lentes intraoculares está íntimamente ligado a una correcta elección de la potencia de la LIO. Es bien sabido que, dependiendo de las características biométricas de cada ojo se puede calcular la potencia de la LIO a implantar para permitir tener en foco las imágenes procedentes de objetos lejanos. Un error en el cálculo de la potencia de la LIO a implantar de 0.5 D, puede reducir el efecto de la corrección de las aberraciones corneales anteriormente citadas, con lo que no se aprovecharía óptimamente el diseño de la LIO escogida. El efecto es aun más importante para las lentes multifocales, pues el error en el cálculo de potencia puede privar al paciente de uno de los focos, con lo que el objetivo de evitar el uso de gafas no se habría conseguido.

Las técnicas de cálculo de la potencia más clínicamente extendidas se basan en los conceptos de la Óptica paraxial, esto es, en una aproximación que no contempla aberraciones, donde el ojo se modela como un sistema óptico compuesto por un dioptrio esférico, la cornea, y una lente delgada, que representa a la LIO. Así, se calcula la potencia de la LIO para cada paciente, en función de los parámetros biométricos medidos en su ojo, que normalmente suelen ser la longitud axial del mismo, así como la potencia corneal. Esta ultima, se calcula utilizando el radio de la cara anterior de la cornea, proporcionado por los keratómetros o topógrafos clínicos y un índice de refracción equivalente. Es bien sabido que el valor de índice 1.3375, que se utiliza en la

mayoría de aparatos clínicos sobre-estima la potencia de la cornea. Esta sobreestimación depende del radio anterior y de la relación entre el radio de la cara posterior y anterior de la cornea, siendo para el modelo de Gullstrand de alrededor de 0.8 D. Además de los datos biométricos, un parámetro esencial para la correcta determinación de la potencia de la LIO es la predicción de su posición una vez implantada en el ojo. Esta última se calcula en función de regresiones empíricas basadas en datos de otros pacientes, siendo especificas dichas regresiones para cada formula. La predicción también contiene una constante, que se optimiza en función del modelo de lente utilizada, el cirujano y la técnica quirúrgica. Es importante hacer notar que debido a las aproximaciones inherentes de la teoría utilizada, a la falta de consideración de aberraciones y al uso de estas regresiones empíricas, la posición calculada de la LIO es un parámetro ficticio, que no se corresponde con la posición real de la lente una vez implantada, si no que es aquella posición que permite resolver la formula, y así obtener un error postoperatorio promedio mínimo. Sin embargo, esta optimización asociada a la posición efectiva de la lente, aunque permite corregir errores sistemáticos, no elimina los errores individuales asociados a cada paciente. Debido a ello, el cálculo de potencia para pacientes fuera de los rangos promedio, así como pacientes con ojos largos o cortos o con configuraciones ópticas poco comunes, suele ser erróneo, al no estar incluidos en dichas regresiones, problema que se trata de solucionar escogiendo aquellas fórmulas que empíricamente muestran mejores resultados en determinados rangos biométricos u optimizando nuevas constantes para diferentes tipos de configuración ocular.

Un caso particular y de especial relevancia son los pacientes de cirugía de catarata que se han sometido previamente a cirugía refractiva. Obviamente, estos ojos presentan unas configuraciones ópticas poco comunes, al haber sido modificadas por la cirugía refractiva previa, y por ello alejadas del ojo modelo. Este grupo es en el que tradicionalmente las fórmulas de cálculo de potencia suelen dar peores resultados. A este punto se une el hecho de que la cirugía refractiva estándar suele incrementar las aberraciones corneales, que no se consideran en los cálculos paraxiales en los que están basadas dichas fórmulas. El resultado es que las fórmulas que se suelen utilizar para el cálculo de potencia de la LIO en pacientes normales no son válidas para pacientes con cirugía refractiva previa. En ojos donde se ha corregido la miopía por medio de cirugía refractiva, las fórmulas convencionales de cálculo de potencia suelen dar como resultado una refracción postoperatoria hipermetrópica, mientras que para pacientes operados de hipermetropía, el resultado suele ser miópico. Esto se debe principalmente a dos fuentes de error asociadas a este tipo de pacientes: la incorrecta determinación de la potencia corneal y la incorrecta predicción de la posición efectiva de la LIO, que se suele basar en la primera. En consecuencia, se ha desarrollado un amplio catalogo de fórmulas para el cálculo de potencia de LIO, que dependen de diversos factores, como la corrección de la potencia corneal por medio de diferentes regresiones empíricas o la consideración de datos pre-cirugía refractiva, no siempre disponibles en la historia de los pacientes. De esta forma, la selección de la fórmula a utilizar para calcular la potencia de la LIO depende de las características biométricas del paciente y del tipo de cirugía refractiva previa a la que se ha sometido, por lo que a efectos prácticos los cirujanos deben considerar diferentes fórmulas para seleccionar la potencia más adecuada. Debido a ello y a la mejora en los instrumentos clínicos para la determinación de los parámetros biométricos, se ha sugerido desde el ámbito clínico la necesidad de crear modelos de cálculo de potencia más deterministas. En esta línea, se han desarrollado algunas aproximaciones teóricas, bien dentro del limite paraxial o mediante trazado exacto de rayos con la introducción de algunas aberraciones, como la aberración esférica de la LIO y la consideración de la asfericidad de la cornea. En ambos casos, se ha demostrado que la predicción de la posición postoperatoria de la LIO es uno de los factores determinantes en la precisión del procedimiento, pues en este caso todas las superficies ópticas han de estar en sus posiciones reales.

Objetivos

En este marco, el principal objetivo de esta tesis es desarrollar un procedimiento para el cálculo de potencia de LIO valido para cualquier tipo de paciente y basado únicamente en sus propios datos biométricos y en el modelo de LIO a utilizar. Para ello, se usarán técnicas para modelar la óptica del ojo basadas en trazado exacto de rayos, considerando por ello tanto las aberraciones de la cornea como las de la LIO a implantar. Se considerará también la aberración cromática de cada uno de los medios a través de los que se realice el trazado de rayos.

Con el fin de determinar la validez de la representación topográfica de la cornea preoperatoria para el procedimiento de cálculo de potencia, compararemos las aberraciones corneales pre y post-operatorias en una serie de pacientes intervenidos con una incisión corneal de 3.5 mm, superior al tamaño habitual, para así poder considerar los efectos mas extremos de la incisión en las aberraciones corneales

Una vez resuelta esta cuestión y en un paso previo a la validación clínica, se comparará la potencia calculada con el modelo personalizado con el resultado predicho por las fórmulas paraxiales que se utilizan clínicamente en la actualidad para un amplio espectro de configuraciones oculares. Con ello es posible extraer conclusiones acerca de las principales diferencias entre los resultados relativos a cada método, así como evaluar el impacto de cada uno de los parámetros introducidos en el modelo de trazado de rayos.

El modelo de trazado de rayos se validará clínicamente tanto en pacientes normales, como en pacientes que se han sometido a una cirugía refractiva previa, con el fin de discernir si este modelo puede utilizarse de manera general para todo tipo de pacientes con probado beneficio clínico frente a las técnicas actualmente disponibles.

Métodos

El modelo de trazado de rayos desarrollado en este trabajo es completamente predictivo y basado en datos preoperatorios del paciente. Se introduce una representación de la superficie anterior de la cornea, basada en la medida de las elevaciones corneales realizada con un topógrafo corneal (Atlas; Carl Zeiss Meditec, Dublin CA, USA). Así, la cornea queda representada tanto por su potencia, asociada a su curvatura como en las fórmulas paraxiales, como por sus aberraciones. Las elevaciones corneales suministradas por el topógrafo en coordenadas polares se ajustan por mínimos cuadrados a una expansión de polinomios de Zernike hasta octavo orden para una apertura de 7 mm. A partir de dicha superficie ajustada, se escogen una serie elevaciones distribuidas en un mallado cartesiano con un espaciado de 0.1 mm cuyos valores intermedios son interpolados mediante un polinomio de grado 3 cuando se introducen en el programa de trazado de rayos que se utiliza en este trabajo. Además, las superficies corneales se recentran respecto de la pupila, para que así las aberraciones calculadas a partir de ellas estén referidas a la línea principal de mirada. Estas superficies reconstruidas de las elevaciones medidas por el topógrafo corneal, se utilizan también para evaluar las aberraciones corneales en un modelo separado donde la focal se considera en el plano donde se minimiza el RMS (root mean square) del radio del spot. Puesto que solo se mide la cara anterior corneal, la potencia de la superficie posterior se considera mediante el uso de un índice de refracción equivalente (IRE), calculado a partir del modelo de ojo de Le Grand, con una dispersión igual a la del agua. Dicha aproximación permite predecir un IRE muy cercano al calculado a partir de datos biométricos considerando medidas totales de la cornea publicadas en la literatura. La predicción de la posición de la LIO se realiza mediante una regresión previamente encontrada entre la cámara anterior preoperatoria, es decir, la posición del cristalino natural, medida con un biómetro óptico (IOL Master, Carl Zeiss Meditec, Jena, Germany), y la posición de la LIO tras la cirugía, medida con un sistema de tomografía de baja coherencia, OCT, (Visante, Carl Zeiss Meditec, Dublin, CA). Los detalles geométricos y ópticos que definen la LIO se introducen también para considerar correctamente su efecto en el modelo. Finalmente, la retina se coloca a una distancia igual a la medida de la longitud axial del ojo. Una vez construido el modelo, se realiza un trazado exacto de rayos utilizando un programa de diseño óptico (ZEMAX Development Corp, Bellevue, WA, USA). Esto permite calcular el camino exacto que siguen los rayos en su refracción y traslación a través de los diferentes medios oculares. Con el fin de realizar un modelado lo más realista posible, se consideran seis longitudes de onda entre 470 y 700nm en el trazado de rayos, cuya influencia en la calidad óptica vendrá pesada por la curva de sensibilidad espectral del ojo en condiciones fotópicas. A partir de este trazado de rayos policromático para 4mm de pupila, se evalúa, como métrica de la calidad óptica del ojo con la LIO implantada, el área bajo el modulo de la función de transferencia policromática promediada radialmente (rMTF) entre 0 y 30 ciclos por grado. La integración numérica se realiza usando la regla del trapecio con un paso de 3 ciclos por grado. Para cada potencia de LIO se construye un modelo a través del que se realiza el trazado policromático de rayos y se calcula la correspondiente área bajo la rMTF. Al final de la evaluación de LIOs, se escogerá aquella potencia que maximice el área bajo la rMTF, que será la que optimiza la calidad de la imagen retiniana. De esta forma, el procedimiento personalizado del cálculo de potencia queda integrado completamente en el programa de trazado de rayos. Los datos biométricos se introducen al comienzo (número de topografías, profundidad de la cámara anterior, rango de potencias de la LIO a evaluar y longitud axial). El procedimiento permite determinar la potencia de la LIO para diferentes niveles de aberraciones corneales. El modelo incorpora una superficie que permite compensar total o parcialmente parte de las aberraciones corneales asociadas a la topografía del paciente.

Resultados

Cambios ópticos temporales en la cornea tras la cirugía de cataratas

Para determinar la validez de las topografías preoperatorias utilizadas en el procedimiento del cálculo de potencia, se evaluó la inducción de aberraciones corneales tras la intervención en 29 ojos. El tamaño promedio de la incisión fue de 3.5mm. Se midieron al menos 4 topografías corneales preoperatorios, repitiéndose el proceso a las 2 semanas, 1, 4 y 7 meses y al año tras la cirugía de cataratas. A partir de esas topografías se calcularon las aberraciones corneales asociadas, referidas a una misma focal para cada paciente, fijada como aquella que minimizaba el radio del spot para las topografías preoperatorias. Esto permitió calcular la evolución de las aberraciones de bajo (para 3mm de pupila) y alto orden (para 4mm de pupila), por mera substracción de la etapa preoperatoria. En el caso de las aberraciones de bajo orden, se calcularon también las evoluciones de las componentes asociadas a la refracción corneal: desenfoque (esfera), astigmatismo (cilindro) y círculo de mínima confusión. De esta forma se encontró un cambio hipermetrópico de 0.3 D y un astigmatismo inducido de -0.4 D, estable a los 4 meses de la intervención. Del resultado anterior se sigue que la posición del círculo de mínima confusión de la cornea se mantiene inalterado tras la cirugía de catarata. Este es un resultado importante, debido a que la potencia de LIO calculada por el procedimiento es aquella que minimiza círculo de mínima confusión, pues las LIOs utilizadas durante esta tesis no son tóricas.

La forma más correcta de calcular la evolución del cilindro corneal es la descomposición vectorial, que realizamos considerando dos ejes diferentes: el preoperatorio, definido como la orientación del cilindro antes de la incisión, y el inducido, definido como el eje donde se realiza la incisión, que está correlacionado con la dirección del astigmatismo inducido a las 2 semanas de la intervención. Cuando el cilindro corneal asociado a cada estadio del estudio se descompone en ambos ejes, es posible realizar una substracción directa y así evaluar de una forma sencilla la evolución del cilindro en cada componente. Así encontramos que el cilindro asociado a la componente preoperatoria permanece constante durante todos los estadios del estudio, con una magnitud similar a la preoperatoria. Sin embargo, pudimos comprobar como la componente del astigmatismo en el eje de la inducción es responsable de la evolución, desde la inducción inicial tras la intervención, hasta la estabilización que ocurre sobre los 4 meses, con un valor de 0.3 D, independientemente del valor inicial de astigmatismo inducido. Es posible por tanto, establecer un modelo de estos resultados que prediga el cilindro tras la intervención. Este será el resultado de sumar vectorialmente el cilindro preoperatorio y un residuo, que para este tamaño de incisión (3.5 mm en promedio) es 0.3 D en la dirección de la incisión. Por lo tanto, esto valida la aproximación clínica en la que el cilindro corneal preoperatorio se suma vectorialmente al astigmatismo inducido por la cirugía, SIA en ingles (surgically induced astigmatism), para predecir el astigmatismo postoperatorio de la cornea.

Con respecto a las aberraciones corneales de alto orden, encontramos que su magnitud antes y después de la cirugía es similar. Sin embargo, cuando se estudia la evolución promedio de ciertos términos, como trefoil y coma, la inducción no fue nula, lo que indica un cambio de orientación. La aberración esférica, mostró una inducción promedio nula, aunque cuando se considera la inducción en función de la aberración esférica prequirúrgica, es posible observar una tendencia, que la hace disminuir para corneas con un valor inicial mayor de 0.058 micras a 4mm de pupila o aumentarla en el caso contrario.

<u>Cálculo de potencia de LIO personalizado por trazado de rayos.</u>

El procedimiento personalizado de trazado de rayos se aplicó a 19 ojos normales, a los que también se les predijo la potencia de LIO a colocar con 4 de las fórmulas paraxiales mas utilizadas en el ámbito clínico. Para cada ojo, se predijo la potencia con el procedimiento de trazado de rayos considerando 3 topografías corneales diferentes, siendo la potencia de la LIO final escogida, la moda de las 3 predicciones. La población incluida en el estudio cubrió un amplio espectro refractivo (-8.5-+4D). Las diferencias entre el procedimiento personalizado y las fórmulas paraxiales fueron mínimas en promedio. Sin embargo la diferencia entre la predicción de nuestro procedimiento y las de las fórmulas paraxiales fue mayor para aquellos pacientes con mayores errores refractivos, alcanzando hasta 1.5 D, con una dispersión del mismo orden entre las diferentes fórmulas paraxiales.

El efecto combinado de las aberraciones corneales y la aberración cromática, fue mas importante para lentes con mayor dispersión cromática, esto es, con menor numero de Abbe, suponiendo cambios entre la predicción de la potencia con nuestro procedimiento considerando luz monocromática (540nm) y policromática del orden de

0.5 D para LIOs con un número de Abbe de 37, que puede considerarse realista en los materiales utilizados para algunas LIO comerciales.

Se compararon las posiciones de la LIO predichas con nuestro algoritmo y con otro también desarrollado para el mismo modelo de LIO. La diferencia promedio fue de 0.11±0.15 mm, siendo la posición predicha por nuestro algoritmo más posterior. El impacto de dicha diferencia se evalúo, calculando la potencia de LIO a implantar por trazado de rayos para el mismo ojo con ambas predicciones de posición post-operatoria. La diferencia promedio entre la potencia calculada considerando ambos algoritmos para predecir la posición de la LIO fue de 0.25±0.31 D, es decir, menor que el intervalo de potencia con el que se comercializan las LIO consideradas en el estudio, que es de 0.5 D

La variabilidad máxima entre la potencia predicha para un mismo sujeto cuando se consideraron diferentes topografías fue, como máximo de 0.5D, que como se acaba de mencionar, es el incremento en potencia para el modelo de LIO evaluado. Se mostró que las topografías corneales con una desviación estándar en astigmatismo superior a 0.05 micras produjeron la variabilidad en la predicción de la potencia.

<u>Cálculo de la potencia de LIO usando trazado de rayos personalizado en pacientes normales de catarata</u>

El estudio anterior mostró la necesidad de un método optimizado para el cálculo de potencia, debido a las diferencias entre las distintas fórmulas paraxiales, y entre éstas y el procedimiento de trazado de rayos. Sin embargo no validó el procedimiento, puesto que los ojos considerados no fueron intervenidos, con lo que la potencia óptima no pudo ser determinada. Para validar el procedimiento, se llevo a cabo un estudio con 18 pacientes normales, con ojos considerados como promedio. Se eligieron así puesto que esta es la población donde mejor funcionan las fórmulas paraxiales, con lo que este estudio puede ser considerado como una validación del procedimiento de trazado de rayos en comparación al estado del arte actual en cálculo de potencia, representado por las fórmulas paraxiales. Se realizaron todas las medidas preoperatorias correspondientes, así como la predicción personalizada por trazado de rayos con y sin la incorporación de las aberraciones corneales, para poder así evaluar su impacto. Se calculó también la potencia de LIO con la formula paraxial SRK/T. Con el fin de calcular la potencia óptima para cada paciente, se añadió a la potencia de LIO implantada, la potencia en el plano de la LIO correspondiente a la refracción realizada al paciente 1 mes tras la operación. Se calculó para cada paciente la diferencia entre la potencia óptima y cada una de las predicciones preoperatorias (trazado de rayos, con y sin aberraciones corneales, y formula paraxial SRK/T), para trasladarla al plano de gafa y calcular así el error refractivo asociado a la elección de dicha potencia. Encontramos que el error refractivo absoluto promedio, así como la varianza no fueron estadísticamente diferentes para ninguno de los procedimientos considerados, lo que valida el procedimiento de trazado de rayos. Sin embargo, el error refractivo promedio fue estadísticamente diferente entre los métodos de trazado de rayos y la predicción paraxial. Este punto puede deberse a la necesidad de un mejor algoritmo de predicción para la posición de la LIO. Este factor no es crucial para la formula paraxial, pues la predicción de dicha posición se basa en una constante que está optimizada a partir de datos post-operatorios de cientos de pacientes que han sido implantados con el mismo modelo de LIO. Así, se calcula la constante, y por lo tanto la posición de LIO que en promedio genera un error refractivo nulo. De esta forma, cualquier error en el procedimiento queda corregido por dicha optimización. Puesto que el procedimiento de trazado de rayos solo considera datos biométricos reales del paciente, la veracidad de dichos datos es el factor limitante de la precisión del método.

Con respecto a la influencia de las aberraciones corneales, la máxima diferencia entre la potencia calculada con y sin aberraciones fue de 0.5 D, que es el incremento en potencia del modelo de LIO utilizada. Se encontró una ligera correlación de los resultados con las aberraciones corneales. Sin embargo, el error refractivo absoluto promedio fue menor cuando las aberraciones corneales no fueron introducidas en el procedimiento. Su impacto queda pues enmascarado por los errores asociados a los datos biométricos y a los propios de procedimiento, ya que el tratamiento por trazado exacto no permite la optimización de ninguno de los parámetros involucrados para incrementar artificialmente la precisión del método, como se hace en las fórmulas paraxiales.

Cálculo de potencia de LIO usando trazado de rayos personalizado en pacientes de catarata post-LASIK

Una vez validado el método para pacientes normales, se realizó un estudio similar involucrando a pacientes post-LASIK con corrección tanto miópica como hipermetrópica, para así verificar si el procedimiento personalizado de trazado de rayos puede ser considerado como un método global de cálculo de potencia de LIO. Los métodos y el protocolo fueron idénticos al caso anterior. Además de la formula paraxial SRK/T, se utilizó con fines comparativos una modificación en dicha formula dependiente de la cirugía refractiva previa a la catarata, referida a partir de ahora como Doble K/Masket, que según la literatura, puede considerarse como el estado del arte en cálculo de potencia de LIO para pacientes post-LASIK. En el caso de pacientes miópicos post-LASIK, se consideró la formula SRK/T Doble K, donde la potencia corneal pre-LASIK se utiliza para predecir la posición de la lente y la potencia corneal post-LASIK se utiliza, una vez corregida, para calcular la potencia de la LIO en la posición anteriormente determinada. Para la corrección de la potencia corneal post-LASIK se utilizó el método de Seitz/Speicher/Savini. Para pacientes hipermetrópicos se utilizó el método de Masket, basado en el cálculo de potencia con la formula SRK/T sobre el que se realiza una corrección basada en el cambio de refracción asociada la cirugía refractiva.

En este caso, no se encontró una diferencia estadísticamente significativa entre los errores refractivos promedio para la predicción Doble K/Masket y el procedimiento de trazado de rayos incorporando aberraciones corneales. Sin embargo, el error refractivo absoluto medio y la varianza fueron estadísticamente superiores para formula paraxial Doble K/Masket en comparación al trazado de rayos incorporando aberraciones corneales. Esto demuestra que el trazado de rayos incorporando las aberraciones corneales es más preciso en pacientes post-LASIK. Cuando las aberraciones corneales no se consideran en el procedimiento de trazado de rayos, estas diferencias con la formula Doble K/Masket dejan de ser significativas. Por lo tanto las aberraciones corneales son las responsables del incremento de precisión del trazado de rayos con respecto a las técnicas actuales de cálculo de potencia para estos pacientes. Además, la diferencia entre el procedimiento de trazado de rayos con y sin la inclusión aberraciones corneales depende de la magnitud de las aberraciones corneales (r^2=0.59). Esta correlación mejora (r^2=0.82) al considerar sólo la aberración esférica.

Esto sugirió la posibilidad de desarrollar un nuevo método para mejorar la precisión de las fórmulas actuales para pacientes con cirugía refractiva previa. Debido a su naturaleza paraxial, no consideran las aberraciones de la cornea ni de la lente. Esta es una de las razones por las que es necesario definir correcciones en la potencia post-

LASIK medida. Se demostró que es posible mejorar la predicción asociada a las fórmulas paraxiales incluyendo la aberración esférica corneal en pacientes post-LASIK. De esta forma, obtuvimos nuevas fórmulas que tienen como parámetros la potencia calculada con las fórmulas paraxiales validas para pacientes normales y la aberración esférica corneal a 4mm. Estas fórmulas se generaron con los datos biométricos de 29 pacientes post-LASIK miópicos. La potencia óptima para cada paciente, obtenida a partir de la potencia implantada y la refracción postoperatoria trasladada ópticamente al plano de la LIO, se ajustó por un procedimiento de mínimos cuadrados a la aberración esférica corneal y a la potencia resultante de aplicar distintas fórmulas paraxiales, sin ninguna corrección propia para pacientes post-LASIK. De esta forma, por cada formula paraxial se genera una nueva formula modificada para pacientes post-LASIK incorporando la aberración esférica corneal. La introducción de la dicho parámetro mejoró la predicción de potencia en los pacientes incluidos en el estudio frente a los resultados asociados a las fórmulas originales. Se calculó la diferencia en valor absoluto entre la potencia óptima y la potencia de la LIO predicha por las fórmulas originales y por las fórmulas modificadas. Este valor, promediado para todos los pacientes incluidos en el estudio fue de 2.48±1.29 D con la formula SRK/T y de 0.81±0.50 D con la formula modificada incluyendo la aberración esférica corneal. En el caso de la formula Haigis, dicho valor fue de 1.44±0.85 D, mientras que en el caso de la nueva formula basada en la misma e incluyendo la esférica corneal el resultado fue de 0.61±0.50 D. Por lo tanto el error de la predicción es notablemente menor con las nuevas fórmulas incorporando la aberración esférica corneal que con las fórmulas convencionales. Las fórmulas con menor error predictivo fueron las basadas en la formula HofferQ y la Haigis. Además, el rango de error (diferencia entre el mayor error hipermetrópico y miópico en valor absoluto predicho por cada fórmula) para estas nuevas fórmulas incorporando la aberración esférica corneal fue 0.56D menor que el que resulta de aplicar la formula Haigis L. De esta forma, cuando el trazado de rayos no está disponible, es posible utilizar la aberración esférica corneal, incorporándola en las fórmulas que están actualmente disponibles en la práctica clínica.

Finalmente y volviendo al procedimiento de trazado de rayos, se estudió el impacto del índice de refracción equivalente (IRE) en los pacientes post-LASIK. El cálculo de IRE se basa en la relación entre el radio de la cara anterior y posterior de la cornea. Esta relación es aproximadamente constante en pacientes normales. Sin embargo, la relación entre el radio de la superficie anterior y posterior de la cornea se ve modificado por el efecto de la cirugía refractiva de diferente forma dependiendo de la corrección refractiva realizada. Como consecuencia de esto, los resultados para pacientes post-LASIK pueden mejorarse si el IRE se modifica para ellos. Se calculó el IRE para 25 pacientes post-LASIK de forma individual y en promedio considerando métodos paraxiales, a partir del radio de la cara anterior corneal, calculado de la topografia corneal post-operatoria por trazado de rayos. El radio de la cara posterior de la cornea, que es necesario para el cálculo del IRE, no se midió en el estudio. Puesto que la literatura muestra que permanece constante tras la cirugía refractiva, se determinó a partir del radio corneal pre-LASIK y la relación promedio entre el radio de la cara posterior y anterior de la cornea para pacientes normales (0.838). En un intento por evitar el uso de datos pre-LASIK, que no están siempre disponibles, el IRE fue también calculado únicamente utilizando datos post-LASIK con la misma metodología paraxial y considerando el radio de la cara posterior corneal fijo para todos los pacientes, igual a valores fisiológicos reportados en la literatura (6.53mm). El IRE promedio calculado por ambos métodos para la población considerada en el estudio, fue de 1.324±0.003 y 1.325±0.004 respectivamente, con un rango similar en ambos casos. Cuando tanto el IRE promedio como el personalizado se consideraron en el procedimiento de trazado de rayos, se encontró en ambos casos un error en la predicción de la potencia media en torno a cero, a diferencia del error medio ligeramente positivo relativo al IRE calculado para pacientes normales. La varianza del error medio de la predicción y el error absoluto medio para la formula Haigis L fue estadísticamente superior a la que resulta del trazado de rayos con un índice equivalente promedio, con lo que la modificación del IRE mejoro los resultados del trazado de rayos personalizado, incluso a un nivel superior al de las fórmulas consideradas como el estado del arte actual para este tipo de pacientes.

Conclusiones

1. Hemos desarrollado un proceso predictivo personalizado que permite calcular la potencia de la LIO óptima para un determinado paciente y un modelo de LIO específica. Este procedimiento esta basado en una serie de medidas biométricas realizadas en el ojo, y en un procedimiento exacto de trazado de rayos policromático.

2. Se ha estudiado la inducción de aberraciones corneales tras la cirugía de cataratas, así como su evolución temporal. Las topografías de la superficie anterior de la cornea pueden usarse para predecir la potencia de la LIO en el procedimiento

personalizado de trazado de rayos, ya que el circulo de mínima confusión asociado a dicha superficie corneal permanece estable tras la cirugía.

3. La precisión del procedimiento de trazado de rayos está limitada por la calidad de los parámetros introducidos, especialmente por las topografías corneales. El tratamiento policromático es especialmente relevante para las LIOs con un número de Abbe bajo.

4. El procedimiento de trazado de rayos y las fórmulas convencionales muestran una precisión similar en pacientes normales promedio. La introducción de las aberraciones corneales no se traduce en una disminución del error en la predicción de la potencia. Sin embargo, la diferencia entre las fórmulas paraxiales y el procedimiento de trazado de rayos es mayor cuanto mayor es la ametropía del paciente antes de la cirugía de catarata.

5. La introducción de las aberraciones corneales en el procedimiento de trazado de rayos para pacientes post-LASIK es necesaria. La precisión del procedimiento incluyendo las aberraciones corneales es mayor que la de las técnicas actuales del cálculo de potencia de LIO para pacientes post-LASIK, tanto miópicos como hipermetrópicos, especialmente debido a la consideración de la aberración esférica corneal.

6. El procedimiento personalizado de trazado de rayos puede considerarse como un método global para el cálculo de potencia, valido tanto para pacientes normales como para todo tipo de pacientes post-LASIK.

7. La precisión del procedimiento de trazado de rayos en pacientes post-LASIK miópicos puede mejorarse si se modifica el índice de refracción equivalente de la cornea con respecto al usado en pacientes normales. Este índice de refracción equivalente se calcula paraxialmente a partir de medidas post-operatorias.

8. La incorporación de la aberración esférica corneal a las fórmulas paraxiales para pacientes normales mejora la predicción de potencia en pacientes post-LASIK. Sin embargo, la precisión de estas fórmulas modificadas es menor que la del trazado de rayos personalizado.

UNIVERSIDAD DE MURCIA

Departamento de Física

Laboratorio de Óptica

Optical quality in pseudophakic eyes: experimental measurements, modeling and applications

Carmen Cánovas Vidal

2012

Index

Chapter 1

INTRODUCTION

1.1. The eye as an optical instrument

1.1.1. Optical elements of the eye

The eye is the responsible of the first step in vision, that is, the optical phase, in what the light reflected or emitted by the objects is focused to create an image at the retina that will be processed by the brain. This image formation is mainly due to two convergent elements in the eye (the cornea and the lens) that actually create an inverted image of the object.

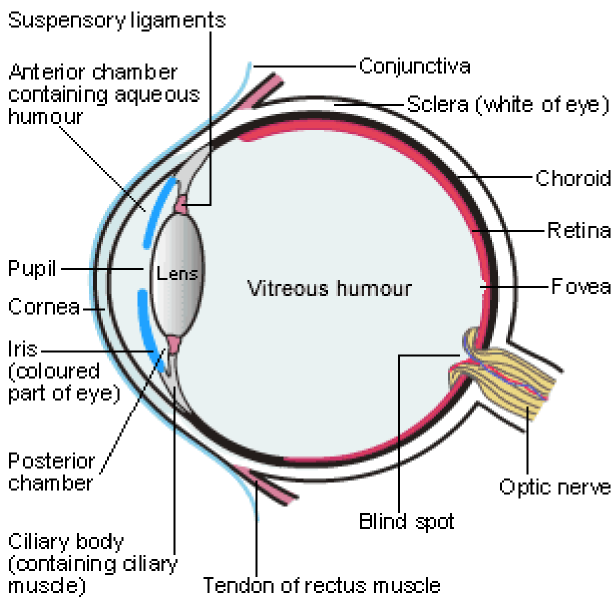

Figure1.1 Schematic view of different structures in the eye.

The different parts of the eye are shown in figure 1.1. Light reaches the eye at the cornea. This transparent surface of about 580 microns (μm) on average is covered by the tear film, that is between 4 and 7 μm thick. The tear film allows for moistening the corneal surface and provides clear vision. Although the cornea is composed by six different layers, the stroma comprises the 90 percent of its thickness. It consists of regularly arranged collagen fibrils that are the main responsible of the cornea's transparency. Optically, the cornea is a convex-concave lens with a mean refractive index of 1.376. It separates the air from the aqueous humor and therefore, it is the element with the highest optical power (approximately two thirds of the total power of the eye, although this fraction is modified when the power of the eye is increased during accommodation). The first corneal surface has an average radius of about 7.8 mm and, because it is the first interface between air and the cornea, it provides the highest optical power. The anterior corneal surface can present some toricity, which generates corneal astigmatism. Due to the fact that the second corneal surface is more difficult to be measured, there is some dispersion in its characterization. While Gullstrand adopted 6.8 mm as its average radius, Le Grand considered 6.5 mm. This generates a difference of about 0.7 D in the total corneal power between their models [Atchinson and Smith, 2000]. Dubbelman [Dubbelman et al. 2006] has shown by using a Scheimpflug imaging technique an average good correspondence with Le Grand's values.

The zone between the cornea and the next structure of the eye is called anterior chamber and it is filled by the aqueous humor, which has a refractive index of 1.336. This fluid serves to hydrate the cornea, due to its lack of vessels.

After being refracted by the cornea and passing the anterior chamber, the light reaches the iris, which is the aperture of the eye. This is opening and closing, depending on the light levels, accommodation state and other factors, like age. The illumination level affects the pupil size, changing from about 2 mm diameter in photopic conditions (luminance of 100 cd/m^2) to about 8 mm in scotopic conditions (for 0.00001 cd/m^2) [Atchinson and Smith, 2000]. The changes in pupil size also affect pupil center position. Yang found that the pupil center shifts temporally as the pupil dilates, although the change in position was not related to refractive error, age or change of pupil diameter [Yang et al. 2002]. The pupil size and location determines the amount and type of aberrations and therefore affects the retinal image quality and optical performance.

The other optical component adding power to the eye is the crystalline lens. It is formed by different fiber layers, which generate a gradient index ranging from 1.406 at the center to 1.386 at the capsule. The lens grows throughout life, therefore, its thickness and radii are highly age dependent. Furthermore, these parameters also change during the accommodation process, when the lens' shape is modified to allow the image formation of objects at different distances. This is possible due to the combined action of the ciliary muscle, the ciliary body on the elastic capsule and lens itself (figure 1.2(a)). According to Helmholtz's theory, when the eye is looking at distant objects, the ciliary muscle is relaxed and the lens is flattened in an un-accomodated state by the zonular fibers. When a near object is focused, the ciliary muscle is contracted, the ciliary body moves forward and toward the axis of the eye, releasing tension in the zonular fiber, that allows a more curved shape of the lens through the elastic capsule. The combination of the forward movement of the lens as well as the increase of the curvature of both anterior and posterior lens surfaces generates an increased power to focus near objects. When accommodation is relaxed, the lens diameter increases, decreasing its thickness and flattening both lens surfaces (figure 1.2.(b)). The power of the lens, and therefore of the complete eye, is lowered, allowing far objects to be in focus [Glasser, 2008]. This mechanism is disrupted by age, generating an eye unable to focus at different distances. This is called presbyopia and it is mainly due to the loss of elasticity at the lens matrix itself. Another alteration in the lens that is mainly due to age, although might be also due to some other mechanisms, is the formation of cataracts, that will be discussed in section 1.2. Both, cataract and partially presbyopia, are solved with the substitution of the cataractous lens by an artificial implant called intraocular lens, which will be specifically treated in the next section.

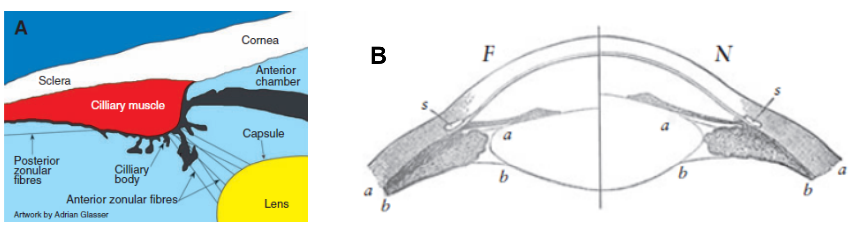

Figure 1.2. (a) Ocular structures responsible for the accommodation mechanism [from Glasser, 2008] and (b) schematic view of the anterior eye when looking at far (F) or near (N) [Helmholtz, 1925]

After refraction in the lens, the light passes through the vitreous chamber, which is the biggest internal structure in the eye, enclosing almost the 80% of the total eye volume. This is filled with the vitreous humor, a transparent gelatin composed by collagen fibrils, with a refractive index of 1.336. Finally, the light focuses into the retina, where it is detected by the photoreceptors and converted in electrical signals, completing the optical part of the vision process

It is important to note that the light experiences different optical processes when passing through the eye. When the light reaches the surfaces separating different media, it is both refracted, this creating an image at the retina, and reflected, this lowering the amount of light that finally reaches the retina. Purkinje images are the specular reflections from a source produced by the corneal and lenticular surfaces. The information provided by these images has been used in order to determine the radii of the lens surfaces and to further develop the understanding of the accommodation process [Helmholtz, 1925]. Purkinje images can also be used clinically to measure the tilt and misalignments between different optical surfaces [Guyton et al. 1990 and Tabernero et al. 2006 (a)]. Most methods to estimate corneal topography are based on the reflection of light in the anterior cornea, as will be described in the next chapter. In addition, light scattering through the different media or floating particles in the humors also may affect the quality of retinal image. A pathological case related to an increase of scatter is the cataract, affecting the retinal image by the creation of a light halo.

Imperfections in different surfaces are the responsible of optical aberrations in the refraction process, whose impact depends on the pupil size. The nature of monochromatic and chromatic aberrations as well as its mathematical description will be the subject of the next section, as well as it impact on the optical quality of image.

1.1.2. Optical quality parameters

An ideal optical system can be described by paraxial optics. Monochromatic optical aberrations are deviations from the paraxial behavior that makes inaccurate the ray propagation described within this approximation. In order to quantify the monochromatic aberrations, the wave aberration function is defined at the exit pupil as the difference between the real wavefront and a reference wavefront, that might be chosen as that described by paraxial optics (figure 1.3) [Born and Wolf, 1989].

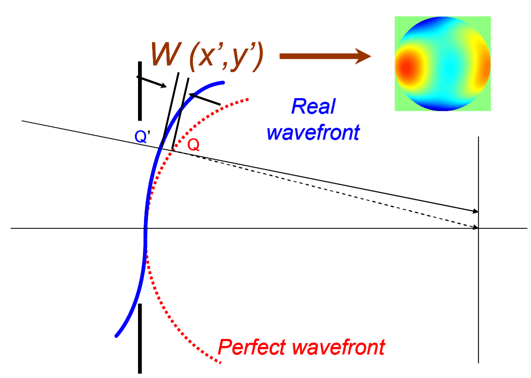

Figure 1.3. Wave aberration in the point x',y' of the exit pupil (W(x',y')) is defined as the optical path length [Q'Q], where Q' and Q are the points of intersection of the ray at the exit pupil x',y' with the real wavefront and the gaussian reference sphere [Born and Wolf, 1989].

The wave aberration is a two-dimensional function that can be decomposed as a sum of weighted polynomials. A modal decomposition is frequently used to describe the wave aberration, being the Zernike polynomials [Noll, 1976] the most common basis used due to its orthogonality properties over a unit circle [Mahajan, 1998]. In polar coordinates, each polynomial is composed by a normalization factor, radial component and angular function. The radial component is a polynomial and the angular function is sinusoidal. They might be specified by a double indexing, where n is the highest power order of the radial component and m the order of the azimuthal frequency of the angular function. Zernike polynomials might also be specified by a unique index [Thibos et al. 2000]. The jth polynomial can be obtained from the row number n and the column number m related to the double indexing description when showed in a pyramid (figure 1.4). The general mathematical expression of the Zernike polynomials is given by:

$$Z_j(\rho,\theta) = Z_n^m(\rho,\theta) = \begin{cases} \sqrt{n+1}\ R_n^0(\rho) & \text{if } m=0 \\ \sqrt{2(n+1)}\ R_n^{|m|}(\rho)\cos(m\theta) & \text{if } m>0 \\ -\sqrt{2(n+1)}\ R_n^{|m|}(\rho)\sin(m\theta) & \text{if } m<0 \end{cases} \qquad [1.1]$$

where ρ is the radial coordinate ranging from 0 to 1, θ ranges from 0 to 2π and the radial component R(m,n) is described as:

$$R_n^{|m|}(\rho) = \sum_{s=0}^{(n-|m|)/2} \frac{(-1)^s (n-s)!}{s!\,[(n+|m|)/2-s]!\,[(n-|m|)/2-s]!}\,\rho^{n-2s} \qquad [1.2]$$

Figure 1.4 shows a 3D representation of the Zernike polynomials up to the 4th order while table 1.1 shows the mathematical representation of these polynomials up to 6^{th} order.

Figure 1.5 shows the convention for Zernike polynomial orientation for ophthalmic optics, where the origin is taken at the center of the eye's entrance pupil. The positive x coordinate is to the right, the positive vertical coordinate is pointing up, being the same orientation for both eyes. Regarding the positive z coordinate, it points out in the same direction as the foveal line of sight in the object space [Thibos et al. 2000].

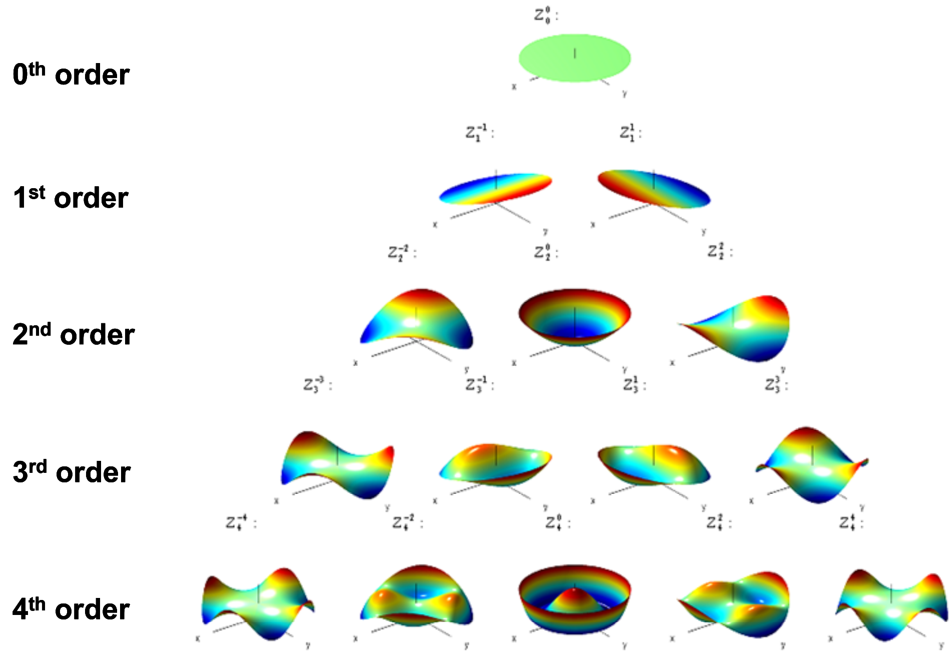

n\m	-5	-4	-3	-2	-1	0	+1	+2	+3	+4	+5
0						j=0					
1					1		2				
2				3		4		5			
3			6		7		8		9		
4		10		11		12		13		14	
5	15		16		17		18		19		20

Figure 1.4. 3D representations of the Zernike polynomials up to the 4th order in pyramid order. With the single indexing ordering z12 is Z(4,0), because it is the 12th when starting from the top and counting from left to right, as it is schematically shown below the pyramid.

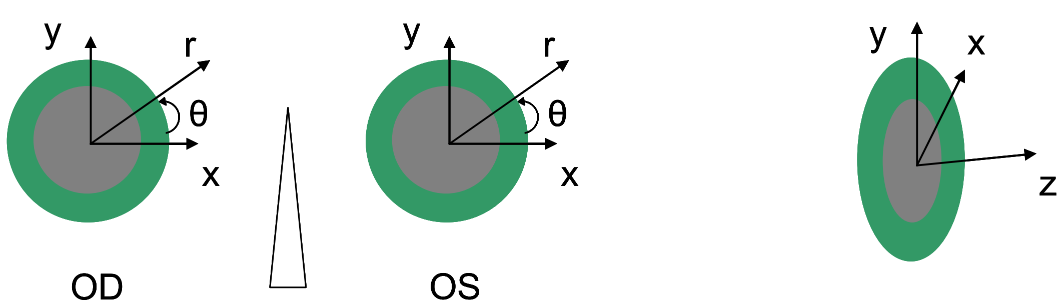

Figure 1.5. The right handed coordinate system (left) is defined for both eyes when looking at front (right).

j = index	n = order	m = frequency	$Z_n^m(\rho,\theta)$
0	0	0	1
1	1	-1	$2\ \rho \sin\theta$
2	1	1	$2\ \rho \cos\theta$
3	2	-2	$\sqrt{6}\ \rho^2 \sin 2\theta$
4	2	0	$\sqrt{3}\ (2\rho^2\text{-}1)$
5	2	2	$\sqrt{6}\ \rho^2 \cos 2\theta$
6	3	-3	$\sqrt{8}\ \rho^3 \sin 3\theta$
7	3	-1	$\sqrt{8}\ (3\rho^3\text{-}2\rho) \sin\theta$
8	3	1	$\sqrt{8}\ (3\rho^3\text{-}2\rho) \cos\theta$
9	3	3	$\sqrt{8}\ \rho^3 \cos 3\theta$
10	4	-4	$\sqrt{10}\ \rho^4 \sin 4\theta$
11	4	-2	$\sqrt{10}\ (4\rho^4\text{-}3\rho^2) \sin 2\theta$
12	4	0	$\sqrt{5}\ (6\rho^4\text{-}6\rho^2\text{+}1)$
13	4	2	$\sqrt{10}\ (4\rho^4\text{-}3\rho^2) \cos 2\theta$
14	4	4	$\sqrt{10}\ \rho^4 \cos 4\theta$
15	5	-5	$\sqrt{12}\ \rho^5 \sin 5\theta$
16	5	-3	$\sqrt{12}\ (5\rho^5\text{-}4\rho^3) \sin 3\theta$
17	5	-1	$\sqrt{12}\ (10\rho^5\text{-}12\rho^3\text{+}3\rho) \sin\theta$
18	5	1	$\sqrt{12}\ (10\rho^5\text{-}12\rho^3\text{+}3\rho) \cos\theta$
19	5	3	$\sqrt{12}\ (5\rho^5\text{-}4\rho^3) \cos 3\theta$
20	5	5	$\sqrt{12}\ \rho^5 \cos 5\theta$
21	6	-6	$\sqrt{14}\ \rho^6 \sin 6\theta$
22	6	-4	$\sqrt{14}\ (6\rho^6\text{-}5\rho^4) \sin 4\theta$
23	6	-2	$\sqrt{14}\ (15\rho^6\text{-}20\rho^4\text{+}6\rho^2) \sin 2\theta$
24	6	0	$\sqrt{7}\ (20\rho^6\text{-}30\rho^4\text{+}12\rho^2\text{-}1)$
25	6	2	$\sqrt{14}\ (15\rho^6\text{-}20\rho^4\text{+}6\rho^2) \cos 2\theta$
26	6	4	$\sqrt{14}\ (6\rho^6\text{-}5\rho^4) \cos 4\theta$
27	6	6	$\sqrt{14}\ \rho^6 \cos 6\theta$

Table 1.1. Zernike polynomials up to the 6th order

There are several approaches to characterize the optical performance from the wave aberration function once found its modal decomposition in Zernike terms. It is possible to refer to the actual value of the different Zernike modes or the root mean square of the wavefront error (RMS), that can be easily calculated as the root square of the sum of all the squared Zernike coefficients. These parameters are usually called pupil plane image quality parameters.

It is also possible to describe the optical quality of the system related to the formed image. This is estimated from the generalized pupil function, defined as a complex function, whose modulus is the pupil's transmission (p(x',y')), and whose phase is related to the wave aberration function [Goodman, 1996]. The image of a point source, the point spread function (PSF), of an aberrated system is related to the Fraunhofer diffraction pattern of the generalized pupil function:

$$PSF(x,y) = \left| FT\left[p(x',y') e^{i\frac{2\pi}{\lambda}W(x',y')} \right] \right|^2 \qquad [1.3]$$

where (x,y) are the coordinates at the image plane, (x',y') the coordinates at the system's exit pupil, FT represents the Fourier transform and λ the light's wavelength.

Even in the case of an aberration free system, the irradiance distribution at the image plane, is not a perfect point, but the diffraction pattern produced by a circular aperture, what is called the Airy disk. Therefore, in the ideal scenario of an aberration-free system, the optical quality is limited by diffraction (figure 1.6).

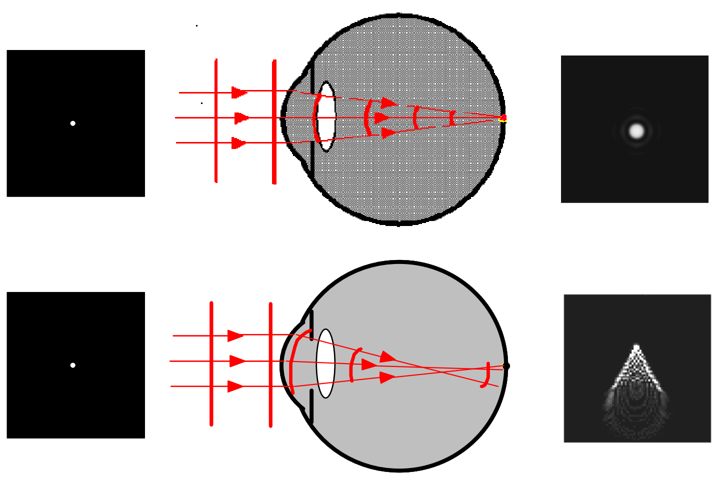

Figure 1.6. The PSF of a non aberrated eye is the Airy disk (top). In the case of an eye presenting aberrations, the image of a point deviates in a manner that depends on the type and amount of those aberrations.

It is possible to calculate the image that the system generates for an extended object for incoherent illumination, as the convolution of the image predicted by geometrical optics with the PSF [Goodman, 1996]:

$$I(x,y) = \iint PSF(x - x', y - y') I_{geometric}(x', y') dx' dy' = PSF \otimes I_{geometric} \qquad [1.4]$$

The normalized Fourier transform of the PSF is the Optical Transfer Function (OTF). The modulus of the OTF is known as the Modulation Transfer Function (MTF) and indicates how the system transfers from the object to the image the spatial frequencies which containes. The MTF of an optical system free of aberrations with a circular aperture is the Fourier transform of the Airy disk, which is a decreasing function that is zero for a specific spatial frequency, meaning that the system is not transmitting spatial frequencies higher than this cutoff frequency. When aberrations are present, the MTF drops faster, and therefore, the effective cutoff is much lower than the diffraction limited.

In addition to the previously discussed monochromatic aberrations, the optical properties are dependent on the light wavelenght. This is called chromatic aberration and it is due to dispersion effects in matherials, that is, the dependence of the refractive index value for different wavelengths. There are two types of chromatic aberrations: longitudinal and transversal (Figure 1.7). In the first case, the amount of longitudinal chromatic aberration is defined as the power difference for different wavelengths (usually the most separated but relevant for the optical system). In the case of the eye, there is a difference of refraction about 2.1 D between 400 and 700 nm [Atchinson and Smith, 2000]. On the other hand, transversal chromatic aberration is the difference between image magnification for different wavelengths.

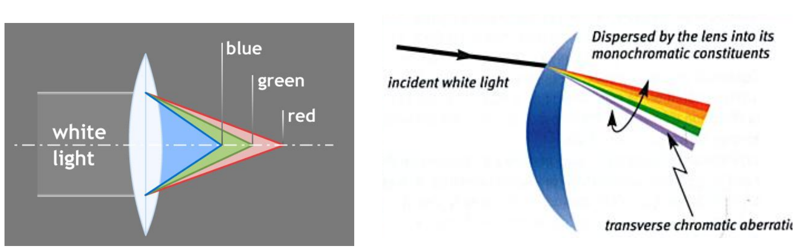

a b

Figure 1.7. Schematic effect of the longitudinal chromatic aberration (a) and transversal chromatic aberration (b).

For polychromatic sources, the optical quality parameters previously described are calculated separately at each wavelength and weighted according the relative spectral sensitivity. As a matter of example, the polychromatic MTF (MTF_{pol}) that is used during this work [van Meeteren, 1974], is calculated from the MTF for different wavelengths ($MTF_{mon}(\lambda)$) and weighted according a specific function, that in the case of the eye is the relative spectral sensitivity:

$$MTF_{pol} = \frac{\sum_{\lambda} MTF_{mon}(\lambda)V(\lambda)}{\sum_{\lambda} V(\lambda)} \qquad [1.5]$$

At equation 1.5, V(λ) represents the spectral luminous efficiency function, which shows the relative response of the eye to different wavelengths. The curve at figure 1.8 represents the visual response for high light levels, which is referred as photopic illumination. The lower luminance limit to be considered within this range is 3 cd/m^2. Low light levels, which are called scotopic conditions, are related to luminance levels below 0.3 cd/m^2. The main difference between the visual response at that light conditions and that showed at figure 1.8 is the fact that the maximum is shifted from 555nm at photopic to 507 nm at scotopic illumination, which is called Purkinje shift [Atchinson and Smith, 2000].

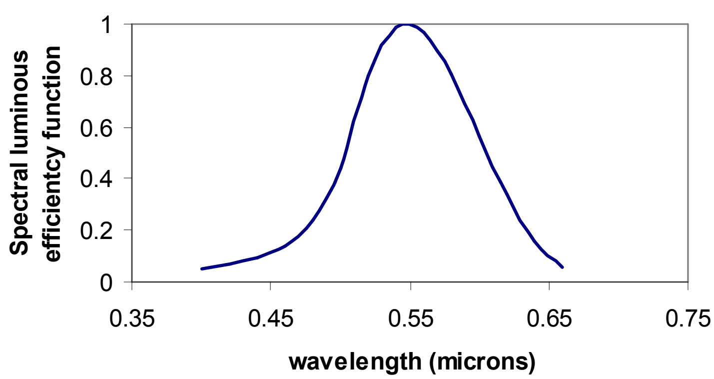

Figure 1.8. Spectral luminous efficiency function at photopic conditions.

1.1.3. Theoretical eye models and optical quality

The ocular anatomical aspects have been briefly discussed in the first section of this chapter. The match between surface curvatures, refractive indexes and distances allows for an adequate image formation. The characteristic of these images might be described from the paraxial point of view, that is, with no concern about large pupils or for incidence angles larger than a few degrees from the optical axis. In this case, paraxial models are used, where different surfaces in the eye are spherical and centered with respect to the optical axis. For a more detailed description based on the incorporation of non-paraxial optical approximations of the eye's optical quality, finite or wide angle schematic eyes are needed, characterized by a lack of alignment between different optical surfaces that deviate from the spherical shape.

From the first physical eye model proposed by Huygens, a great number of paraxial eye models have been developed. An extensive summary of some of these paraxial schematic eye models has been compiled [Atchinson and Smith, 2000]. As an example of one of these paraxial eye models, Figure 1.9 shows the geometrical and optical parameters defining the Le Grand's full theoretical eye model [Le Grand and EL Hage, 1980], that consists on 4 centered, spherical refractive surfaces, where all refractive indexes are considered as constants. This model is able to predict the paraxial properties of an average real eye, such us its power as well as the position of the entrance and exit pupil and its focal, principal and nodal planes. In the figure, only the relaxed form is shown, although, there is an accommodated version. In addition, there is a simplified version of this eye model, where the cornea is reduced to a unique refractive surface and the thickness of the lens is neglected. In general, simplified models are considered adequate for reproducing the paraxial properties of the average eye. At the same time, the complexity of the calculations is substantially reduced. On the limit of simplicity, the so called reduced schematic eyes, are simply composed by a unique refractive surface. This surface is not anatomically real, because the radius is smaller than the cornea to reproduce the power of the whole eye. Although, these eye models are useful within the paraxial region, more realistic models of the eye are needed in order to include some non-paraxial effects as the eye's monochromatic aberrations.

One characteristic of the human eye is that, in general, the optical axis does not contain neither the fixation point nor the point of the retina where the image is formed (figure 1.10). Therefore, the visual axis is defined as the line joining the fixation point and the foveal image through the nodal points. In average, the visual axis is located 5 degrees nasal at the object space to the optical axis at the horizontal orientation. The angle between the optical and visual axis is referred as alpha angle. The eye is not a centered system, due to the fact that the centre of curvature of the cornea, lens and pupil do not lie on one single line. An approximate optical axis can be defined as the line of the best fit through the centres of curvature of the best fit spheres to each ocular surface

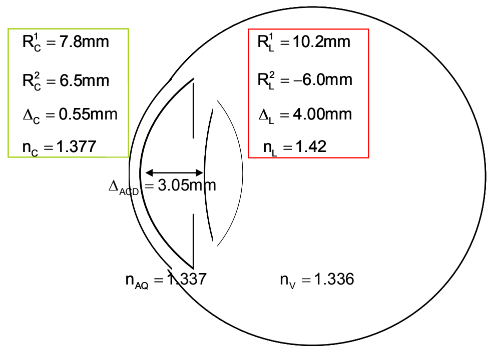

Figure 1.9. Le-Grand full theoretical eye [Le Grand and EL Hage, 1980].

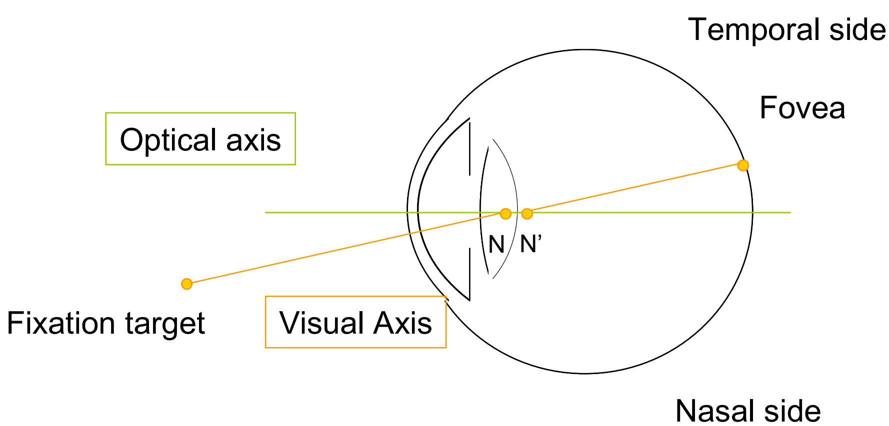

Figure 1.10. Visual axis and optical axis

The ocular surfaces are not spherical and this characteristic should be taken into account if the model should predict spherical aberration. More sophisticated models should then include aspheric surfaces. The most common rotationally symmetric aspheric surface used for modeling the eye is the conicoid. The elevation (z) in a point (r) is defined as follows:

$$z = \frac{cr^2}{1 + \sqrt{1 - (1+Q)c^2r^2}} \qquad [1.6]$$

where c is the curvature, which is the inverse of the radius, and Q is the conic constant (less than -1 for hyperbolas, -1 for parabolas, between -1 and 0 for ellipses, 0 for spheres, and greater than 0 for oblate ellipsoids). In the human eye both the radius and aspheric terms change between individuals, although it is possible to consider average values in order to define general eye models.

When all these factors are considered together, it is possible to define models that allow for a more realistic representation of the eye, reproducing characteristics as spherical aberration. In table 1.2, the radius and aspheric terms corresponding to the eye surfaces as defined in different finite eye models are listed. For the anterior cornea, the conic constant is between 0 and -0.3, with an average value of about -0.2. This means that in the anterior cornea the radius grows with the distance to the axis. A consequence of this is that anterior corneal spherical aberration although it is positive, is smaller than that related with a spherical surface [Guirao et al. 2000].

Eye model	**Anterior cornea**		**Posterior cornea**		**Anterior lens**		**Posterior lens**	
	R (mm)	**Q**	**R (mm)**	**Q**	**R (mm)**	**Q**	**R (mm)**	**Q**
[Kooijman, 1983]	7.8	-0.25	6.5	-0.25	10.2	-3.06	-6	-1
[Navarro et al., 1985]	7.72	-0.26	6.5	0	10.2	-3.13	-6	-1
[Liou and Brennan, 1997]	7.77	-0.18	6.4	-0.6	12.4	-0.94	-8.1	0.96

Table 1.2. Radius and aspheric terms in some published finite eye models

Liou and Brennan eye's model appears to give a good overall estimation of average optical quality in real eyes [Liou and Brennan, 1997]. This is achieved because the eye's geometry and the index of refraction are realistic, due to the fact that were taken from some experimental studies, as well as the consideration of the pupil decentration of 0.5mm nasally from the optical axis and the consideration of a 5 degrees alpha angle. This eye model is able to reproduce spherical aberration values within empirical levels. With respect to chromatic aberration, this eye model is able to reproduce only 1.1 D from the 2.1 D present on average in the human eye. When a retina with a radius of -12 mm is incorporated to the model, also provides reasonable estimations of the saggital and tangential power errors as well as astigmatism and field of curvature.

The modification of spherical aberration with accommodation has been also modeled. Navarro et al. developed a model, based on a modification of the Le Grand's schematic eye model, where the lens' geometrical parameters and placement depends on the accommodative state [Navarro et al. 1985]. This model is able to predict the decrease of spherical aberration in accommodated states. Escudero-Sanz developed a wide angle model simply by adding a spherical retina with a radius of -12mm [Escudero-Sanz and Navarro, 1999], which provides good off-axis predictions in comparison to experimental data.

Norrby [Norrby, 2005] developed ray tracing eye model by using the parameters defining the different ocular surfaces measured by corrected Scheimpflug technology [Dubbelman et al. 2001, 2002 and 2004]. Although it predicts correctly the decrease of spherical aberration with accommodation, the net spherical aberration values retrieved by the model were slightly negative with respect to those measured in the real eyes, becoming even more negative with age. This discrepancy might be solved by increasing slightly the measured conic constants and including the non significant dependence in aspheric terms found with age.

Although these eye models predict some of the average eye aberrations, such us spherical aberration and partially, chromatic aberration, their performance is limited, because also their inputs are limited. Ocular surfaces are restricted to rotational symmetry. However, it is well known that this is not the case. For example, the anterior cornea usually shows two different radii, being the cause of the corneal astigmatism. A more realistic modeling would therefore have a toric cornea.

Furthermore, individual eyes are not identical and because of that, its optical properties are also different. On average, only spherical aberration is different from zero, but population studies of aberrations have shown a large inter-subject variability. [Castejon-Monchón et al 2002 and Porter et al. 2001], being the aberration pattern specific for each individual. Therefore, the best scenario to model the eye is a complete customized eye description where individual measurements allow for a complete eye characterization. At this respect, the use of customized models has been proposed

[Tabernero et al. 2006 (b) and Rosales and Marcos, 2007]. They will be further described in the next chapter.

1.2. The pseudophakic eye

1.2.1. Cataracts and cataract surgery

A cataract is the opacification of the natural lens of the eye. This loss of transparency is caused by age, although there are some other causes, as traumatisms or some previous eye diseases. Although there are no studies showing prevention factors, it is widely accepted that diminishing UV exposure may delay cataract development [Chen, 1989].

Cataracts are clinical identified by slit lamp examination and graded by using the Lens Opacity Clasification Sytem III (LOCSIII) [Chylack et al. 1993]. Figure 1.11 shows the chart that is used to subjectively classify the degree of cataract. However, some objective procedures has been developed based on image analysis from slit lamp [Duncan et al. 1997] or Scheimplug images [Vivino et al. 1993], as well the analysis of the degradation of the retinal image quality from double pass images [Artal et al. 2011].

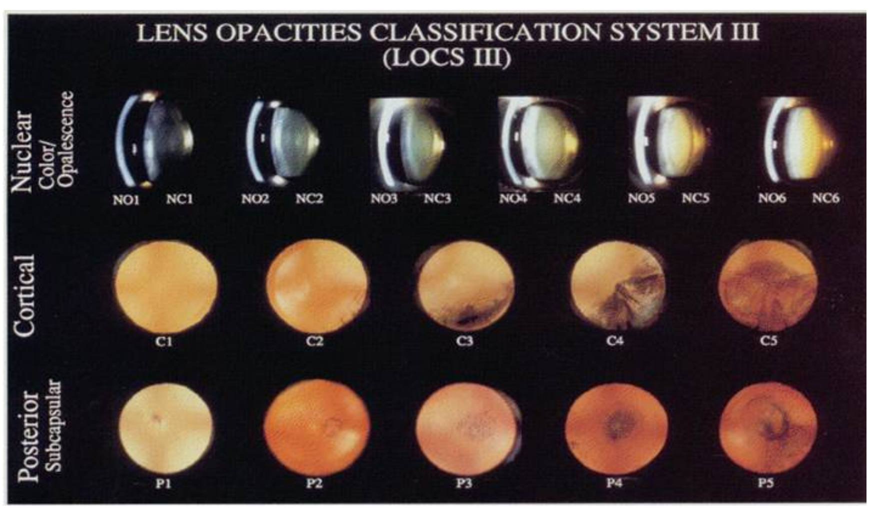

Figure1.11 LOCSIII card used to clarify the degree of cataracts

A cataratous lens causes glare and halos, resulting in vision impairments and, in the most extreme cases, blindness. According to the Word Heath Organization (WHO), age related cataract is responsible for 48% of world blindness, which represents about

18 million people. This is paradoxical due to the fact the solution of cataract is a simple and ambulatory surgery. Figure 1.12 presents the global surgical rates in 2004, showing that in developing countries cataract surgery is still not widely practiced.

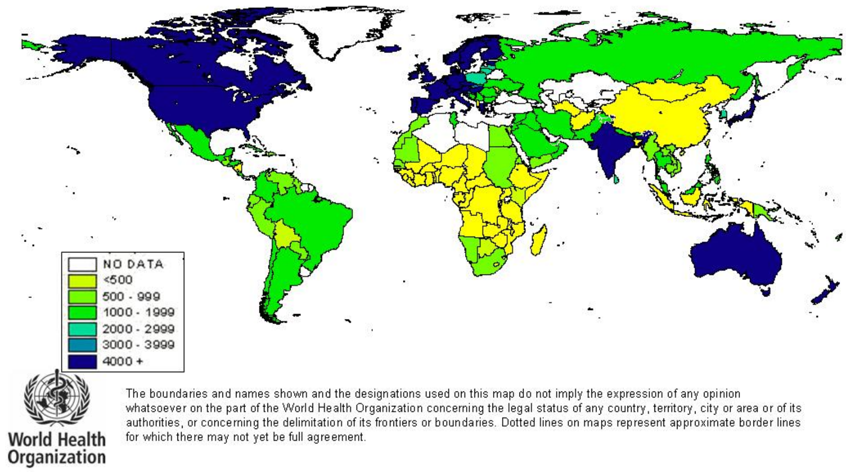

Figure 1.12. 2004 global cataract surgical rates.

The technique of couching, the traditional treatment for cataract, goes back to the Assyrian Code of King Hammurabi around 1700 BC and the Hindu surgeon Susruta around 700 BC. Couching was the only choice for treatment for more than three thousand years until the late 19th century. This traditional treatment is a mechanical dislocation of the lens usually performed with a sharp artifact (Figure 1.13) or by blunt manipulation [Schrader, 2004]. The use of this primitive technique has been shown as the responsible of endophtalmitis, uveitis and glaucoma. The potential problem related to the dislocated lens migration to the visual field was also an important point to consider.

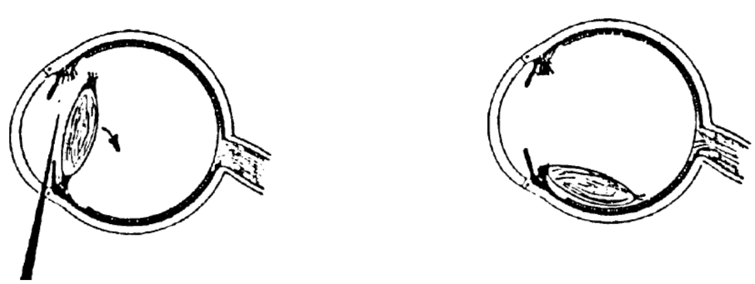

Figure 1.13 Couching procedure [Schrader, 2004].

The extraction of the cataract was shown as the solution to the drawbacks of couching. Although there are some references from the 10h century, when a bronze oral suction instrument was used, it was not until 1748, when Jaques Daviel successfully extracted a lens for the first time. Although the cloudy lens was removed, vision was not restored, due to the high residual hyperopia that resulted of the lens extraction. Sir Harold Ridley started what can be considered nowadays as the state of art in cataract surgery, when he implanted 1949 an artificial, prosthetic lens in place of the extracted lens, after seeing the absent of rejection when plastic pieces were inserted in pilot's eyes during the Second World War. The first IOL permanently implanted dates from 1950 (figure 1.14).

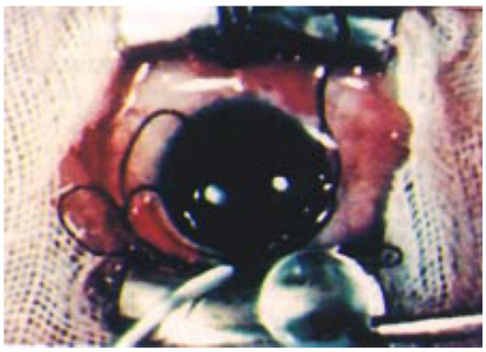

Figure 1.14 (a) Photograph extracted from an original film and subsequent video tape of Ridley's eighth IOL implantation, performed at St. Thomas' Hospital, May 8, 1951 [Apple and Sims, 1996] and (b) Plaque to Sir Harold Ridley in St Thomas' Hospital, where he implanted the first permanent IOL

Charles Kelman introduced in 1967 the phacoemulsification, a technique that breaks the cataratous lens by ultrasounds. Then, those small fragments in what the lens results are suctioned by a small incision. This is the reason that makes cataract surgery almost painless and ambulatory. Nowadays, cataract surgery is the most common eye surgery. The Organization for Economic Co-operation and Development (OECD) reported in 2010 a ratio of 756 surgeries per 100000 population in Europe on average, what means approximately 4 million cataracts procedures.

1.2.2. IOLs. Types and description

An IOL is an artificial lens used to replace the crystalline lens, that is usually placed inside of the bag through a small incision performed in the cornea (figure 1.15). Another type of IOL is that implanted in addition to the natural lens in order to correct for refractive errors, called phakic IOLs. However in this Thesis, when IOL is mentioned through the manuscript, it is referring to posterior chamber or in the bag IOLs.

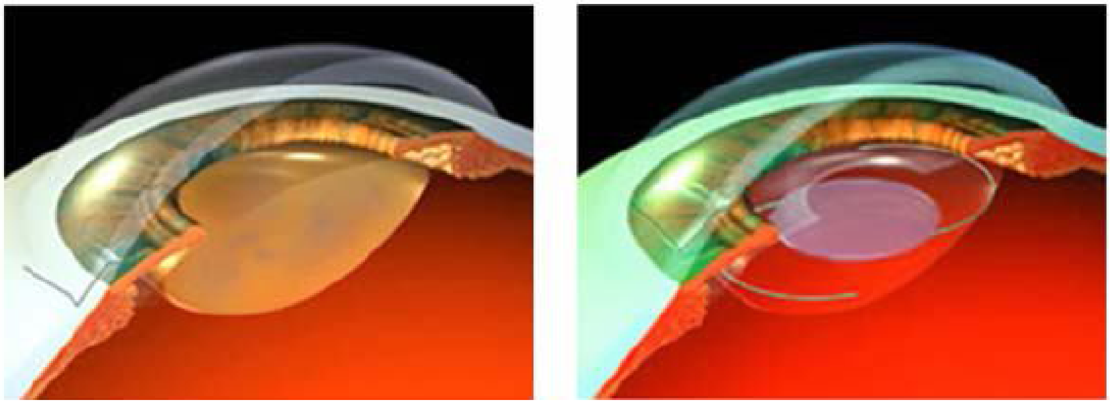

Figure 1.15 Natural condition and in the bag IOL placement in the eye.

The role of IOLs has been broadened since Ridley's first prototype. If the initial IOL objective was to add the needed power to the eye in order to compensate for the natural lens replacement, the idea of today's IOLs is to compensate for some other optical defects and therefore, improve as much as possible the overall ocular optical performance. Therefore, there are different types of IOLs depending on patient's needs. Standard IOLs are monofocal, providing one best focus position (Figure 1.16a). Toric IOLs to compensate for corneal astigmatism, have also been developed (Figure 1.16b). These IOLs have a low and high power meridian, whose power difference is the cylinder correction provided by the lens. In clinical practice, the IOL should be oriented with its low power meridian in a position determined by the corneal's steep meridian. Correct IOL orientation and rotation stability are the most important factors since one degree of misalignment with respect to the intended axis is related to a reduction of a 3.3% of the overall astigmatism correction, with a complete loss of the benefit when the IOL is rotated by 30 degrees [Bauer et al. 2008]. Clinical studies have shown an average rotation is of about 3 degrees [Bauer et al. 2008] and a mean rotation after implantation of about 0.23 degrees [Hoffmann et al. 2011]. Thus, toric IOL implantation has been shown as a safe a predictive method to manage corneal astigmatism.

Presbyopia correcting IOLs have been developed in order to provide additionally near vision and thus increase patient's spectacle independence. Multifocal IOLs have an added power to the base IOL power, which allows for having two simultaneous images at the retina. There are several strategies to achieve this objective. Diffractive IOLs (Figure 1.16c, left) incorporate a diffractive surface, whose step height and ring diameter are calculated in order to achieve a phase difference that generates different orders of diffraction. The first order creates an additional foci, used for near vision, to that provided by the lens geometry, which allows for far vision. Those parameters which characterize the profile define the light distribution between both foci as well as the add power to provide the near focus. Multifocal IOLs may also be refractive (Figure 1.16c, right). In this case, one of the surfaces of the IOL is divided into different zones of alternating refractive power. Therefore, those lenses have a different power depending on the zone where the light impinges its surface. The mayor drawback of multifocal IOLs, both diffractive and refractive, is the superimposition of the light coming from both near and far foci. Thus, when the patient is looking at a far object, the near focus is in front of the retina and then the corresponding image is defocused (Figure 1.17). The opposite behaviour has the far focus when looking at near object. The result of this superimposition is a halo, reducing the contrast of the retinal image.

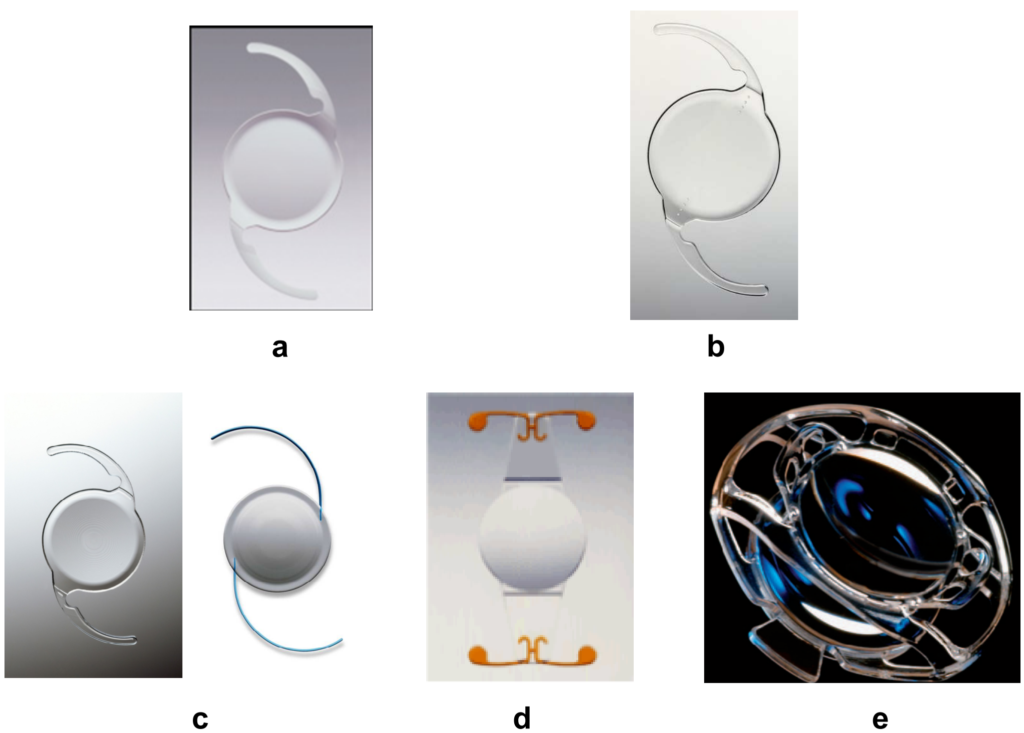

Figure 1.16 (Top) Monofocal IOLs: monofocal aspheric IOL (a), toric aspheric IOL (b). (Bottom) Presbyopia correcting IOLs: Multifocal IOLs, both diffractive (left) and refractive (right) (c), single optic accommodating IOL (d) and dual optic accommodating IOL (e).

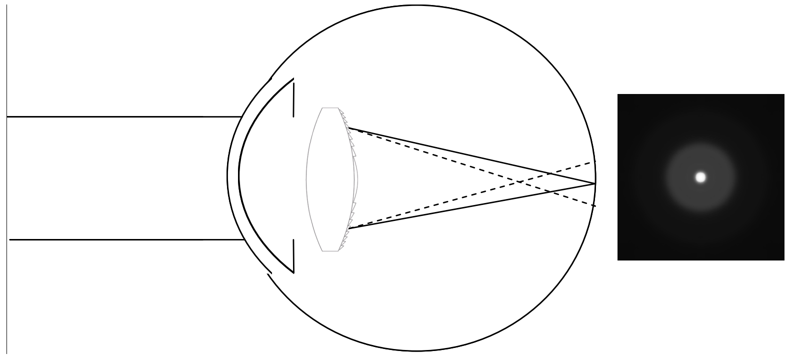

Figure 1.17 Schematic view of an eye implanted with a multifocal IOL. The defocus image corresponding to the near focus when looking at far generates the halo.

The ideal scenario to avoid this problem would be an IOL with similar accommodative capabilities as the natural lens. It is well accepted that presbyopia is mostly due to lens stiffness [Glasser and Campbell, 1999]. Therefore, the cilliary muscle is probably able to drive a more elastic artificial lens. Different simplified options have been proposed under the name of accommodating IOLs. Those IOLs with a unique optic that may enhance near vision by moving forward (Figure 1.18a) can be considered as one category, usually referred as single accommodating IOLs. The AT-45 Crystalens (Bauch&Lomb) (Figure 1.16d) is the most relevant example because it is until data the only accommodating IOL approved by the US Food and Drug Administration (FDA) and therefore, the only lens that can be commercialized as accommodative lens in the United States. In spite of good far and near clinical performance [Cumming et al. 2001], there are evidences showing a backward movement [Menapace at al. 2007] contrary to its theoretical operating principle. Some other factors further than the accommodative response have been proposed in order to explain these favorable clinical results, as the senile miosis [Nakazawa and Ohtsuki, 1984] or a particular shape of the IOL that might enhance the corneal aberrations leading to a extended depth of focus [Oshika et al. 2002]. Another approach to use ciliary body forces, are dual optic IOLs. In this case, the Synchrony (Abbott Medical Optics, Santa Ana, CA) might be one representative (Figure 1.16e). This IOL is composed by a posterior stationary optic with a negative power which depends on patient's biometry. The anterior +32 D optic is the responsible of moving and therefore, of achieving different foci (Figure 1.18b). It has been shown that the theoretical change of power due to the dual optics is double than that achieved by a single IOL for the same axial displacement [Menapace et al. 2007]. Ray tracing analysis reveals that in the case of the single optics the power change depends strongly on the

IOL base power, while the dual optic provides more stable accommodation range through the base IOL power range (Figure 1.18c) [McLeod et al. 2007]. This IOL is actually implanted in European countries as well as some other nations and it is under FDA approval for US commercialization.

Lens refilling is another interesting approach based on inserting an elastic material mimicking the natural lens. The proper polymer refractive index, in order to achieve emmetropia, and the development of new cataracts in the refilled material are factors that need to be further investigated to make this solution feasible [Glasser, 2008].

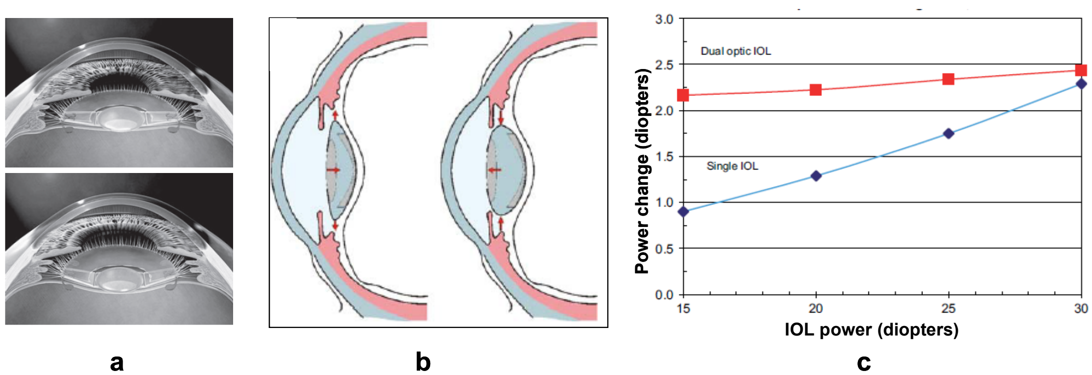

Figure 1.18. AT-45 Crystalens accommodated (a, top) and unaccomodated states (a, bottom) [Glasser 2008], Synchony relaxed (b, left) and accommodated (b, right) [Menapace et al. 2007] and increased power for 1 mm displacement in dual versus single optic IOL for different IOL powers (c) [McLeod et al. 2007].

The success in providing spectacle independence of all approaches to restore visual performance described until now is based on the correct IOL power calculation prior to the surgery. This is in fact challenging, as will be discussed next in this chapter. Light Adjustable Lenses (LAL) developed by Calhoun Inc area a different approach. LALs are similar to standard 3-piece lenses, but contain photosensitive molecules that enable postoperative adjustment of the final refractive power using safe levels of ultraviolet light of 365 nm [Schwartz, 2003]. The principle of this technique is shown in Figure 1.19. When UV light is used to irradiate the lens with a specific spatial profile determined by a prior refraction, the macromers in that area are polymerized. The diffusion of the material produces a change in the lens radius and therefore, in its optical power. Once the desired power change is achieved, the entire lens is irradiated to polymerize all the remaining macromers to prevent future changes in the lens power, in a process called “lock-in”.

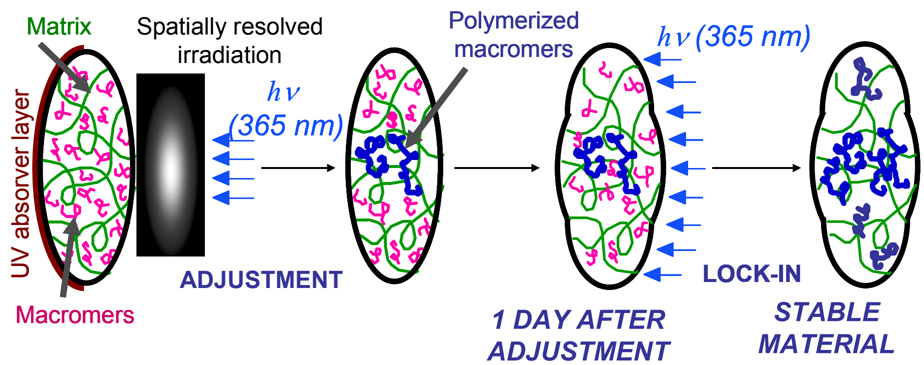

Figure 1.19. LAL Adjustment procedure.

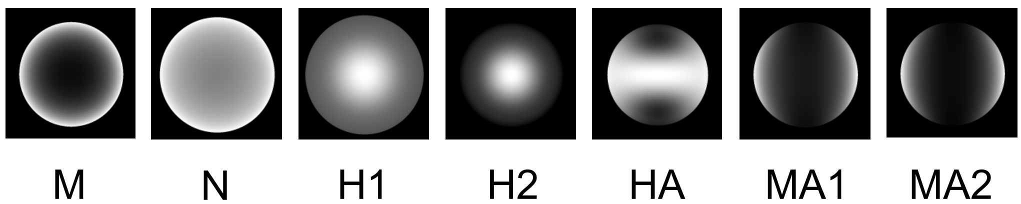

Figure 1.20. Different light profiles for light treatment in the LALs. From left to right: Myopic (M), neutral (N), hyperopic of different power (H1, H2) and different toric treatments combined with sphere (HA, MA1 and MA2).

In clinical practice, the complete procedure for adjusting and blocking the LAL is what follows: the IOL is implanted in a conventional surgical procedure using a 3.5 mm average corneal incision. Two weeks after the surgery, the first treatment is applied based on a prior refraction. Two days after the first adjustment, an additional treatment may be performed, if the refraction target is not achieved. Otherwise, the first lock-in is directly performed. Two days after the first lock-in, a second lock-in is applied in order to avoid undesired changes after the treatments. Patients must wear UV blocking glasses until the last lock-in to avoid the effect of spurious UV light that could affect the LAL state. Figure 1.20 shows different intensity profiles that may be applied in order to correct for either sphere (M, H1 and H2) or sphere and astigmatism (HA, MA1 or MA2). In addition, a neutral (N) treatment was included for patients who don't require a change in refraction. Related to the maximum change in optical power, it has been shown that the LAL can achieve a posterior adjustment of about 2D both for sphere and cylinder, either in vitro [Schwartz, 2004] or in vivo [von Mohrenfels et al. 2010]. In vivo studies have also proved the stability in the induction of either sphere or cylinder [Lichtinger et al. 2011], providing a predictive refraction after cataract surgery. It is also important to note that further than low order aberrations, it has been postulated that this lens has the ability to modify also higher order aberrations [Sandstedt et al. 2006].

1.2.3. Optical quality of IOLs and the pseudophakic eye

One of the aims of cataract surgery, together with providing spectacle independence, is to improve the patient´s optical performance by correcting some corneal aberrations. We are able to start to achieve this objective due to the fact that corneal topography allows us to gain better knowledge of the human cornea [Guirao and Artal, 2000]. Several years ago, it was shown that intraocular lenses with excellent optical quality as measured in an optical bench [Norrby, 1995a] produced lower than expected optical performance when they were implanted in normal eyes. Different measurements supported this result, when the MTF for subjects implanted with IOLs was measured by using a double pass instrument [Navarro et al. 1993, Artal et al. 1995]. The average MTF measured for old phakic subjects was similar to that measured in pseudophakic patients implanted with monofocal lenses. These values were significantly lower than those measured in the young eye. This apparent paradox was solved when corneal topography showed that corneal spherical aberration remains stable while total eye's spherical aberration increases with age [Artal et al. 2002]. This suggested a compensation mechanism between the cornea and the lens in the young eye which is disrupted with age. To further emphasize this finding, it was found that lens spherical aberration increases with age, as supported by in vitro measurements, which showed that the spherical aberration of the natural lens changes from negative to positive [Glasser et al. 1998]. When all these results are considered together, the best approach is not to have an IOL with positive, or even without spherical aberration. The idea is to mimic the amount of spherical aberration of young the lens which compensates for the positive spherical aberration introduced by the cornea (Figure 1.21) [Guirao et al. 2002]. From this result, new aspheric IOL designs correcting corneal spherical aberration were developed [Holladay et al. 2002 and Artal, 2009]. When implanted, an average zero ocular spherical aberration was measured in comparison to the positive spherical aberration yielded by conventional spherical IOLs [Mester et al. 2003], clinically validating this lens. Aspheric IOLs are nowadays available (Figures 1.16 a,b and c) showing a superior visual outcomes in cataract patients [Packer et al. 2002, Bellucci et al. 2005]. This proved that corneal aberrations should be taken into account in order to improve optical performance in cataract patients. On the other hand, spherical aberration is not the only corneal aberration that impacts visual performance. A new optical design has been proposed in order to compensate also corneal coma [Tabernero et al. 2007].

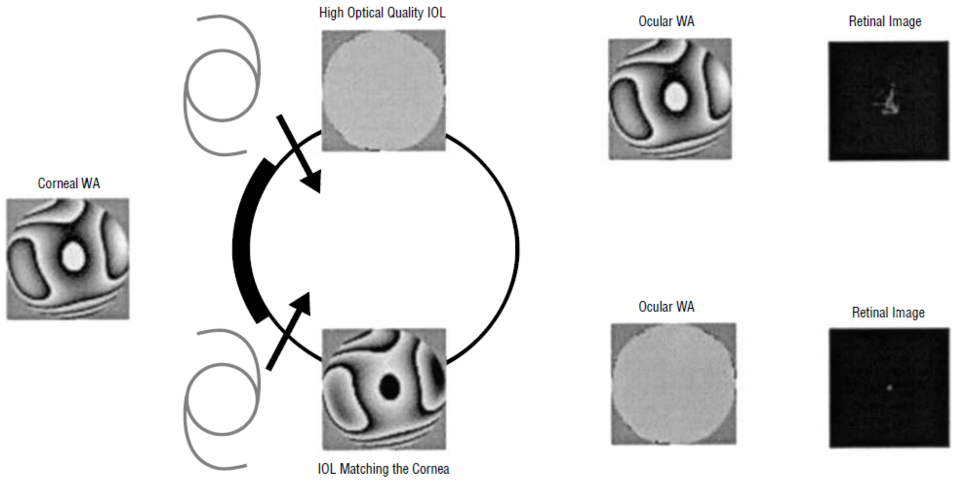

Figure 1.21 The best IOL design is not a lens with a perfect isolated optical performance but such lens that contains the opposite to the corneal aberrations [Guirao et al. 2002].

Other factors may also affect the optical quality of the pseudophakic eye. Because an aspheric lens has a net value of spherical aberration, the impact of misplacements, as tilt and decentration, should also be considered due the induction of undesired non symmetric aberrations. Clinical studies reported typical values of about 0.3 mm and 3˚ for decentration and tilt, respectively [Mutlu et al. 1998 and Mester et al. 2009]. These amounts of misplacements are not enough to produce a significant reduction in the optical quality of the pseudophakic eye with an aspheric lens to those levels related with spherical lens implantation [Piers et al. 2007]. The maximum IOL decentration and tilt in which an eye with an aspheric IOLs presents lower optical quality than implanted with spherical lenses were 0.8 mm and 10˚, respectively [Piers et al. 2007]. Therefore, under clinically realistic conditions of tilt and decentration, eyes implanted with aspheric IOLs have superior optical behaviour than those implanted with spherical IOLs.

Another important factor in the pseudophakic eye is chromatic aberration. Figure 1.22 shows the chromatic difference of refraction as a function of the wavelength in the visible spectrum (longitudinal chromatic aberration) for eyes implanted with IOLs having different Abbe numbers [Zhao and Mainster, 2007]. The Abbe numbers for IOL materials range between 35 and 60. The chromatic aberration for the phakic eye is also shown at the figure as a reference (dashed line). An eye implanted with an IOL with an Abbe number of about 50 resembles the chromatic aberration of the phakic eye. Adaptive optics served to proof that the combined correction of monochromatic aberrations when chromatic aberration is avoided improved contrast sensitivity with respect to the uncorrected case [Yoon and Williams, 2003]. It has been recently reported that a combined correction of spherical aberration and longitudinal chromatic aberration provided an improved visual performance, mainly a better contrast sensitivity, than either the uncorrected condition or the case when only spherical aberration was compensated [Artal et al. 2011]. Naturally following this, an aspheric monofocal diffractive lens that compensates for corneal spherical aberration and the chromatic aberration of the aphakic eye as well as for that related to the IOL material has been also proposed. A theoretical study showed the benefit of such correcting device in presence of corneal higher order aberrations and realistic conditions of tilt and decentration [Weeber and Piers, 2012].

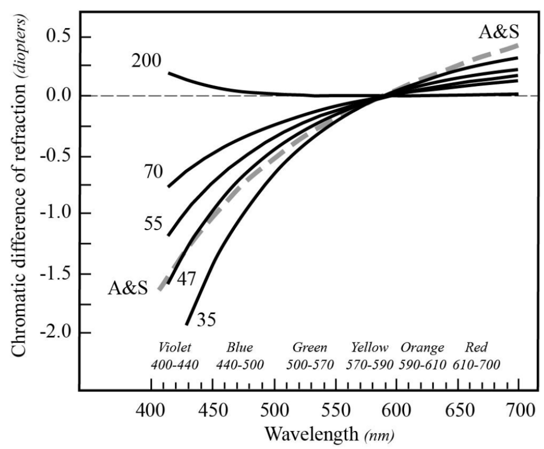

Figure 1.22 Chromatic difference of refraction for pseudophakic eyes implanted with IOLs having different Abbe numbers compared to the chromatic aberration for the average phakic eye [Zhao and Mainster, 2007].

Other factors are related with the surgery itself. The corneal incision, performed to remove the fragments of the cataratous lens and to implant the IOL, modifies the corneal shape and the amount and type of corneal aberrations. The most widely reported effect is the surgically induced astigmatism (SIA). It depends on the incision size, orientation and type of incision, ranging from 0.3 D to 0.7 D on average [Kohnen et al. 1995, Masket and Tennen 1996, Masket et al. 2009, Tong et al. 2008, Hayashi et al. 2009]. In fact, SIA is considered to select the cylinder power when a toric IOL is implanted [Hill, 2008]. In addition to astigmatism, some other aberrations can result from the cataract incision. The induction is related to non rotationally symmetric aberrations, mainly at the incision's orientation [Guirao et al. 2004]. It would be therefore desirable to be able predict and quantify the impact of these induction in the optical quality of the pseudophakic eye.

1.2.4. **IOL power calculation review**

The selection of the appropriate power of intraocular lenses (IOL) remains a challenge in cataract surgery [Dupps, 2000]. The initial approach was to implant a fixed IOL power. In the Gullstrand eye model the crystalline lens has a power of about 19 D. A clinical study showed that the average refraction when such fixed IOL power was implanted was -0.76±2.13 D, with 5% of the patients presenting a residual refraction higher than 5 D [Olsen, 1988]. Therefore, in spite of an acceptable average residual refraction, the need of a proper algorithm to calculate the personalized IOL power is evident.

Although apparently IOL power calculation from biometric data is a simple problem from a theoretical point of view, it becomes complicated when is applied in some type of patients [Haigis et al. 2009], especially in those that have undergone a previous refractive surgery [Hoffer et al. 1995]. The inaccuracy in the calculation affects specially the new types of IOLs with the potential of correcting different aberrations [Holladay et al. 2002, Tabernero et al. 2007] due to the fact that errors in defocus larger than 0.5 D may reduce the potential visual benefit of correcting high order aberrations [Tabernero et al. 2006 (b)].

In the next section, most common IOL power calculation techniques used nowadays will be reviewed when applied both for normal and post-LASIK patients.

1.2.4.1. IOL power calculation for normal patients

Different approaches have been considered for IOL power calculation since Sir Harold Ridley implanted the first IOL. It is curious to mention that this first cataract patient presented a residual refraction of -14 D. The main reason was the IOL design. Although Ridley copied the geometrical properties of the crystalline lens, he did not account for the difference in refractive index between the natural lens and the IOL material [Apple and Sims, 1996]. After this, appropriate modifications of the IOL power were made, resulting in a subsequent residual error of about one diopter, that was considered as acceptable by that time.

Before 1975, the IOL power was calculated based on the clinical history [Shammas, 2004]:

$$P = 18 + 1.25 * R \qquad [1.7]$$

where R is the preoperative refractive error, prior the development of the cataract. By using this formula, 50% of the eyes had a residual error higher than 1 D. Since then, a catalogue of formulas has been developed, although almost every IOL power calculation can be defined as a theoretical or a regression formula or a combination of both.

The paraxial formula which is the base of most of the IOL power calculations procedures can be easily deduced. When the IOL is considered as a thin lens, its power is retrieved by:

$$P = \frac{n}{S_L'} - \frac{n}{S_L} \qquad [1.8]$$

where n is the refractive index of the media in what the IOL is placed (by simplicity, the same refractive index is considered for the anterior and posterior segment) and S_L and S_L' are respectively the position of the object and the image position that the IOL retrieves. The situation at the eye is schematically shown in figure 1.23.

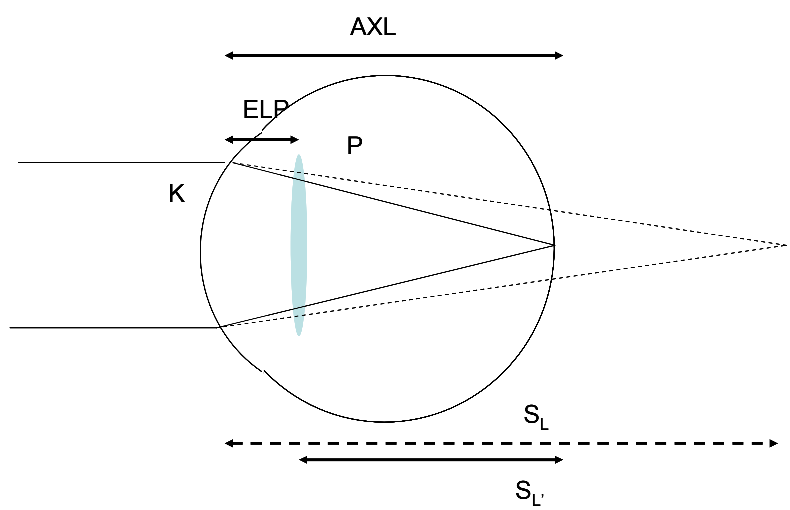

Figure 1.23 Schematic view of the parameters involved in the paraxial formula for IOL power calculation

To be focused at the retina, the image (S_L') is placed from the IOL at a distance corresponding to the difference between the axial length of the eye (AXL in the schema) and the thin IOL position or effective lens position (ELP). Regarding the IOL's object, this is the image that the cornea forms for objects placed at an infinite distance of the eye. This is the focal length of the cornea, that should be referred to the IOL position in order to be introduced at [1.8]. Therefore, the object position with respect to the IOL (S_L) is the focal length of the cornea minus the distance between the cornea and the IOL, that is, the effective lens position (ELP). Because the cornea is considered as a unique refractive surface, its focal length is n/K, where n is the refractive index of the image space of the cornea, which is the same as the media in which the IOL is placed, and K the power of the cornea. When all this is considered together, the power of the thin IOL under paraxial approximation is:

$$P = \frac{n}{AXL - ELP} - \frac{n}{\frac{n}{K} - ELP} \qquad [1.9]$$

To keep the IOL power in dioptres, all dimensional parameters, as ELP or AXL should be introduced in meters. A small modification can be made at [1.9] to calculate the IOL power to produce a desired refraction R at the spectacle plane. In that case, such refraction, translated to the corneal plane by considering the vertex distance (d), should be added to the corneal power K, yielding to:

$$P = \frac{n}{AXL - ELP} - \frac{n}{\dfrac{n}{K + \dfrac{R}{1 - Rd}} - ELP} \qquad [1.9b]$$

Equation [1.9] or its variant [1.9b] is at the basis of all original theoretical formulas [Colenbrander, 1973, Fyodorov and Kolinko, 1967 and Fyodorov et al. 1975, van der Heijde, 1976, Binkhorst, 1979]. All these formulas are almost identical in spite of small correction factors. For example, an overall increase of 0.05 mm to the ELP is introduced at the Colenbrander formula (Figure 1.24) in order to take into account that the principal plane of the cornea is in front of the anterior corneal vertex according the Gullstrand eye model [Colenbrander 1973]. However, such correction was not shown as clinically relevant [Retzlaff, 1980]. Another modification to equation [1.9] used the corneal radius instead of the corneal power reading, with the incorporation of 1.333 as equivalent refractive index to convert such radius to power [Binkhorst, 1979]. Because most of the keratometers were using 1.3375 as keratometric index, the IOL power predicted by Binkhorst differed about 0.5 D from the power calculated from the rest of formulas [Shammas, 2004]. In general, a correction factor to the axial length ranging from 0.25 mm to 0.5 mm was also introduced, depending on the formula. The reason for that correction was that the ultrasound devices used for measuring the AXL retrieved the distance between the corneal surface and the vitreoretinal interface, not to the photoreceptor layer.

$$, F_L = \frac{n_1}{l - v - 0{\cdot}00005} - \frac{n_1}{\frac{n_1}{F_C} - v - 0{\cdot}00005}$$

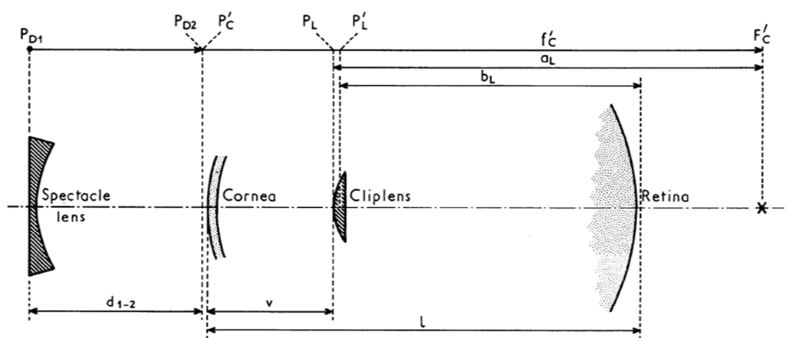

Figure 1.24 Schematic view of the parameters involved at the IOL power calculation from the Colenbrander's original paper, together to his formula [Colenbrander, 1973]. F_L and F_C represent the IOL and corneal power respectively, while l is the AXL and v the ELP.

Retzlaff presented a comparison between the outcomes of the different theoretical formulas up to that date for 176 implantations [Retzlaff, 1980]. In all the formulas and all the subjects, the ELP was considered as 3.46 mm. The standard deviation of the predicted IOL power error was similar between all the theoretical formulas, with a value of 1.5 D for the Fyodorov [Fyodorov and Kolinko, 1967 and Fyodorov et al. 1975] and Colenbrander formula [Colenbrander, 1973] and 1.7 D for the Binkhorst [Binkhorst, 1979]. In all the cases, the range of IOL power error, defined as the difference in between the most hyperopic and the most myopic IOL power error, was of about 9D.

In an attempt to offer an alternative to the low accuracy provided by the equation [1.9], regression analysis was proposed. For the same population as described before, a simple linear regression formula provided a standard IOL power calculation error of 1.3D with a range of 7.7 D. In order to generate such formula, different presurgery measurements were correlated with the IOL power generating emmetropia after surgery. The first general regression formula was the SRK I [Sanders and Kraff, 1980]:

$$P=A-2.5*AXL-0.9*K \qquad [1.10]$$

where P is the IOL power, AXL the axial length of the eye in mm, K the averaged corneal power in diopters and A is a constant which depends on the IOL model chosen for the surgery. This first regression formula did not result accurate for the whole axial length range. Because of that, some years later the SRK II formula was proposed [Sanders et al. 1988], with a correction of the IOL power dependent on the patient's axial length:

$$P=\{A-2.5*AXL-0.9*K\}+F \qquad [1.11]$$

where the portion of the formula between brackets is the same as [1.10], that is, the SRK I formula, and F is a correction factor which depends on the patient's axial length:

F (D)	AXL range (mm)
-0.5	>24.5
0	[22,24.5]
+1	[21,21.9]
+2	[20,20.9]
+3	<20

Table 1.3 Axial length's dependent SRK II correction factor

Although, these formulas are rarely used nowadays in the clinical practice, the A constant established by them is the base of the modern IOL power calculation formulas in combination to thin lens theory, that is, equation [1.9] with improved methods to predict the ELP.

A second generation of theoretical formulas arose around the same time [Hoffer, 1981 and Shammas, 1982]. The AXL was considered to predict the ELP, which until that moment, had been kept constant in all theoretical formulas. Thus, the ELP was deeper in long eyes than in shorter. The results of these formulas and the previously mentioned SRK II were similar in accuracy [Sanders et al. 1988].

The term modern formulas was adopted to group those which are using the corneal curvature, in addition to the AXL, to predict the ELP [Shammas, 2004]. These are also called third generation formulas. The first modern IOL power calculation formula was the Holladay 1 [Holladay et al. 1988]. It is based on the Binkhorst formula [Binkhorst, 1975] and incorporates an algorithm to predict the ELP as the sum of the anatomical ACD and a constant factor, termed as “Surgeon Factor” (SF) (Figure 1.25). The anatomical ACD (aACD) was defined as the distance between the corneal vertex to the anterior iris plane. In order to estimate this value Holladay considers a method similar to that proposed by Fyodorov [Fyodorov et al. 1975], where the corneal height is defined as the height of a spherical segment, with radius is equal to the corneal radius and transversal diameter corresponding to the external corneal diameter. The latest is considered to be proportional to the AXL value, introducing a correction factor for extreme AXL. Finally, a constant value of 0.56mm is added to account for the corneal thickness. The complete ELP is calculated in the Holladay 1 formula by adding a constant, the SF, to that previously defined aACD. This constant depends on the IOL model and biometric technique and should be optimized for every surgeon in order to achieve the optimum outcomes. The optimization is performed by solving the formula for a large number of patients.

In order to provide a theoretical formula to the SRK umbrella, Retzlaff et al developed the SRK/T (SRK/theoretical) formula [Retzlaff et al. 1990]. The formula [1.9] gives the theoretical basis, while different regression factors were developed in order to account for the ELP prediction. The corneal height concept was adopted from Holladay’s approach, although the constant used in this case was the A constant, consistently with the rest of formulas developed by the same authors, which is transformed to generate an offset similar to that related by the Holladay’s SF. Different other regressions were added to the formula, as the determination of the corneal diameter from corrected axial lengths and from the corneal power.

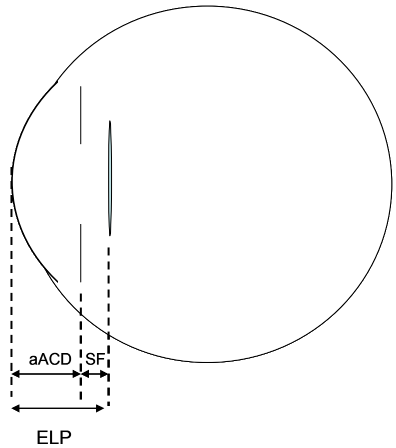

Figure 1.25 At the Holladay 1 formula the ELP is defined as the anatomical ACD (aACD), which is the distance from the cornea to the anterior iris plane, and the surgeon factor (SF), a constant distance from that position to the IOL plane

The Hoffer Q formula is also based on equation [1.9]. The main difference between this and the previous formulas is that the ELP prediction is not based on the corneal height concept [Hoffer, 1993]. Contrary, the ELP is calculated from an axial length factor, which is linear with the axial length, a corneal power factor, which is related to the quadratic tangent of the corneal power, a correction factor for extreme axial lengths and constant, the pACD, that in the same way as the SF, should be further personalized.

More recently, the Haigis formula, which is also based on equation [1.9], considers three different constants that relate linearly the ELP with the AXL and the preoperative anterior chamber depth (ACD) [Haigis, 2004]:

$$\mathrm{ELP} = a_0 + a_1\mathrm{ACD} + a_2\mathrm{AXL} \qquad [1.12]$$

The three constants at the Haigis formula may also be optimized, although it has been found that a fixed value of a_1=0.4 and a_2=0.1 can be used [Haigis, 2004]. It has been reported that when only the a0 constant is optimized, the results provided by this formula and the rest of modern formulas are similar. However, the triple optimization generates extra accuracy, although a number of cases between 500 and 1000 is needed to achieve such optimization [Hoffer, 2011a].

The Holladay 2 formula uses even more parameters, as the measured external corneal diameter (clinically called, white to white), lens thickness, age or preoperative refraction. However, this formula has never been published, residing in the Holladay IOL Consultant software.

All previously described modern formulas, although based on optical theory, contain several approximations and assumptions. One of them is the introduction of the corneal power. Keratometers or corneal topographers measure the front corneal radius, but in order to provide a correct estimation of the total corneal power, the posterior corneal power should also be considered. An equivalent refractive index (ERI) has been developed to overcome this problem. There are several values adopted for this ERI, depending on the topographer or keratometer used, ranging from 1.3375 to 1.332. Therefore, a corneal radius of 7.7mm would be translated to 43.83D or 43.12D, depending on the ERI used. Olsen, by considering the cornea as a thick lens as well as the Gullstrand's ratio between anterior and posterior cornea, calculated 1.3315 as equivalent refractive index [Olsen, 1986]. Nevertheless, because the ERI has been usually considered as 1.3375, it is straightforward to conclude that it overestimates the corneal power. This overestimation depends on the anterior corneal radius and it is of about 0.8D for the cornea of the Gullstrand eye model. The difference is even greater if the ratio between posterior and anterior corneal radius is lower than in the mentioned model [Dubbelman et al. 2006]. In addition to the inaccuracy on the corneal power determination, there are some other factors that cannot be addressed by IOL power calculation formulas, as the spherical aberration at both the lens and the cornea.

IOL power calculation formulas deal with these assumptions by optimizing the IOL constants and therefore, changing the IOL position. Equation [1.9] predicts that the more anterior the IOL position, the lower the IOL power, while if the IOL is placed more posteriorly, the higher IOL power calculated. Those formulas which include corneal power by using 1.3375 as refractive index should shift posteriorly the ELP to account for the overestimated corneal power. The IOL spherical aberration can also be included in the IOL constant. A practical example are the Ceeon 911A and the Tecnis Z9000 IOL models (Abbott Medical Optics, Santa Ana, CA). They have same paraxial properties, with the only difference that the latter is an aspheric lens. The A constant differs from 118.3 for the spheric lens to 119.0 for the aspheric version. Therefore, considering an average eye the ELP for the aspheric lens is more posterior than that related to a spheric lens and the power calculated for the aspheric IOL results higher than the corresponding spherical lens [Norrby, 2011]. Thus, the ELP cannot be considered as the anatomical position of the IOL after the surgery or the principal plane of the IOL, since it is an artificial position that retrieves the correct IOL power under the assumptions contained at the formula [Norrby, 2008].

All the systematic errors that might impact the residual refractive error predicted by the formula and the surgical technique or the biometric device are overcame by the IOL constant optimization. Therefore, the average improvement of results is in the basis of this optimization procedure. And because of that, IOL power calculation incorporating this principle cannot be accurate in all possible eye's configuration, but in the most common or average, since the optimization process can only correct for systematic errors. An example of the effect of the IOL optimization is shown at figure 1.26, which corresponds to a retrospective clinical study involving more than 6000 eyes [Aristodemou et al. 2011]. The residual spherical equivalent (SE) prediction error is defined as the difference between the actual spherical equivalent and that predicted by the IOL power calculation formula. At the figure, the residual prediction SE is shown both when the IOL power calculation formula is applied using the IOL constants provided by the manufacturer and for optimized constants. While the IOL constants provided by the manufacturer retrieve a systematic hyperopic refractive error, this average error is corrected when the optimized constants are considered for the prediction. However, the optimization process was not able to reduce the spread of the values, which is the error at the individual level.

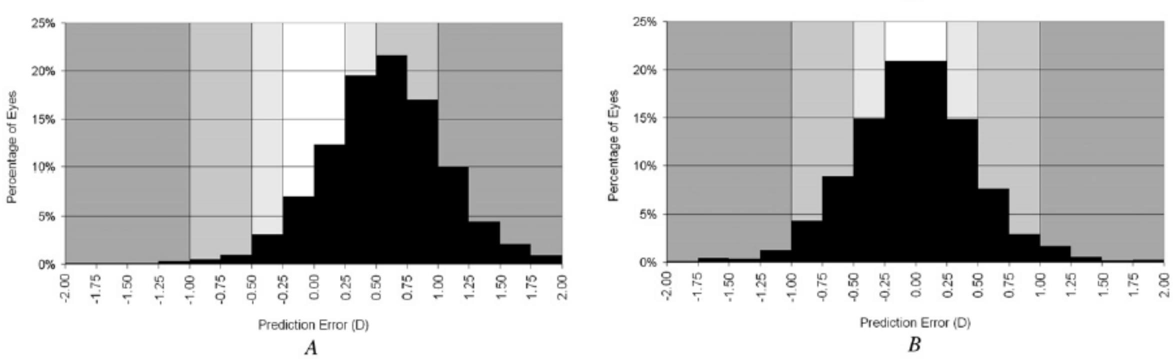

Figure 1.26. Residual SE prediction error for a large number of patients with the IOL constant provided by the manufacturer (a) and with an optimized constant (b) [Aristodemou et al. 2011].

Furthermore, due to the use of a different ELP prediction algorithm, not all formulas present the same accuracy for the whole AXL range. Table 1.4 shows the mean absolute error for the formulas providing the least mean absolute error (MAE) for different range of axial lengths when optimized constants are used [Hoffer, 2000]. It is possible to observe that a different formula has to be chosen in order to retrieve the best performance, that is also different related to axial length range. Therefore, the combination between the paraxial treatment and the regression analysis is far from retrieving a unique formula valid for all eye's configurations.

Axial Length	Number of Eyes	Formula	MAE (D)	SD (D)	MAX (D)	Pers ACD	SD
Short	10	Hoffer Q	0.72	0.29	1.08	6.17	0.05
		Holladay 2	0.72	0.40	1.07	6.20	0.08
Average	231	Holladay 1	0.42	0.49	−1.44	5.63	0.02
		Hoffer Q	0.43	0.50	−1.61	5.67	0.02
Medium long	52	SRK/T	0.35	0.40	−1.06	5.64	0.05
		Holladay 1	0.37	0.43	−1.18	5.59	0.06
Very long	24	SRK/T	0.44	0.56	1.10	5.93	0.17
All long	76	SRK/T	0.38	0.47	1.10	5.73	0.07

Table 1.4. Mean absolute error for those formulas retrieving the least MAE by axial length range [Hoffer, 2000]. In this study, the Holladay 1, Holladay 2, Hoffer Q and SRK/T were evaluated.

Other authors have attempted to overcome the limitations of previously described IOL power calculation formulas, which represent the current state of art. Olsen developed a formula based on paraxial thick lens theory [Olsen, 2004]. Because of that the position of the IOL is not the ELP, but the exact IOL placement in the eye. Therefore, an accurate estimation of that parameter was needed. In order to answer this question, Olsen back calculated the effective ACD achieving the postoperative refraction with his formula in 6698 cases [Olsen, 2006]. The results were then fitted by multiple linear regression to different biometric parameters in order to generate the prediction. The position of the IOL was estimated by means of 5 biometric parameters:

$$ACD = ACD_{const} - 1.04 + 0.19AXL + 0.49ACD + 0.28LT - 0.81R + 0.028R_x \quad [1.13]$$

where ACD_{const} is a constant value, representing average distance between the corneal surface and the IOL surface in a representative patient sample, AXL the patient's axial length, ACD the preoperative anterior chamber depth, LT the lens thickness, R the average corneal radius and R_x the preoperative refraction [Olsen, 2006]. In a further development, the axial length measured with partial coherence interferometry was corrected to compensate for its calibration against the inmersion ultrasound [Olsen and Thorwest, 2005]. The axial length measurement as well as the inherent approximations to that method will be further discussed in the next chapter. When this is combined to the Olsen formula, it retrieves results similar to the Haigis formula and also similar to those presented in table 1.3 [Hoffer, 2000]..

Norrby also presented a paraxial ray tracing IOL power calculation procedure that could be programmed in an Excel spread-sheet [Norrby, 2004]. His approach, based on forward ray tracing, included a spectacle, the cornea and the IOL. The focus criterion is that the ray height at the retina should be zero. For that purpose, the radius of the anterior spectacle surface can be modified, giving therefore, the corresponding refraction. All lenses are considered as thick lenses. Inputs for the calculation are the mean corneal anterior radius and the AXL. The posterior corneal radius is calculated from the Gullstrand ratio between the anterior and posterior corneal radius (7.7/6.8mm), as well as the corneal thickness and refractive indexes of the different ocular media, which are also taken from the same model. The geometrical and optical IOL parameters were facilitated by the manufacturer. The IOL position was calculated according a previous author's concept, the combination of lens haptic plane (LHP) and the compressed vault height (CVH) [Norrby, 1995b]. The LHP was defined as the plane where the IOL haptics make contact with the ocular tissue. This value was supposed to be only dependent on the eye's anatomy. In fact, it was predicted by multiple linear regression in a posterior study, showing a significant relation with the AXL and corneal radius [Norrby et al. 2005]. The dependency of the IOL model at the IOL position is given by a constant value, the CVH, which is specific for every IOL model [Norrby, 2004]. When this paraxial ray tracing was clinically applied, the results were not statistically significant to those provided by standard IOL power calculation formulas [Norrby et al. 2005]. However, these procedures were a step forward because there are no parameters to be adjusted when thick lens treatment is applied, contrary to the IOL formulas, that adjust for systematic errors with the IOL constant. However, the paraxial nature of both approaches does not consider corneal and IOL aberrations

Preussner [Preussner et al. 2002] proposed the use of exact ray tracing for IOL power calculation. His procedure is based on backward ray tracing, where rays travel from the retina to the cornea. To fine tune the result, a visual impression may be generated by blurred Landolt rings superimposed at the retina. A large clinical study using this exact ray tracing procedure with a fixed corneal excentricity showed similar results to that provided by modern IOL power calculation formulas [Preussner et al. 2008].

An analysis of all the errors affecting IOL power calculation was performed considering a ray tracing procedure [Norrby, 2008]. Figure 1.27 shows the impact of different biometric parameters in final refraction error. The prediction of the actual lens position was the highest contributor of the error in IOL power calculation, followed by the accuracy at the refraction procedure and the AXL determination. The accuracy of the AXL determination was related to ultrasound biometry in contact mode, which is less precise than the measurement provided by optical biometry, as will be discussed in chapter 3. However, a different study of the sources of errors in IOL power calculation which used optical biometry still showed axial length measurement as the second contributor in the IOL power prediction error [Olsen, 2007].

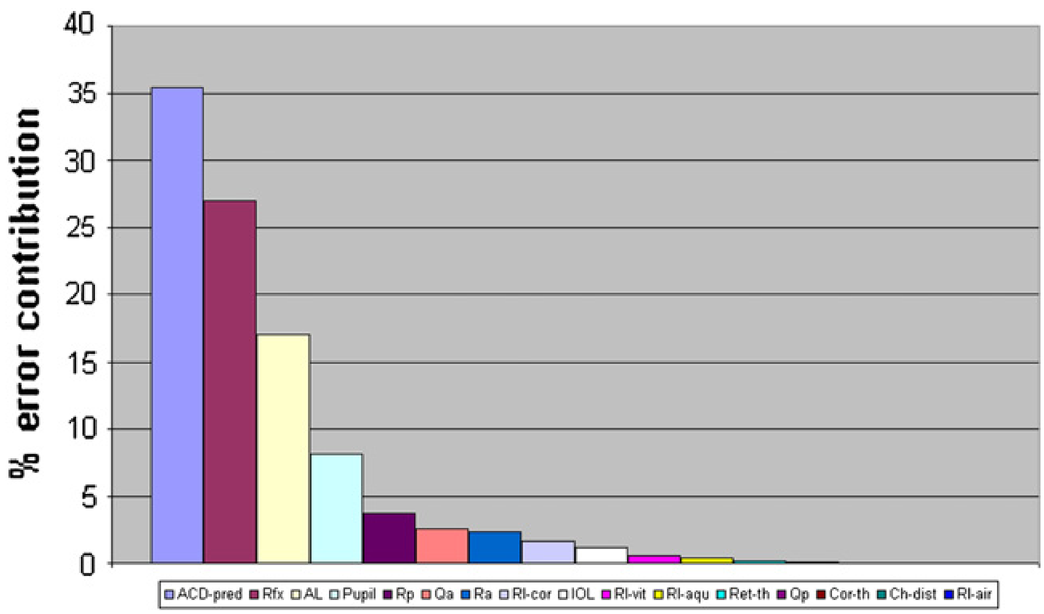

Figure 1.27 Percentage of error contribution in IOL power calculation. Ordered by increased value: ACD-pred=prediction of postoperative IOL position; Rfx=postoperative spectacle refraction; AL=axial length; Pupil=pupil size; Rp=corneal posterior radius; Qa=corneal anterior asphericity; Ra=corneal anterior radius; RI-cor=corneal refractive index; IOL= IOL power; RI-vit=vitreous refractive index; RI-aqu=aqueous refractive index; Ret-th=retinal thickness; Qp=corneal posterior asphericity; Cor-th=corneal thickness; Ch-dist=chart distance; RI-air=air refractive index. [Norrby, 2008].

It was shown that in the best case scenario, when the variability due to all inputs included at that calculation procedure was brought to the smallest as clinically achievable by that time and considering optical biometry, the mean absolute error in the prediction is of about 0.4D [Norrby, 2008]. Therefore, biometrical inputs limit the accuracy of the procedure. It should be noted, that in this study, only spherical aberration is considered and the optical treatment is limited to monochromatic light.

1.2.4.2. IOL power calculation for post-LASIK patients

The proper selection of the intraocular lens (IOL) power to implant is particularly important for post-LASIK patients, who have undergone a previous surgery to be spectacle free. However, IOL power calculation is more challenging for them [Holladay, 1989 and Hoffer, 1995]. Postoperative hyperopia is a common outcome in patients who have undergone myopic LASIK, whereas myopia is a common outcome for post-hyperopic LASIK patients [Gimbel and Sun, 2001 and Speicher, 2001].

For those patients who have previously undergone LASIK surgery, regular formulas should be modified to account for several factors that lead to previously mentioned IOL power calculation errors. One of these errors is that corneal power after LASIK is wrongly measured by corneal topographers and keratometers [Hoffer, 1995, Holladay, 1988 and Gimbel and Sun, 2001] The total corneal power is estimated from only anterior corneal measurements by using an ERI that accounts for the power of the posterior cornea. This ERI is based on a fixed ratio between anterior and posterior corneal radius. That ratio is modified after LASIK, since the procedure changes the curvature of the anterior cornea by keeping the posterior corneal shape [Perez-Escudero et al. 2009 and Zang and Wang, 2010]. Therefore the asymmetric modification imposed in the anterior cornea with respect the posterior cornea, changes the ratio between both corneal radius on what the ERI is based. Naturally following from this, the ERI for normal patients is no longer valid in post-LASIK patients. Furthermore, it is well known that its value may vary in post-LASIK patients [Hammed et al. 2002 and Savini et al. 2007]. An additional source of error in the corneal power determination is the measurement of the corneal radius. Because the cornea is much more flat after myopic LASIK, the corneal zone measured is substantially bigger in a normal cornea. Therefore, the measurements are not referred to the central portion of the cornea, which is the flattest area of the cornea in this patients, leading to an extra overestimation of the corneal power [Haigis, 2008 and Olsen, 2007].

Aramberri identified the ELP estimation as another source of error for myopic post-LASIK patients [Aramberri, 2003]. This was based on post-LASIK corneal power values, which underestimated the ELP and then the IOL power between 1 and 3D. He solved that problem using the pre-LASIK corneal power for calculating the ELP and the corrected post-LASIK corneal power for the IOL power calculation in the ELP previously calculated. This new procedure that can be applied to all IOL power calculation formulas is called Double K method. The potential disadvantage of this procedure is its dependency on clinical patient's history, which is not always available.

Different approaches have been pointed out in order to account for these errors in IOL power calculation for post-LASIK patient. They can primarily be divided into three groups: 1) based on LASIK pre-op data [Holladay, 1989, Feiz et al. 2001, Walter et al. 2006 and Arramberri, 2003] , 2) based on the change of manifest refraction [Hamed et al. 2002 and Masket and Masket, 2006] and 3) based on new regressions [Shammas et al. 2003 and Haigis, 2008]. The main problem of the two first groups is their dependence on historical clinical data, which are not always available and/or accurate. Additionally, it has been shown recently that methods using surgically induced changes in refraction, corrected corneal powers combined with the Double K procedure when estimating the pre-LASIK corneal power and methods using no previous data yield smaller IOL power error [Wang et al. 2010]. Therefore calculations with adjusted values and no dependency on clinically historical data can be considered to be the current state of art. One of the representatives among these calculation procedures is the Hagis-L [Haigis, 2008]. Haigis recalibrated the corneal radius measured by the IOL Master in order to overcome those factors previously discussed in determining the corneal power for myopic post-LASIK patients. This corrected radius is incorporated to the regular Haigis formula [Haigis, 2004]. By using this formula, Wang found a mean absolute error of 0.65±0.51D [Wang et al. 2010].

However there is another factor that is not considered by any of these formulas: anterior corneal aberrations. It has been widely reported that standard refractive surgery increases corneal aberrations, [Moreno-Barriuso et al. 2001, Kohnen et al. 2005 and Benito et al. 2009]. Spherical aberration is the most prominent although some other aberrations can result after LASIK, as coma terms, linked to a decentred ablation pattern [Mrochen et al. 2001]. The amount of the induction depends on several factors, making difficult its prediction. Because of the paraxial nature of the corneal power determination in the majority of standard IOL power calculations, these changes are not considered. In a step further in this direction, personalized corneal eccentricities, calculated from anterior corneal topography, were introduced an exact ray tracing procedure [Preussner et al. 2005]. A hyperopic shift up to 2D in IOL power was found for myopic post-LASIK patients. The effect of the rest of anterior corneal aberrations was not considered in the calculation, although a visual impression could be generated to judge subjectively their impact. The calculation is limited to monochromatic light. Nevertheless, as has been previously mentioned, empirical regression formulas can be considered the current state of art for this type of patients.

Chapter 2

JUSTIFICATION AND OBJECTIVES

2.1. Justification

Nowadays cataract surgery is one of the most common surgeries. All aspects related to that procedure have been improved, from the surgical technique to the IOL design, that allows for correcting some corneal aberrations and provide partial solutions for some other age related eye problems, such as presbyopia.

Those improvements will have a limited impact in patient's optical performance if the IOL power is wrongly selected. The transparency of the media will be restored but once the technique has advanced, the patient's requirements have increased and one of them is spectacle independence after surgery. This only can be achieved if the IOL power is properly selected. On the other hand, the impact of corneal aberrations correction is related to the blur imposed by the defocus induced by the implantation of a wrong IOL power. The possible inaccuracy in the calculations affects the new types of IOLs with the potential of correcting different aberrations [Holladay et al. 2002 and Tabernero et al. 2007], due to the fact that errors in defocus larger than 0.5 D may reduce the potential visual benefit of correcting higher order aberrations [Tabernero et al. 2006 (b)].

Although there are some theoretical approaches for IOL power calculation, the most common used formulas bases are paraxial optics and regressions retrieved from a large number of previous patients. Therefore, it is common sense to think that these calculations would be accurate on average but not individually as desired. To further support this point, it was recently reported that claims relating to biometry errors leading to wrong intraocular lens powers were the second most frequent cause of patients' claim after cataract surgery [Ali and Little, 2011]. It is then well understood that although current IOL power calculation procedures provides good outcomes on average, results at individual scale needs still to be improved. This is especially evident in those cases where patients present some peculiarity, such as extreme eye geometry or abnormal corneas.

Especially post-LASIK patients might be considered as subjects presenting abnormal corneas, due to the corneal ablation performed in the prior LASIK surgery. In fact, this change is usually related to induction of different corneal aberrations, as spherical aberration or coma, depending of the ablation pattern and centration. Due to the paraxial nature of common used formulas, corneal aberrations are totally ignored.

Furthermore, the decoupling between anterior and posterior corneal radius results in an inaccurate corneal power measurement when the same approach as normal patients is used. In addition, the effective lens position (ELP) estimation is also compromised in these formulas which consider the corneal power for its calculation. The correction of corneal power with new population based regressions and the use of pre-LASIK data have been proposed as solutions for IOL power calculations in post-LASIK patients. It should not be forgotten that these patients are especially sensitive to spectacle independence due to the fact that have undergone a prior surgery only to avoid wearing spectacles.

There have been some other attempts to approach IOL power calculations in a more theoretical way. Those attempts are not describing the eye in a complete customized fashion, due to the fact that depending on the approach some parameters are not included, such as aberrations (in paraxial ray tracing or thick lens methods) as well as a complete description of corneal aberrations or even chromatic aberration (in other ray tracing procedures). Accurate eye models have been developed, including also tilt and decentration of different optical surfaces [Tabernero et al. 2006 and Rosales and Marcos, 2007]. These are accurate procedures, because good correspondences between computed and measured aberrations have been shown. These models are of great importance to study the impact of some parameters on optical quality, such as tolerances to tilt or decentration, as well as depth of focus. However, IOL power is an input of these procedures, and therefore cannot be calculated from these models.

2.2. Objectives

The main objective of this thesis is to develop customized eye models for IOL power calculation purposes, based on more sophisticated inputs and techniques, as well as a better understanding of the optics of the eye. This procedure should be evaluated in comparison to the current state of art to assess at which customization level provides superior refractive outcomes. Furthermore, the limitations of the procedure will be studied. Therefore, the objectives of this work may be summarized as follow:

- To develop a customized IOL power calculation procedure based on polychromatic exact ray tracing. This predictive model will incorporate patient's corneal topography and biometry as well as the exact design of the IOL model.

- The impact of the incision on the cornea will be studied, both in low order and higher order aberrations, to establish the validity of considering preoperative corneal topography in the ray tracing procedure.

- IOL power calculation in normal patients: as a first approach, the IOL power calculated with the ray tracing procedure and some other current IOL power calculation procedures will be compared for a group of healthy subjects covering a wide range of refractions to identify potential differences between procedures, as defined in literature. The impact of the different parameters involved in the procedure will be discussed, as the polychromatic treatment, the incorporation of corneal aberrations and the IOL placement prediction. The customized ray tracing procedure will be validated in a clinical study. Its accuracy will be compared with the current stated of art in IOL power calculation, as well as the impact of considering corneal aberrations as an input.

- IOL power calculation in post-LASIK patients: the accuracy of the procedure will be evaluated in comparison to paraxial formulas especially developed for this population in a clinical study involving both myopic and hyperopic post-LASIK patients. The essential parts of the method affecting the accuracy of the procedure will be identified, such as corneal aberrations and the equivalent refractive index of the cornea.

- Possible applications that can be immediately translated into clinical practice will be developed based on the conclusions of the prior points, combining the current state of art and the incorporation of the parameters that most impact IOL power calculation in the herein developed ray tracing procedure.

Chapter 3

METHODS

This chapter is divided in two parts: the first describes the clinical instruments used to get the patient's data needed to build the customized eye models on what this work is based. The latter is a full description of the different ray tracing procedures used during this thesis, either for calculating corneal aberrations or the complete customized ray tracing procedure for IOL power calculation.

3.1. Instruments to eye's characterization

The clinical instruments used to measure ocular distances and geometries will be discussed during this section.

3.1.1. Axial length measurement

There are two main methods to measure axial length in clinical practice. Because both have been used through this work, the principles of these two procedures as well as their main differences are described through this section.

3.1.1.1. Ultrasound biometry

This type of biometry is based on the ability of measuring the distance between internal eye structures by using reflecting sound waves. The probe of the instrument which is placed in front of the eye is an electro-acustic transducer (figure 3.1(a)), able to transform electric energy into mechanical energy in the form of sound of waves and viceversa. Therefore, it can produce the initial ultrasound signal that goes into the eye and measure the reflected signal from the different eye's structures. In a echo-graph (figure 3.1(b)), each individual echo impulse, corresponding to the reflected sound in a particular eye surface, appears as a spike in the graph, plotted against the time of flight, that is the time that takes for the impulse to travel from the transducer, to a given interface, and back.

The axial length or some other distance in the eye can be calculated considering the time of fight and the sound velocity in the corresponding media, from:

$$d = \frac{tv}{2} \qquad [3.1]$$

where t is the time of flight, v the sound velocity and d de resulting distance. It is possible to define an average sound velocity for the complete eye (from 1548 to 1556 m/s depending on the biometric unit), and therefore, only the time difference between the spikes corresponding to the anterior cornea and the retina are considered. However, there are also some other units that makes a segmental measurement and therefore the sound velocity of every eye media should be specified (1532 m/s for the aqueous humor and vitreous body, 1640 m/s for the lens and the cornea). Segmental measurements allows for avoiding errors associated to the average sound velocity. It is overestimated for long eyes and underestimated for short eyes, which yield an error in the axial length determination of about 0.1 mm.

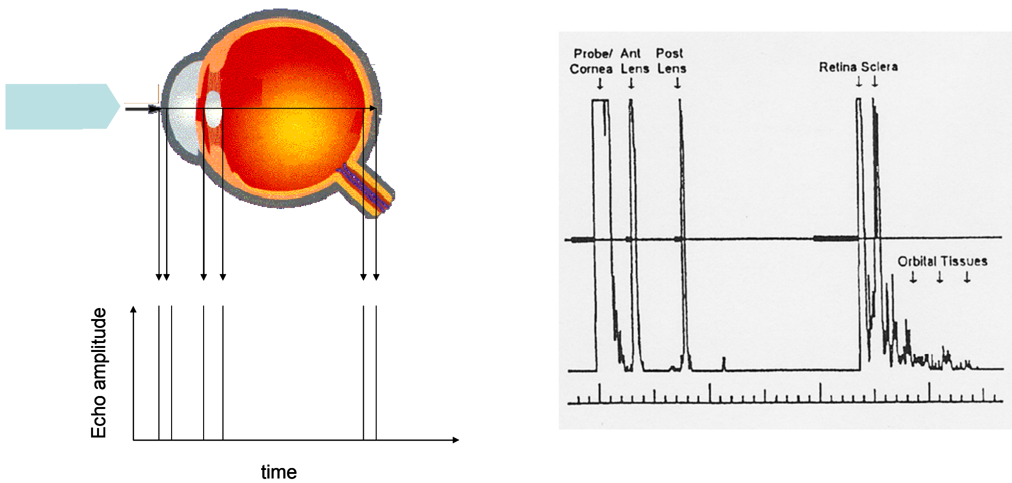

a b

Figure 3.1 Schematic representation of the ultrasound biometry principle (a) and a real echograph, where all the spikes are not of the same height, due to attenuation effects and with non negligible width (b).

There are two main types of ultrasound biometry, depending on the transducer surface. A-scan is related to a transducer with a flat anterior surface. Due to that surface shape, the emitted sound beam is not focused. On the other hand, B-Scan is performed with a concave surface that therefore emits a focused sound beam. The main drawback of the latest is the fact that it retrieves accurate measurements only in those eyes where the retina is in the area where the sound beam focuses, limiting its performance in a wide range of axial lengths. Therefore, the most used for ocular biometry is the A-Scan mode. Regarding the ultrasound beam, higher frequencies produce higher resolution, while lower frequencies provide better penetration. In a compromise between both characteristics, biometry units use ultrasound frequencies ranging between 8 and 25 MHz.

When A-Scan biometry is considered, there are two main measurement modes: immersion and contact. In the immersion A-Scan biometry mode, the eye is not touched directly by the probe. Therefore, the immersion technique of biometry is accomplished by placing a small scleral shell (figure 3.2a) between the patient's lids, filling it with saline or another specific solution, and immersing the probe into the fluid, being careful to avoid contact with the cornea. Another important point of this measurement mode is the fact that the subject is placed in supine position (figure 3.2b).

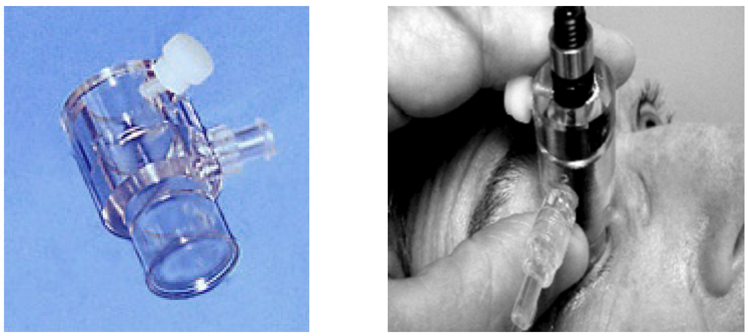

a b

Figure 3.2 Prager shell used for immersion ultrasound (a) and immersion ultrasound operation (b).

The other measurement mode is the contact A-Scan biometry. In this case, the ultrasound probe is placed directly on the cornea. It is of capital importance not to press on the eye, because this affects the final measurement. Therefore, the probe should be glided on the corneal surface avoiding indentation. This is the most common used A-Scan technique because its simplicity although it is well known that only experienced operators can retrieve repetitive measurements. There are variations in the axial length measurement due to the different examination technique. When the same eye is measured, the contact mode retrieves shorter measurements than the immersion technique [Olsen and Nielsen, 1989 and Schelenz and Kammann, 1989]. This difference is between 0.1 to 0.2 mm [Shammas, 1984 and Byrne, 1995]. Although the indentation during the contact procedure is the most accepted cause, there are some other factors that may explain also the discrepancy, as the difference in the patient position.

The ultrasound unit used in this thesis (OcuScan RxP, Alcon, Forth Worth, Texas, USA) works in the contact operational mode. It contains a 10 MHz probe for biometry, and measures axial length in a range between 15 and 40 mm, with an accuracy of 0.1 mm.

3.1.1.2. Partial coherence interferometery

Partial coherence interferometry was proposed by Fercher [Fercher et al. 1998] as an alternative method for axial length measurement. The optical biometer (IOL Master; Carl Zeiss Meditec, Jena, Germany) used in this work is based on such technique. The optical arrangement of the device is a Michelson interferometer, as shown in Figure 3.3. A beam of 780 nm with a short coherence length (c=160 μm) goes through a beam splitter that divides the light in two paths. The first goes into a fixed mirror (M1) while the second is reflected in another mirror (M2) whose position can be adjusted (referred on the scheme as a distance d). The light reflected by both, the static (A1) a movable mirror (A2), delayed by 2d, goes into the eye and is reflected thought the different eye surfaces. Reflexions coming from the anterior cornea (C) and the retina (R) corresponding to the beam reflect on the fixed mirror (A1c and A1r) and to the movable mirror (A2c and A2r) are directed by a second beam splitter into a photo detector. When the difference between the optical paths 2L and 2d is smaller than the coherence length of the light, an interference between A2c and A1 occurs and therefore its signal is recovered by the photo detector. Therefore, to measure the optical path L, the mirror M2 is moved through different positions, being d the distance that maximizes the signal at the photo detector.

Due to its interferometric nature, the result of the measurement is optical path, or more precisely, two times the optical path because the light has to travel into the eye and be reflected back at the retina. To translate the optical path into physical distances, a group refractive index is needed. This is an average refractive index corresponding to the different optical structures within the eye, that in the IOL Master is taken as 1.3549 [Hitzenberger, 1991].

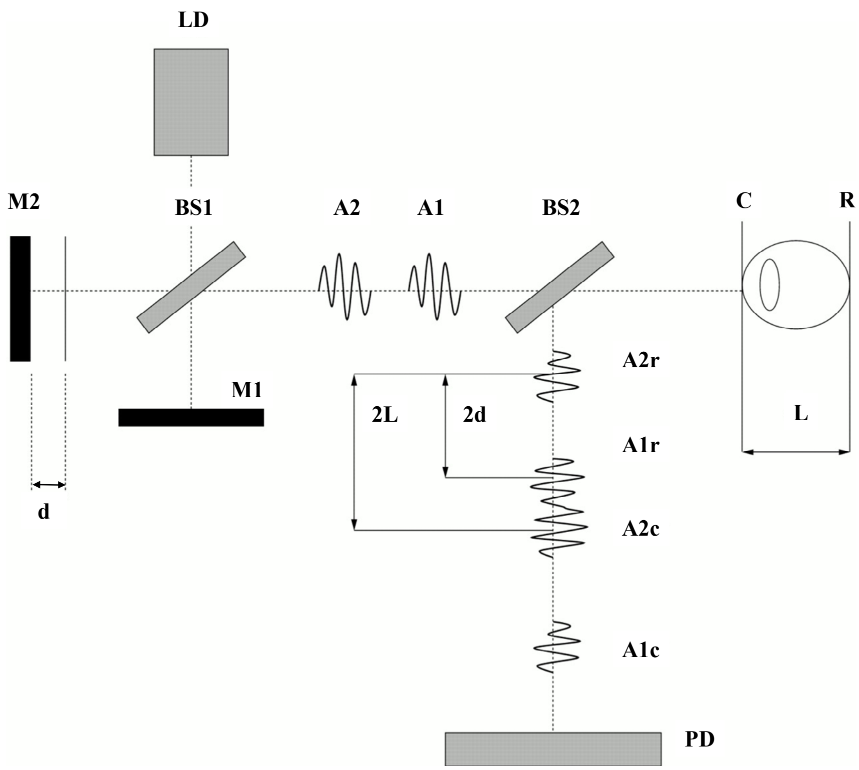

Figure 3.3 Scheme showing the principle of partial coherence interferometry

Because of the short coherence length and the precision of the motor moving the mirror M2, the accuracy of measurements is around 30 μm [Hitzenberger, 1991]. The reproducibility is 22 μm, similar to that provided by inmersion ultrasound [Haigis et al. 2000]. When optical biometry is compared to contact ultrasound, both reproducibility and repeatability of the latest are worse. Sheng reported a standard deviation for repeated measurements of 0.03 mm and 0.15 mm for partial coherence interferometry and contact ultrasound respectively when 20 young subjects where measured by the same operator [Sheng et al. 2004]. Furthermore, the reproducibility for ultrasound measurements was also worse, since the standard deviation of the repeated measurement depended on the operator contrary to optical biometry, that was shown as subject independent [Sheng et al. 2004]. Optical biometry cannot always be performed, since it depends on the transparency of the ocular media. Freeman reported that 20% of the patients could not be measured by partial coherence interferomety due to the presence of dense cataracts, although ultrasound measurements were possible in all the patients [Freeman and Pesudovs, 2005].

There are differences between outcomes retrieved by optical and acoustical biometry. One of the reasons for that difference is that due to the first is using light and the second is using sound, the structures reached in the retina are different, yielding to a different axial length measurement. Ultrasound biometry measures until de inner limiting membrane while optical biometry retrieves the axial length up to the retinal pigment epithelium. Because of that, the axial length measured optically would always be greater than measured by any ultrasound device. It is possible to consider an average value of 0.2 mm [Lim et al. 2005]. There is another difference between devices that makes also a discrepant outcome and this is the fact that the ultrasound biometry is performed in the optical axis while the optical biometry is performed in the visual axis.

Because of these differences, it was decided to calibrate the commercially available optical biometer against an immersion ultrasound device [Haigis et al. 2000]. Therefore, the IOL Master retrieves the same measurements a highly accurate immersion ultrasound, with the advantage that the operational mode is much simpler. Some authors have proposed the conversion of those calibrated optical axial lengths into true optical axial lengths, back applying the same calibration performed by the manufacturer [Olsen and Thorwest, 2005], showing an increased accuracy in the IOL power calculation procedures when thick lens theory in considered [Olsen, 2006].

While the optical biometer and the immersion ultrasound A-Scan retrieve the same axial length after calibration, the contact ultrasound method has reported differences between 0.1 to 0.2 mm, as has been previously mentioned. In addition, the latest is the biometer with respect to the IOL manufactures refer the A constants related to each IOL model [Haigis, 2011]. Therefore, IOL constants should be recalculated for optical biometry. In order to solve this problem the ULIB (User Group for Laser and Interference Biometry) periodically updates the IOL constants for a wide number of IOL models based on registries from surgeons all around the word. In this way, the IOL constants related to the most common paraxial regression formulas are optimized to retrieve zero refractive error on average. This is done from the preoperative data as well as from the knowledge of the IOL power implanted and the residual refraction resulting in a large set of patients. It is obvious from this optimization process, that IOL constants are also optimized in order to improve refractive outcomes with the IOL power calculation procedures currently available, as has been discussed in the first chapter.

3.1.2. Corneal topography. Videokeratoscope

The cornea is the most important refractive surface that remains in the eye after cataract surgery. Therefore, an accurate determination of corneal power and cylinder is crucial to properly select the optimum IOL that provide best patient's optical performance. In addition, the complete description of the corneal topography is also important. During this work, reflection based systems that considered the tear film as a convex mirror has been used for characterizing the cornea. This methodology might be applied in different levels of complexity from keratometry to computer based videokeratoscopy, as will be further described below.

Historically, the interest in measuring corneal properties by using the reflection principle can be dated on 1820, when Cuignet developed a keratoscope based on the observation of a reflected pattern on the patient's cornea. Helmholtz made possible the quantification of the corneal radius by the development of the keratometer in 1854, based on the measurement of the distance between two reflected points in the central cornea. Figure 3.4 schematically shows the image formation by a convex mirror. The ratio between the image (I) and object (O) size is proportional to the ratio between the distance of the image (b) and the object (a). If the object position is assumed to be large in comparison to the corneal radius, the image is located at the focal point of the mirror, that is half of its radius of curvature, and therefore:

$$\text{Magnification} = \frac{I}{O} = \frac{b}{a} = \frac{r}{2a} \qquad [3.2]$$

or alternatively:

$$r = 2a\frac{I}{O} \qquad [3.3]$$

Keratometers measure the radius of the cornea by using the previous relationship. There are two distinct variants of determining r: Javal-Schiotz type keratometers have a fixed image size, whereas Bausch and Lomb type keratometers used a fixed object size.

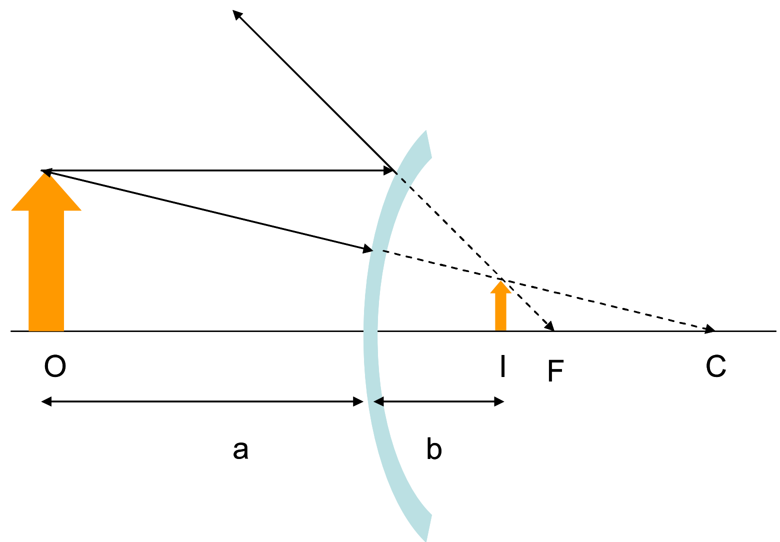

Figure 3.4 The image yielded by a convex mirror is virtual, depending its size on the radius of the mirror. This is the principle behind keratoscopy to measure corneal radius.

However, keratometry mapped only the central zone of the cornea under the assumption of symmetry, that is, a perfect spherocylindrical cornea. However, such information is not sufficient to describe the optical quality of the cornea when there are corneal irregularities or pathologies in the periphery. In 1882, Antonio Placido designed a target based on alternating black and white concentric circles, whose reflections could be observed by looking at the center of the target. Although with technical improvements, this pattern is still used by most current videokeratoscopes. It is possible to qualitatively estimate some corneal properties just by the observation of the Placido ring reflections. A steeper cornea would produce a smaller image with less spacing between rings (Figure 3.5). On the other hand it is also possible to detect astigmatism, due to the generation of elliptical rings, as well as some other corneal irregularities, such as scars or ulcers.

Gullstrand invented in 1896 the photokeratoscopy by incorporating photography to keratoscopy. It made possible to take ring images to quantify the corneal radius by comparing the pictures of reflected patterns on spheres of known radius. Since then, the mayor advantage in the development of devices to measure corneal topography was the incorporation of computer based calculations allowing topographic characterization, with a high degree of precision in what is called videokeratoscope. It was not until early 1990s that corneal topography began to introduce into the clinical practice.

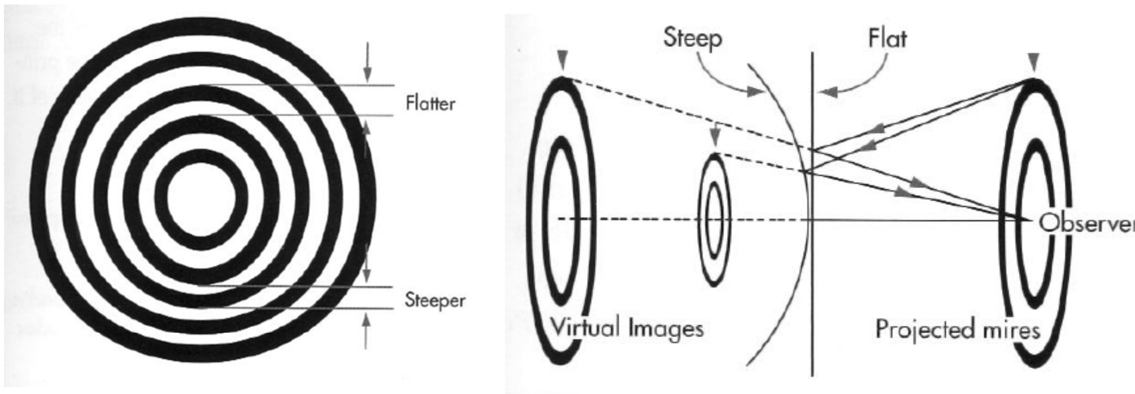

a b

Figure 3.5 Deformations in the Placido ring's due to a reflexion in a steep or flat cornea (a). The size of the image also depends on the corneal power (b) [Mckay, 1998]

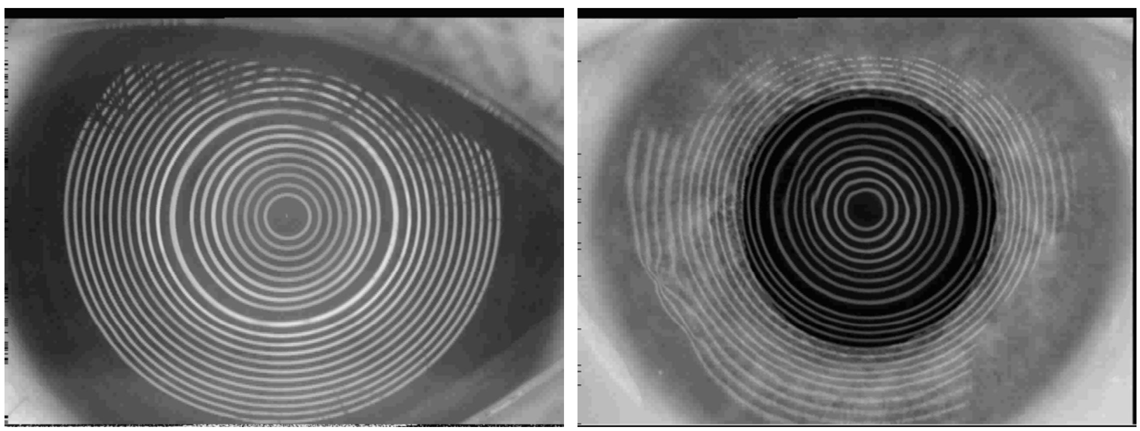

a b

Figure 3.6 Photography of the Placido rings in a post-LASIK cornea from the Humphrey ATLAS (Zeiss)(a). The quality of the tear film is an important factor about the quality of the corneal topography (b).

The corneal topographers used in this thesis are the Atlas models 991, 995 and 9000 (Carl Zeiss Meditec, Dublin CA, USA) (Figure 3.6). For example, ATLAS 9000 has 22 rings, being digitalized in 180 points per ring. Therefore, more than 3900 points are analyzed. One of the rings is placed closer than the rest (figure 3.7). Because of that, its position at the image change differently than the rest when the instrument is moved axially. It is possible to calculate the position of that ring relative to the rings at each side and therefore localize the surface itself.

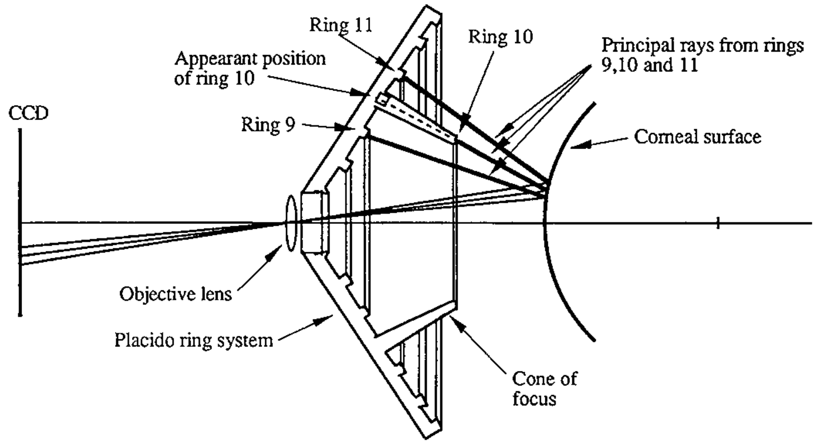

Figure 3.7 One of the rings is placed in front of the rest to localize the corneal surface and start the iteration process [Campbell 1997]

The reconstruction of the corneal shape is performed iteratively. The cornea is sliced in meridians determined as the intersection between the reconstruction plane and the corneal surface [Campbell, 1997]. This reconstruction plane is defined by the principal ray, which pass from the CCD plane, through the central portion of the lens aperture to the point on the corneal surface from where it is reflected, and the videokeratoscopic axis, defined as which passes through the central portion of the lens aperture and starts in the center of the inner ring image of the CCD (figure 3.8).

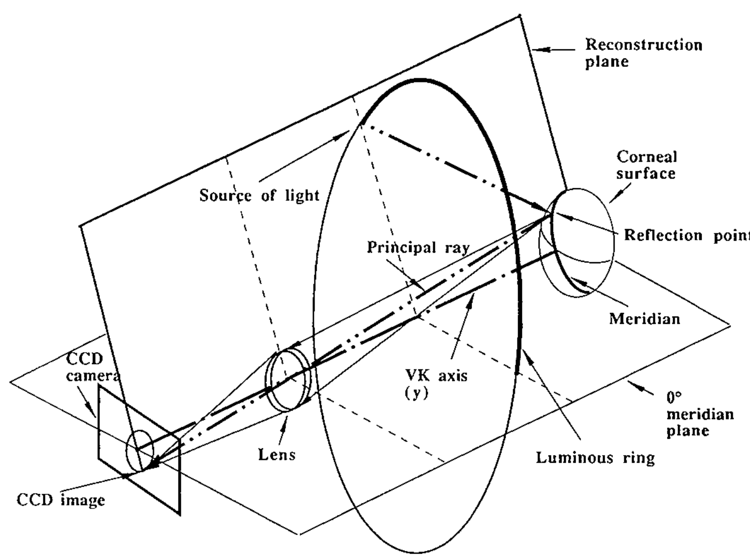

Figure 3.8 Videokeratoscope geometry [Campbell, 1997]

The geometry of the cornea is reconstructed at each meridian from the recorded image of the rings, the known geometry of the instrument and the illumination pattern. This is done under the assumption that the incoming ray is reflected about the normal of the meridian and therefore, the incident ray and the reflected ray at the cornea are lying at the reconstruction plane. The algorithm which reconstructs the corneal shape from the digitized images of the rings is called arc step method. Each meridian is divided in arcs defined as the zone between two different neighbouring points, to ensure a smooth transition. The axial and radial coordinates, as well as the slope of the normal at every measured point of the meridional curve, is found from its nearest neighbour in an iterative process that ensures an accuracy of 0.001μm [Campbell, 1997].

As result of the iteration process on the digitalized images obtained by the videokeratoscope, a discrete set of data in cylindrical coordinates, corresponding to the radial, angular and axial position (usually refer as elevation) for every measured point is retrieved. This is used to describe corneal surface in customized eye models and to compute corneal aberrations as will be described in the next section.

3.2. Ray tracing procedures

Ray tracing techniques are used to develop realistic eye models that are further validated and can therefore be used to perform predictions in future patients. The basis and principles of ray tracing are described in this section as well as the different implementations.

3.2.1. Exact ray tracing

The aim of ray tracing is to find the direction and spatial location of the ray after passing through an optical system defined by different surfaces described by its geometrical (radius, aspheric or toric terms, thickness) and optical (refractive index) properties. Two basic algorithms are iteratively solved: transfer and refraction equations. The former is translating the ray from one surface to another and determine the exact location where the ray intersects the next surface. This is done by calculating the intersection between a straight line (a ray propagates in straight line when it passes through a homogeneous and isotropic medium) and a surface, that in the most general case is solved by iterative algorithms [Welford, 1986].

Refraction equations determine the ray direction after passing through a surface separating two different media. When the most general case is considered, the aim is to determine the direction of the refracted ray after passing through a surface by using the vectorial form of the Snell's law, that is:

$$n'(\vec{r'} \times \vec{B}) = n(\vec{r} \times \vec{B}) \qquad [3.4]$$

where $\vec{r'}$ and $\vec{r}$ are the unit vectors along the incident and the refracted rays, $\vec{B}$ is the unit vector normal to the interface and n and n' the refractive indexes of the two media. Equation [3.4] ensures the co-planarity of incident and refracted rays as well as the normal to the surface at the point where the ray impinges. In order to generate a suitable form of equation [3.4] for ray tracing purposes, such equation is multiplied vectorially by $\vec{B}$,

$$n'(\vec{r'} - \vec{B}(\vec{r'} \bullet \vec{B})) = n(\vec{r} - \vec{B}(\vec{r} \bullet \vec{B})) \qquad [3.5]$$

that can be expanded in scalar form by considering (L,M,N), (L',M',N') and (α,β,γ), the components of $\vec{r'}$, $\vec{r}$ and $\vec{B}$ respectively, yielding:

$$\begin{aligned} n'L' - nL &= k\alpha \\ n'M' - nM &= k\beta \\ n'N' - nN &= k\gamma \end{aligned} \qquad [3.6a]$$

where

$$k = n'(\vec{r'} \bullet \vec{B}) - n\ (\vec{r} \bullet \vec{B}) = n' \cos\theta' - n\cos\theta \qquad [3.6b]$$

where θ and θ' are the angles of incidence and refraction, related by the scalar version of the Snell's law [3.4]

$$n' \mathrm{sen}\theta' = n \mathrm{sen}\theta \qquad [3.7]$$

that can be also expressed as:

$$n' \cos\theta' = \sqrt{n'^2 - n^2(1 - \cos^2\theta)} \qquad [3.8]$$

Therefore, to get the components of the refracted ray (L',M',N') from those of the incident ray (L,M,N), equation [3.6a] is used. Previously, the normal to the surface (α,β,γ) at the point where the ray impinges should be determined as the gradient of the surface. After that k at [3.6b] is calculated from cos θ and cos θ'. The former is got as the scalar multiplication $\vec{r} \bullet \vec{B}$ and cos θ' is calculated from [3.8].

The ray tracing procedure includes two other steps, related with the opening and closing equations. These two stages are used only at the beginning and the end, to start the ray into the system and the final determination of the ray intercept, respectively. Ray tracing procedures can be applied in different levels of complexity by considering those so called skew rays, which are the most general rays, or meridional rays, being those rays which are coplanar with the optical axis of the system. Due to the increased computation speed in modern machines, rays traced are mainly skew rays, being meridional rays traced as special case of general rays [Smith 1990].

It is possible to calculate optical quality parameters from ray tracing procedures. The wave aberration may be calculated in the pupil plane as the optical path difference between the rays passing through defined pupil positions and a reference ray. For each ray traced, a local value of the wavefront is calculated. This is defining a discrete set of local values of the wavefront through the pupil that once fitted by modal reconstruction, yields a set of aberration coefficients. Some other optical quality parameters can be retrieved from the wavefront aberration function, such as the PSF or the MTF.

The software used in this thesis for ray tracing and optical quality evaluation was the ZEMAX optical design package (ZEMAX Development Corp, Bellevue, WA, USA). The different surfaces and options within the program used for modeling the eye's surface will be described through the next sections.

3.2.2. Corneal optical quality evaluation

Corneal topography allows to generate the most realistic representation of the corneal surface. Because the topographer provides corneal elevations in polar coordinates, to generate an adequate input for the used ray-tracing package which requires data in rectangular coordinates, we fit this raw data by a least square procedure to the eighth order Zernike expansion for an aperture diameter of 7-mm. This area was chosen as optimal because the fitted surface should be larger than the analyzed area in the eye model and should also avoid edge effects in the adjustment and throughout the ray tracing procedure. In addition, since we chose a 4-mm pupil size for the image quality calculations in the eye, we consider 7-mm corneal aperture to be a suitable value. A prior step to the fitting is of course the check of the raw data to ensure that they were supplied up to that size.

Zernike polynomials have been chosen as a basis for decomposing and analyzing corneal surfaces since are defined over a unit circle and that lower terms represent familiar corneal shapes, such as sphere and cylinder [Schwiegerling et al. 1995]. There are some other procedures that can be used to expand the discrete sample of corneal elevations in term of Zernike polynomials further than the least square method used here. It would be also possible to consider the orthonormality properties or the Zernike polynomials and then calculate the expansion by integration over the basis determined by the polynomials. However, Zernike polynomials are only orthogonal over a continuous unit circle, and because corneal elevations are supplied as a discrete set of points, the condition of orthogonality is not accomplished. Therefore, it is needed to use orthogonalization methods to find a new basis [Schwiegerling et al. 1995 and Guirao and Artal, 2000]. Salmon reported that the accuracy on the least squares procedure for fitting corneal elevations is similar to that related to the orthogonalization procedures previously mentioned and, in any case, the difference is negligible when compared to the measurement accuracy of the original data [Salmon, 1999].

From this fitted surface, a regular grid of points in Cartesian coordinates is retrieved, as required for surface representation in ZEMAX. Any arbitrary inner point within the supplied regular grid defining the corneal surface is reconstructed by bi-cubic spline interpolation when the ray tracing is performed, from which corneal wavefront aberrations can be calculated. Some other procedures have described to calculate corneal wavefront aberrations. Guirao and Artal developed an analytic procedure that retrieves the Zernike polynomials related to the corneal wave aberration from those coefficients resulting from the corneal elevations fitting [Guirao and Artal, 2000]. This procedure retrieves as good results as the ray tracing described here. However, the main objective of this work is to have a complete ray tracing procedure for modelling the eye and this is the reason of choosing the former.

In addition, the reconstructed surface is re-centered with respect to the pupil. Because clinical instruments, like the Hartmann-Shack wavefront sensors, use the line of sight as reference (because the wavefront aberration maps have their origin in the center of the entrance pupil) [Appelgate et al. 2009], it is convenient to use the same reference, especially when corneal surfaces are integrated in eye models or when internal aberrations are estimated from the subtraction of corneal aberrations from total aberrations [Artal et al. 2006].

The keratometric axis is the axis used for alignment in corneal topography. It joins the fixation target with the centre of curvature of the anterior corneal surface [Atchinson and Smith 2000]. The origin of the Placido rings reflected by the cornea is contained in that axis, which does not correspond to the line of sight (Figure 3.9a). Therefore, the reconstructed surface obtained from corneal elevations, is decentered with respect to the pupil (Figure 3.9b). In order to have the cornea referred to the line of sight, the reconstructed surface should be displaced to the pupil centre, in a distance that can be calculated from the image retrieved by the corneal topographer (figure 3.9b). This procedure, previous to the ray tracing, is performed by locating the center of the pupil and the center of the eighth ring, which is previous ring to that used for locating the corneal surface. The distance between these two centers is introduced in the file containing the Cartesian representation of the corneal surface and therefore, the cornea is centered with respect to the pupil, and the calculated aberrations in ZEMAX referred to the light of sight.

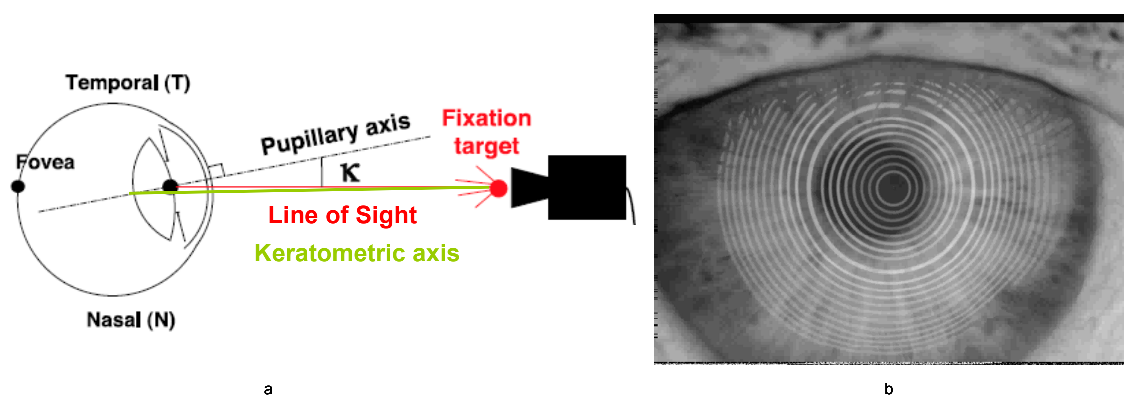

Figure 3.9 Schematic view showing the decentration between the line of sight and the keratometric axis (adapted from [Artal et al. 2006])(a) and actual view in the image retrieved by the corneal topographer (b)

There are some other details that characterize the ray tracing procedure to calculate corneal aberrations. One of them is the position of the image plane. The focal distance is set in order to minimize the root-mean-square (RMS) spot size at the image plane [Barbero et at. 2002]. We have chosen that criterion because in the case of the cornea, the image plane is arbitrary, although its position influences the wave aberration, since it defines the radius of the reference sphere. Therefore, by placing the image plane where the RMS spot size is minimized, the influence of the image plane position is dismissed at the corneal wave aberration values. Another important point is the sampling of the ray tracing. Because the number of rays is finite, the accuracy of the wave aberration results depends on the sampling of the ray grid used. After evaluating different of the available options, we found no differences in results for lower or higher samplings in normal corneas. Therefore, the smallest sampling was used in those cases (32x32). However, the scenario was different for post-LASIK corneas. Due to the higher amount of aberrations present in these corneas, the sampling needed to be doubled to obtain consistent results. In any case, the computing time is still practicable.

Zemax has an own programming language that allows for generating routines, commonly called “macros” that guide that general ray tracing procedure. In this case, a specific macro was developed to automate the corneal wave aberration calculation from the file containing the corneal discrete set of corneal elevations and the corresponding decentration values with respect to the pupil. Once the name of the file was introduced, the focal is set under the previously mentioned criterion and the ray tracing is performed at the selected pupil size. A file containing the corresponding aberrations following OSA standards [Thibos et al. 2000] result from the computation as well as the corresponding sphere, cylinder and axis related to the spherocylindrical prescription, which is calculated from the second order aberration terms [Thibos et al. 1997 and 2004]. Although the sphere calculated has not a physical meaning, it can be used in order to monitor temporal corneal power changes. For that purpose the focal length should be fixed during different stages. This procedure will be further described in chapter 4.

3.2.3. Customized eye models

In this section we present a ray-tracing approach developed to calculate the optimum IOL power [Cánovas and Artal, 2011]. It is based on customized eye models similar to those previously used to model the optical performance in normal eyes [Artal et al. 2006 and Artal and Tabernero, 2008] and, post-operatively, in eyes implanted with IOLs [Tabernero et al 2006 (b) and Rosales and Marcos 2007]. Both studies showed a good correspondence between measured and computed eye´s aberrations. In both cases, all IOL parameters were known, including IOL power used in the surgery as well as its placement in the eye, and tilt and misalignments measured with Purkinje systems [Tabernero et al. 2006(a)]. Our aim was to further develop customized models to be based on preoperative data so that they can be used as a predictive tool.

3.2.3.1. Custom IOL power calculation

Different biometric data (anterior corneal topography, ocular axial length and anterior chamber depth) were measured prior to the surgery and introduced into the calculation procedure in order to allow for customization. Figure 3.10 shows a schematic view of the complete procedure. All the surfaces introduced in the model correspond to those in the real patient´s eye. Here, we sequentially describe the surfaces considered in the customized eye model from the cornea to the retina.

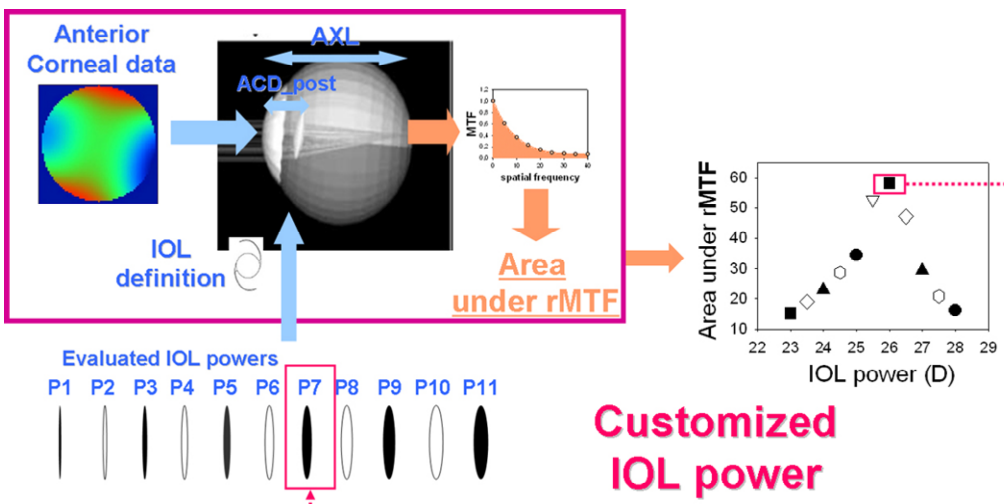

Fig. 3.10 Schematic diagram of the customized eye model for predicting IOL power. For every IOL power, an eye model is built from patient´s biometric data from which the area under the radial MTF is calculated, being chosen the IOL power that maximizes this metric.

The anterior corneal surface is introduced as a discrete Cartesian grid selected from the fitted elevation map which is obtained from the raw data acquired from a Placido based corneal topographer, as described in the previous section.

We considered the contribution of the posterior cornea by using an equivalent refractive index for the anterior surface. It is determined to achieve the power of the complete cornea in the Legrand's eye model [Le Grand and El Hague, 1980] while only considering the anterior surface of the cornea by the use of a similar procedure to that described by Olsen [Olsen, 1986]. The resultant value 1.33 agrees well with the value previously calculated from anatomical data [Dubbleman et al. 2006]. Because our procedure is performed in polychromatic light, we use the dispersion values of water for the equivalent refractive index. The axial position of the pupil of the system was set in the anterior chamber depth prior to the surgery, considered as the distance between the anterior cornea and the anterior surface of the lens.

The prediction of the IOL position after the surgery is especially relevant for the calculation [Norrby, 2008] and especially for short eyes [Olsen, 2007]. Although whatever algorithm predicting actual lens position can be used in this customized procedure, we decided to use the relationship between the anterior chamber depth prior to the surgery (ACD_pre), measured with anterior segment slit-lamp images (IOL Master; Carl Zeiss Meditec, Jena, Germany) and the actual IOL position (called here anterior chamber depth after the surgery (ACD_post)) measured with an anterior chamber OCT instrument (Visante, Carl Zeiss Meditec, Dublin, CA) found in a previous study (Figure 3.11). The relationship between these two parameters was linear (eq. 3.9) with a high degree of correlation (r^2=0.8).

$$ACD\_post = 0.88 \times ACD\_pre + 1.63 \qquad [3.9]$$

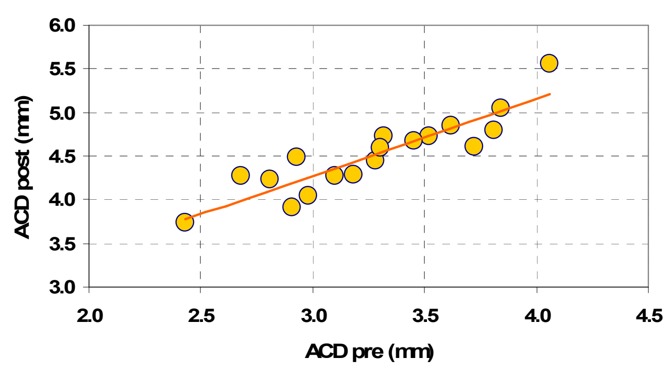

Fig. 3.11. Anterior chamber depth prior to the surgery as function of the anterior chamber depth after the surgery. From this result, we extracted the predictive model described by eq. 3.9.

The particular geometry of the IOL (surfaces radius and aspheric terms, thickness) and its optical properties (refractive index and dispersion) should be introduced into the model. All IOL types (monofocal, spheric, aspheric, toric or multifocal) and designs can be considered if these design parameters are known.

The calculation is performed at the circle of least confusion by correcting corneal astigmatism in the eye model. To perform this correction, we introduce a surface containing the opposite amount of both components of corneal astigmatism, that is c_3 and c_5, and therefore, J_{45} and J_0 according to power vector notation [Thibos et al. 2004]. Because these have zero spherical equivalent power [Thibos et al. 1997], the IOL power calculated by the procedure corresponds to that provided by the averaged corneal power meridians. As a practical example, the corneal astigmatism terms c_3 and c_5 are determined at every moment of the calculation. The correction of both terms corresponds to a cylinder of $+2\sqrt{\frac{6C_3^2+6C_5^2}{r^2}}$ and a sphere of $-\sqrt{\frac{6C_3^2+6C_5^2}{r^2}}$ [Thibos et al. 1997 and Thibos et al. 2004]. Therefore, the spherical equivalent of the correction is zero and does not change that of the corneal surface. Naturally following this, the IOL power calculated by the ray tracing procedure corresponds to the use of averaged corneal power meridians, as in current IOL power calculations.

The retina is placed at a distance corresponding to the axial length measured for each individual subject. The refractive index for the media is considered as that of the Gullstrand model (1.336) with a dispersion corresponding to water. All calculations are performed in white light, by considering 6 wavelengths between 470 and 700 nm weighted by the spectral sensibility curve under photopic conditions.

To select the customized IOL power, from the polychromatic ray tracing performed at 4mm pupil, the area under the radially averaged polychromatic MTF [van Meeteren, 1974] up to 30 cycles per degree (eq. 3.10) is evaluated for each individual IOL power tested. The numerical integration was performed using the trapezoidal rule with a step size of 3 cycles per degree.

$$\mathrm{Area\_under\_MTF} = \int_0^{30} \mathrm{radialMTF}(f)\,df \qquad [3.10]$$

The selected IOL power is that maximizing this image quality metric.

An important feature of this procedure is the ability to use the model to determine the optimum IOL power for different levels of corneal aberrations. This allows studying their impact on the IOL power prediction. We can modify these aberrations in the same way as the corneal astigmatism is neutralized, using the same surface to add different amount of aberrations to the cornea or compensate for their presence. The calculation of anterior corneal aberrations, as described in the previous section, is an important preliminary step in the procedure because it is used to evaluate the anterior corneal topographies that are going to be used in the IOL power prediction. Aberration differences among different independent topographies help to understand possible changes in the final estimation of the IOL power, as will be shown in chapter 5, where also the impact of each individual input in the procedure will be evaluated. Finally, in the next chapter the impact of the change on corneal low and higher order aberrations before and after cataract surgery will be studied in order to understand whether presurgery anterior corneal topographies can be used as valid representation of the corneal surface after the surgery for IOL power calculations purposes.

The complete procedure is written in the ZEMAX programming language. Therefore, the IOL power prediction is fully integrated in a unique routine that should be fed with the abovementioned inputs, that is, corneal elevations files in the corresponding Zemax convention, axial length, anterior chamber depth and IOL model and powers. After that, the routine performs the corresponding calculations herein described, sequentially introducing the different IOL powers into the eye model, and provide the optimum IOL power for that patient, as well as the area under the radial MTF calculated for all the IOL powers evaluated.

Chapter 4

TEMPORAL OPTICAL CHANGES IN THE CORNEA AFTER CATARACT SURGERY

IOL power calculations are based on the spherical equivalent power of the cornea and therefore, a change in the cornea due to the surgery could lead to an incorrect IOL power selection. Most of the earlier studies were only focused on the surgically induced corneal astigmatism (SIA) [Kohnen et al. 1995, Masket and Tennen, 1996, Oshika and Tsuboi, 2002, Feil et al. 1994, Shepherd, 1989]. With the increasing use of toric IOLs, an accurate prediction of the final corneal cylinder is becoming more important due to the fact that an incorrect estimate can reduce the benefit provided by this type of IOLs.

Although there have been studies comparing the corneal aberrations prior to and following cataract surgery in the past [Guirao et al. 2004, Marcos et al. 2007], as far as we know, there is not any attempt in the literature to study the changes in both low (corneal power, cylinder and spherical equivalent) and high order aberrations after surgery. In this context, we study in this chapter the change in both, low and higher order aberrations to generate a complete characterization of the corneal state after surgery and therefore establish whether anterior corneal topographies measured prior the surgery may be considered as a valid representation of the posterior state of the anterior corneal surface.

4.1. Patients and protocol

The study involved 29 patients between the ages of 52 and 78, measured at 6 different times between 2007 and 2009. In the presurgery visit, patients were selected and informed about the nature of the study. The rest of the follow-up visits were conducted at 2 weeks, 1, 4, 7 months and 1 year following the cataract surgery. All clinical examinations, surgeries and measurements were conducted at the Ophthalmology Service at the “Virgen de la Arrixaca” hospital (El Palmar, Murcia, Spain). Prior to the surgery, clinical examinations were performed following the standard procedure for cataract patients (ultrasound biometry, corneal topography, intraocular pressure and slit lamp exam). Exclusion criteria were restricted to any ocular pathology except cataract in order to have a population resembling those usually treated by cataract surgeons. In all the cases, surgery was performed by a single surgeon under topical anaesthesia. The corneal incision was on average 3.5 mm both in temporal or nasal location, following the standard procedure. No sutures were used. The IOL implanted was a light adjustable lens (LAL) (Calhoun Vision, Pasadena, CA). These are foldable 3-piece lenses, having a

6mm, squared edge optic. LALs contain a photosensible material, which allows for postoperative changes in refractive power. At all follow-up visits, a standard ophthalmic exam was performed to ensure that no ocular pathologies were developed. VA was measured and controlled in order to monitor any visual change. In addition, at least 4 corneal topographies were recorded during each visit. For this, all the patients were measured under natural viewing conditions.

4.2. Cornea modeling: refraction and aberrations

The wave aberration (WA) of the anterior corneal surface was obtained by ray tracing through the elevations provided by a Placido-based corneal topographer (Atlas; Carl Zeiss Meditec, Dublin CA), as described in the methods section. The ray tracing was performed at 3 mm pupil for calculating corneal refraction (defocus and cylinder), while 4 mm pupil was used for calculating the rest of higher order corneal aberrations (Figure 4.1). The main difference of the procedure performed here with respect to the standard one previously described is that we are able to also monitor differences in relative defocus, this is, power changes. The focal length of the cornea is calculated for the pre-sugery state and kept for all the other visits. This distance is set in order to minimize the root-mean-square spot size at the image plane [Barbero et al. 2002].

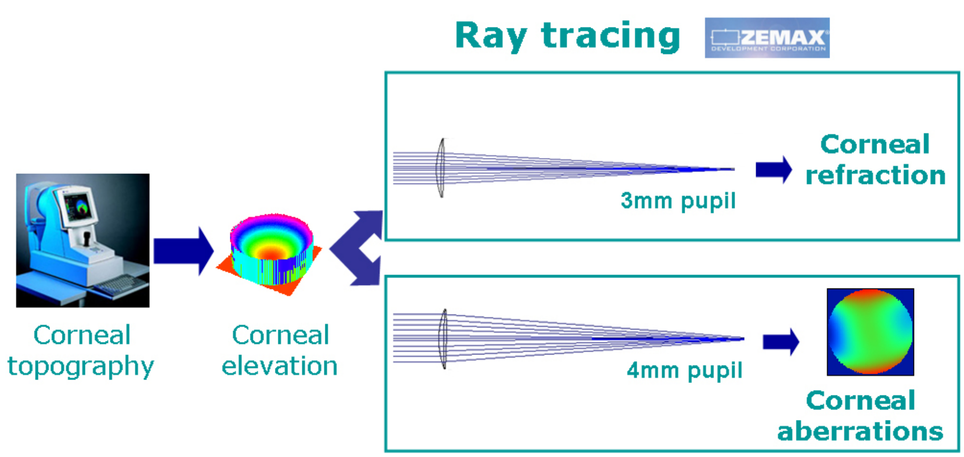

Figure 4.1 Diagram illustrating the procedure for characterizing the cornea from corneal topography.

The corneal WA was based on the average of at least 4 different topographies in every case. The difference between the corneal WA measured at every visit and the one measured for the pre-surgery visit is the induced corneal WA due to the surgery. From the corneal WA and the induced corneal WA, different parameters were analyzed to better understand all the changes due to the surgery in the anterior cornea.

4.3. Defocus and cylinder evolution

Low order corneal WA terms and their induced changes with respect the pre-surgery visit (defocus, horizontal and 45º astigmatism) were calculated for a 3 mm pupil diameter. This pupil size is used to minimize the effect of higher order aberrations. Both, the Zernike coefficients corresponding to every visit, as well as these related to the induced change were converted to the spherocylindrical refractive error in power vector notation [Thibos et a. 2004], according to:

$$\begin{aligned} M &= \frac{-c_2^0 4\sqrt{3}}{r^2} \\ J_0 &= \frac{-c_2^2 2\sqrt{6}}{r^2} \\ J_{45} &= \frac{-c_2^{-2} 2\sqrt{6}}{r^2} \end{aligned} \qquad [4.1]$$

where r is the pupil radius. The sphere, cylinder and axis, as well as the spherical equivalent magnitude corresponding to the clinical minus cylinder convention were calculated from that values [Thibos et al. 1997]. Therefore, the actual and the induced spherocylindrical error is monitored for all the visits along their evolution.

4.3.1. Average and individual changes

The average induced sphere (top left), cylinder (top right) and spherical equivalent (bottom) are shown in Figure 4.2 for the different visits. The incision tends to reduce the power of the cornea, since a positive difference is found. This induced change is reverted between 1 and 4 months post-surgery and stabilizes after that visit. Induced cylinder shows a similar temporal average behaviour. A consequence of these two combined factors is that the induced spherical equivalent remains near to zero during visits (Figure 4.2 (bottom)). This means that both sphere and cylinder are being modified by the incision but since they are coupled, there are no changes in the spherical equivalent. Notably, cylinder and sphere evolution, that tends to reduce their individual value with respect to the initial induced value, are also coupled thereby not altering the average spherical equivalent at any visit.

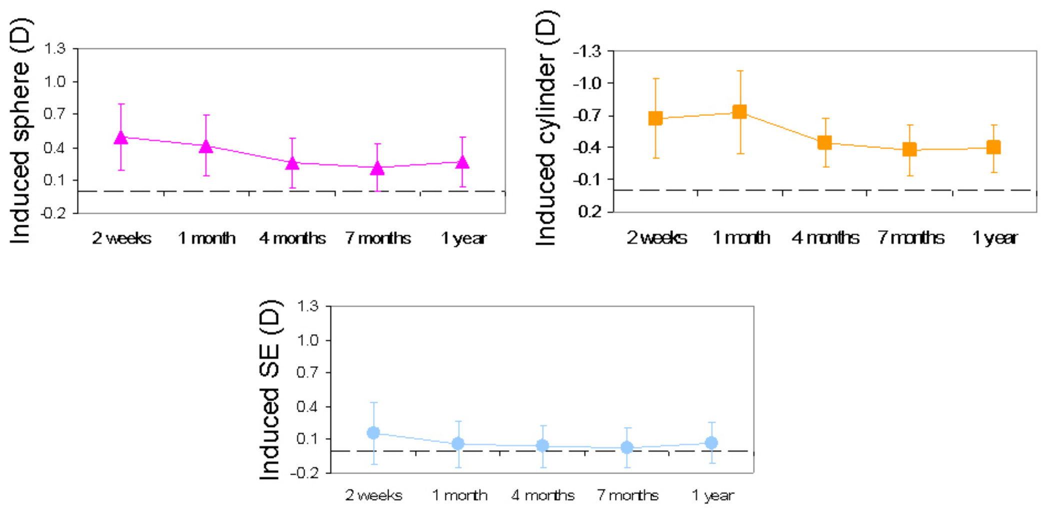

Figure 4.2 Averaged induced low order aberrations evolution. (Top left) Sphere, (Top right) cylinder and (Bottom) spherical equivalent. Error bar represent standard deviation (SD).

Induced effects at the cornea highly dependent on the incision size [Kohnen et al. 1995 and Hayashi et al. 2009]. Nowadays, incisions smaller than 2mm (microincisions) can be performed. In our patients, the average incision size was 3.5mm, and the surgery therefore cannot be considered as microincision surgery. We consider relevant this incision size because it is still commonly used in surgical practice and because not all lenses can be implanted with microincisions. Some of the next generation of accommodating lenses and light adjustable lenses, as these considered in this study, require this type of incision [Ossma et al. 2007]. In addition, this incision size may be considered as extreme. Therefore, the larger effects on the corneal surface are related to that incision size and the impact of smaller incision could be then considered to be within the ranges presented here.

It is important to note however, that corneal spherical equivalent did not change on average at any moment following the surgery. Because IOL power calculations are based on this optical parameter [Olsen et al. 2007], sphero-cylindrical changes due to the surgery do not need to be taken into account to improve these calculations and therefore preoperative corneal topographies can be used to represent the state of the cornea when the IOL power calculation is performed at the circle of least confusion.

The aim of this analysis was not just to study corneal induction and evolution after cataract surgery, but to develop a better understanding of whether we are able to predict what the corneal response will be to small incision surgery and whether this response will be stable. With respect to the sphere's behaviour, we found that the incision causes a significant hyperopic shift in the cornea at early visits, that is almost nullified when the cornea stabilizes. Merriam studied corneal power changes due to incisions of different sizes and locations by comparing keratometric values but found no resulting changes in curvature for a 3mm incision [Merriam et al. 2003]. In our case, the incision was 0.5mm greater on average. Furthermore, the results presented in this chapter are based on ray tracing and therefore the precision of the method may explain the difference at the earlier visits.

When the surgically induced astigmatism (SIA) is considered, it is widely accepted that it depends on the incision´s characteristics [Kohnen et al. 1995, Masket and Tennen 1996, Masket et al. 2009, Tong et al. 2008, Hayashi et al. 2009]. A literature review reveals different values for surgically induced corneal astigmatism for similar incision sizes can be found after different stabilization periods: 2 weeks [Masket and Tennen, 1996, Oshika and Tsuboi, 1995], 1 month [Feil et al. 1994], 6 weeks [Masket et al. 2009] and 3 months [Shepherd, 1989]. After evaluating Figure 4.2, we can conclude that in our population stabilization of corneal astigmatism occurred between 1 and 4 months, since it is after 4 months when the sphero-cylindrical change at the cornea remains stable on average. It is also important to mention that this stable state of the induced corneal astigmatism is reached after an average reversion of 0.3D. In addition, our SIA was -0.4D on average, which is very similar to values previously reported [Kohnen et al. 1995, Masket and Tennen, 1996, Masket et al. 2009]. We did not study the effect of location in SIA, because the number of patients was not enough for a proper statistical analysis.

The progression of induced individual changes is shown in figure 4.3 both for sphere (left) and cylinder (right), where the initial induced value at 2 weeks is plotted versus the induced value both at 1 month and 1 year after the surgery for all the patients. There is a good correspondence between both the induced sphere and cylinder at 1 month and the corresponding initial induction at 2 weeks (r^2=0.46 for sphere and r^2=0.54 for cylinder). However, the correlation between the induction at 1 year and 2 weeks is strongly reduced for sphere (r^2=0.19 for sphere), being almost zero for cylinder

(r^2=0.07). The final induction is lower than the initial value, although the correlation between both parameters is very low. It is important to note that in this comparison the cylinder axis was ignored. The impact of this reversion may be different if the axis of the induction is also modified by the evolution. In order to further understand this point, the axis of the induction will be also considered in the next section.

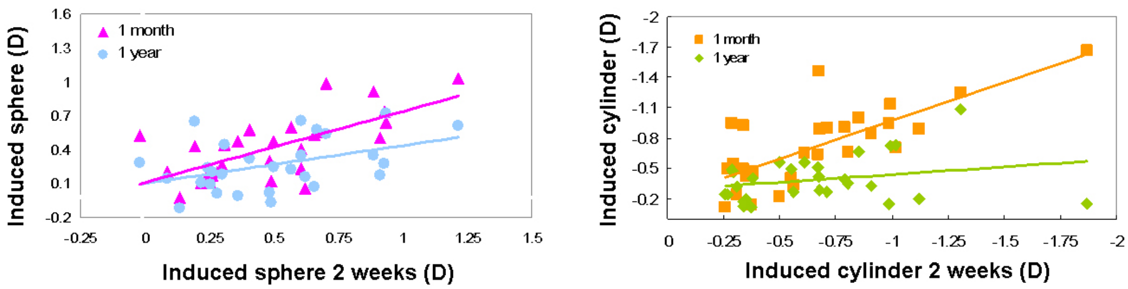

Figure 4.3. Scatter plots showing the individual evolution of induced sphere (right) and cylinder (left).

4.3.2. Cylinder evolution as vector decomposition

The actual cylinder corresponding to every visit was decomposed in two different axes by means of vector summation (Figure 4.4). Cylinder is defined as a vector, whose direction represents the axis and its length the magnitude. Pre-surgery axis (dashed black line) is defined as the axis of the corneal cylinder prior the surgery. Induced axis (dashed red line) is calculated by vector decomposition from cylinder measured two weeks after the surgery (continuous green line) and pre-surgery cylinder (Figure 4.4, left). At later visits, measured cylinder (continuous green line) is decomposed in both defined axis and their evolution can be exactly studied per component (pre-surgery or induced) (Figure 4.4, Right), since the components have been calculated to be referred to the same axis. Then, direct comparison is possible.

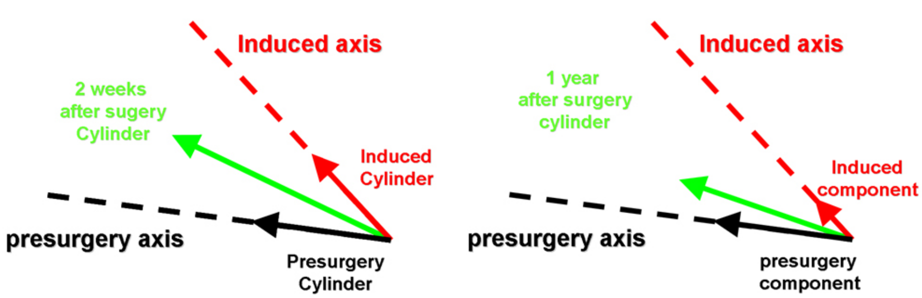

Figure 4.4 Cylinder decomposition procedure.

Cylinder decomposition in the preoperative and induced axis was performed in 20 of the 29 eyes. In the remaining 9 eyes the induced axis was very close to the presurgery cylinder axis. Figure 4.5 shows the incision location in our population. The incision was performed temporally for all right eyes (near 180 degrees), while for left eyes the incision was either nasal (near 180 degrees) or temporal (near 0 degrees). Figure 4.6 shows the induced cylinder at 2 weeks for all the patients in the study both in magnitude and axis. Due to the equivalence between 0 and 180 degrees at cylinder notation, Figure 4.6 shows that the induction was primarily in the direction of the incision.

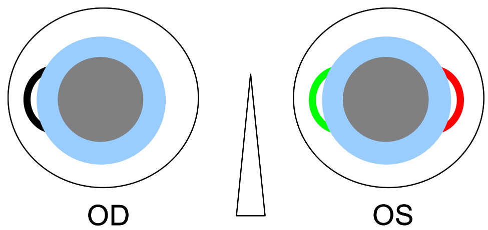

Figure 4.5 Incision locations in the population study depending on the eye which receives the surgery.

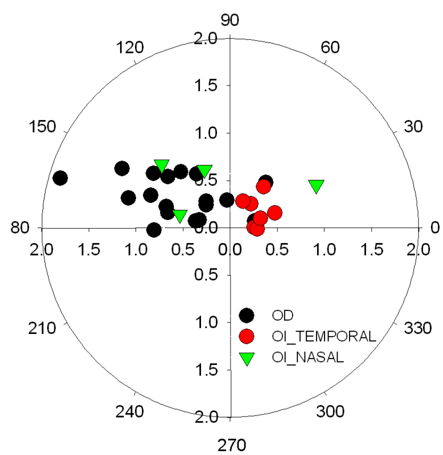

Figure 4.6 Initial induced cylinder both in magnitude and orientation plotted for right eyes (black circles, for left eyes with temporal (red circles) or nasal (green triangles) incision.

Cylinder decomposed in the pre-surgery axis at 1 month and 1 year visit, versus its initial value for every patient is shown in Figure 4.7 (left). The pre-surgery component of the cylinder measured 1 month after the surgery correlates with the pre-surgery cylinder value (r^2=0.54) as well as that measured after 1 year (r^2=0.89). Therefore, the incision does not modify the cylinder at the pre-surgery axis in any visit. Figure 4.7 (right) shows the cylinder component in the induced axis for both the 1 month and 1 year visits, plotted versus the initial induced cylinder. The induced component measured after 1 month of the surgery shows a good correlation with the initial value (r^2=0.44), although the induced value after 1 year does not correlate with the initial induction (r^2=0.02). This shows that the cylinder evolution occurs in this component. Furthermore, the larger induced cylinder values lead to larger changes, reaching an average fixed value after stabilization for all the induced amounts.

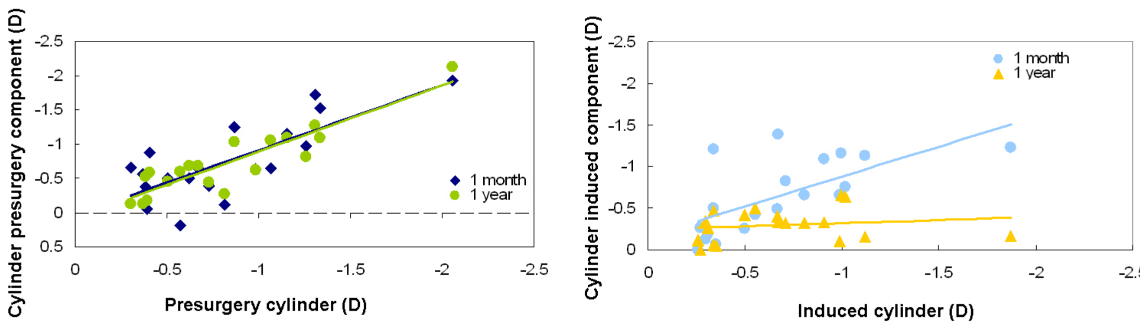

Figure 4.7 Cylinder components (pre-surgery on the left and induced on the right) measured both at the 1 month and 1 year visit versus its initial value.

Figure 4.8 shows the average cylinder in the induced axis for all the visits in the study. It decreases with time reaching -0.3±0.2D at 1 year post-op.

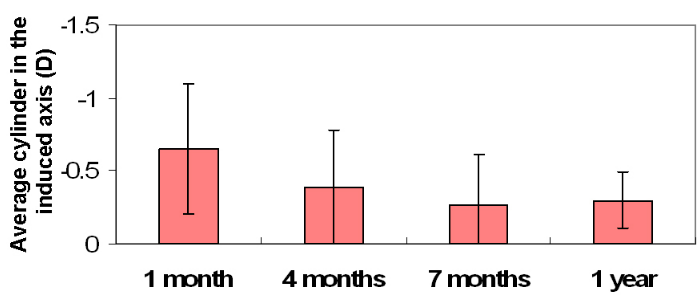

Figure 4.8 Average cylinder in the induced axis for the different measured stages.

Figure 4.9 shows an example for one patient. The preoperative corneal cylinder was -0.5 D at 80 degrees (pre-surgery axis). The cylinder 2 weeks after the surgery was -0.4 D at 16 degrees, therefore the induced cylinder was -0.8 D at 2 degrees (induced axis) (figure 4.8 left). At the 1 year visit, the corneal cylinder was -0.2 D at 61 degrees. By vector decomposition in both presurgery (80 degrees) and induced axis (2 degrees), the presurgery component kept stable, with a value of -0.5 D, being the induced component reduced to -0.3 D (figure 4.9 right). Therefore, the evolution of the cylinder occurred only at the induced axis, reaching the value found for all subjects.

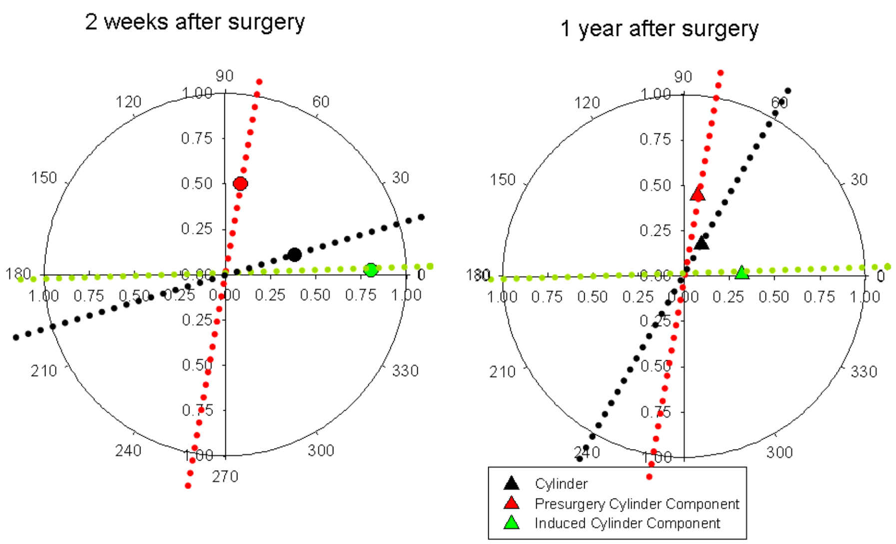

Figure 4.9 Example of cylinder axis decomposition for an individual subject, at 2 weeks (left) and 1 year visit (right).

We have herein demonstrated the clinical common rule that assumes the corneal cylinder after the surgery as the vector summation between the preoperative corneal cylinder and the SIA in direction of the incision [Hill, 2008]. Being more precise, we have demonstrated that we could indeed predict the final cylinder following the surgery by means of a simple model: it will be a vector summation of the preoperative cylinder in its axis and the residual cylinder induced component in the incision axis. This was shown in Figure 4.6 to be equivalent to the induced axis. Regarding the residual cylinder at the induced component, it showed a magnitude after stabilization of -0.3D, according Figure 4.8. Furthermore, once stabilizes, the residual cylinder induced component presents the same value as the SIA found at Figure 4.2 by direct subtraction of the final and preoperative astigmatism. This is possible due to the fact that all the evolution occurs in the induced axis, when the presurgery component is kept. The small divergence between the average residual cylinder at the induced component and the initial SIA found at Figure 4.2 could be due to fact that cylinder decomposition was not possible for all patients in this study because the presurgery axis was the same as the induced axis. It is important to note that the both the SIA and the residual cylinder induced component is found to be independent on the initial induction, since all patients were found to present a constant cylinder in the induced axis at 1 year.

4.4. Evolution of higher order aberrations

Net and induced values for higher order corneal aberrations were evaluated for a 4mm pupil diameter.

Averaged higher order RMS (root mean square of all corneal wavefront terms excluding defocus and second order astigmatism) is shown in Figure 4.10 (top Left) for all visits. With respect to the preoperative value, higher order RMS is increased by the incision at measurement points that closely follow surgery. This amount is reduced approaching preoperative values at 4 months postoperative. Its value remains constant on average for all measurement points past 4 months. Third order RMS trefoil (root mean square of its two third order components, Figure 4.10, Bottom Right) is the main responsible for the initial increase in the higher order RMS because it presents the same temporal behaviour. Contrary to third order trefoil, spherical aberration (Figure 4.10, Top Right) and third order coma RMS (Figure 4.10, Bottom Left) remain stable on average at all the measurement points. This suggests that small incision cataract surgery does not systematically increase corneal aberrations in the long term. The data also indicates that the incision does not change the nature of corneal higher order aberrations.

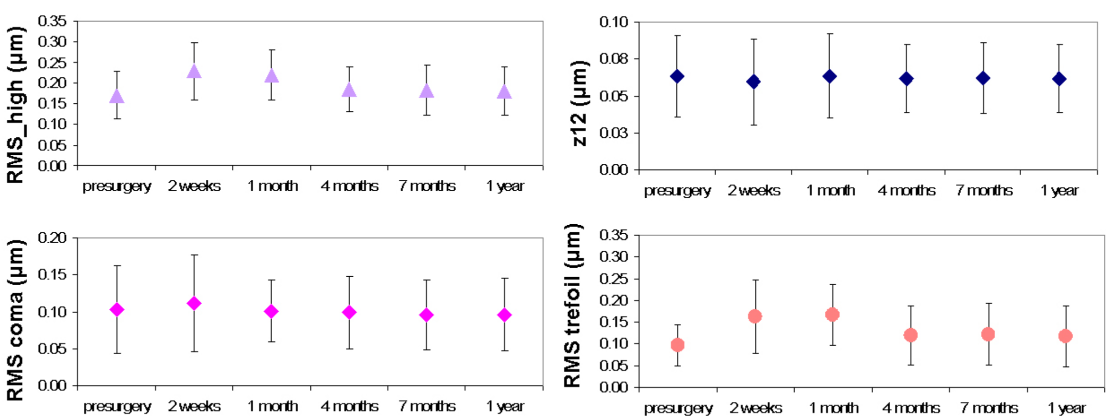

Figure 4.10 Graphs showing optical aberrations averaged for all the patients of the study in all the measured stages at 4mm pupil. (Top Left) Root mean square of higher order terms (RMS_high), (Top right) spherical aberration (z12), (Bottom left) root mean square of third order coma terms (RMS_coma) and (Bottom right) root mean square of third order trefoil terms (RMS_trefoil).

In order to better understand this point, we also calculated the induced aberration with respect to their preoperative values for all the measurement points. There is an induction of higher order RMS that decays with time (Figure 4.11, Top Left). This is consistent with what was found for the average total RMS (Figure 4.10, Top Left). Additionally, the averaged induced value is 65% of the initial higher order RMS after 1 year. This indicates that the incision generates a significant amount of higher order aberrations but it is important to note that the total amount of aberrations was not increased at the latest measurement stages with respect pre-surgery values. Naturally following from this, the orientation of the aberrations should be changed by the incision. The data presented in Figure 4.11 supports this statement, because it shows that on average there is no induction in spherical aberration. However, the induced aberrations are mainly third order coma RMS (Figure 4.11, bottom left) and trefoil (Figure 4.11, bottom right). Therefore, non-rotationally symmetric aberrations are on average most affected by the surgery.

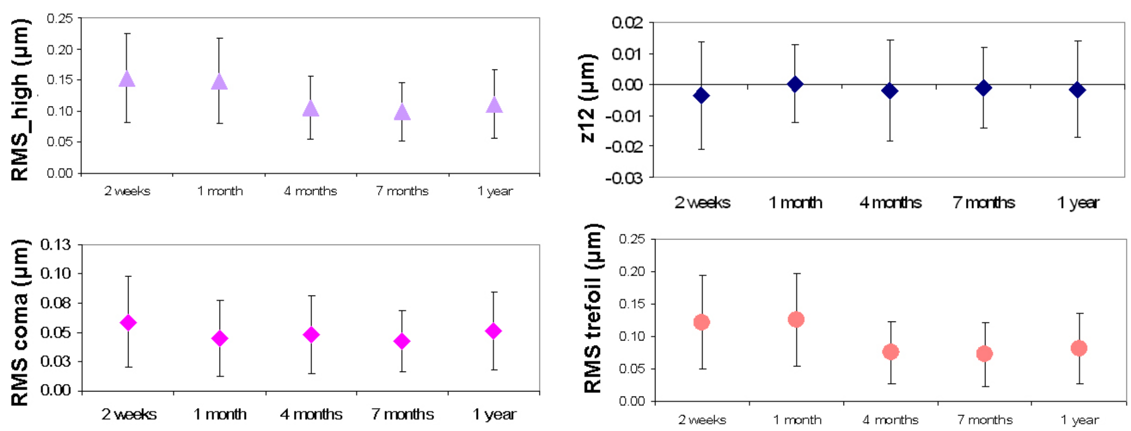

Figure 4.11 Graphs showing induced optical aberrations averaged for all the patients of the study in all the measured stages after the surgery at 4mm pupil. (Top Left) Root mean square of higher order terms (RMS_high), (Top right) spherical aberration (z12), (Bottom left) root mean square of third order coma terms (RMS_coma) and (Bottom right) root mean square of third order trefoil terms (RMS_trefoil).

In Figure 4.12, pre-surgery values for all higher order aberrations are plotted for every subject versus both the induction and final value at 1 year. This type of plots help to understand whether any correlation is found, having in this case a predictive value for the final amount of aberrations from the presurgery stage. Then for example, prior to the surgery a corneal wavefront measurement could be used to predict the final ocular aberration values. Additionally, studying induced values is also interesting because it has been shown that in spite of the fact that the average final amount of the aberrations remain almost unchanged, in some cases, induced aberrations may not be consider negligible. Here we plot only the one year postoperative stage because we have shown that the induced aberrations are stable at this stage and this can be considered the long term state of the cornea following the surgery.

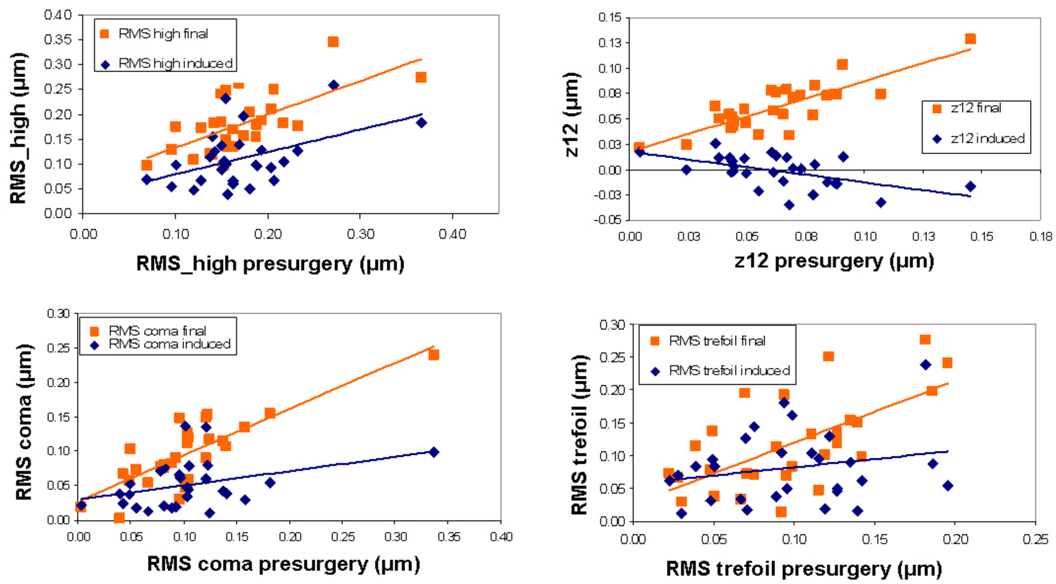

Figure 4.12 Scatter plots showing the initial values for different optical aberration at 4mm pupil versus both the net (orange squares) and induced values (blue rhombus) after 1 year. (Top Left) Root mean square of higher order terms (RMS_high), (Top right) spherical aberration (z12), (Bottom left) root mean square of third order coma terms (RMS_coma) and (Bottom right) root mean square of third order trefoil terms (RMS_trefoil).

In the case of higher order RMS (fig 4.12, Top Left), the higher the pre-surgery value the higher the induced aberrations will be (r^2=0.22). Although the average trend maintains the amount of higher order aberrations, some dispersion may be observed. There are subjects where the induced aberrations increase their final amount of aberrations and others where there is a compensation of part of the presurgery values which lead to a decrease in the final higher order RMS. This is particularly clear in the case of third order coma RMS (figure 4.12, bottom left). The subject originally with the highest amount of this aberration (0.34 µm) was the same subject that experienced the highest amount of surgically induced aberration (0.10 µm), compensating part of his initial aberration value. In the case of trefoil (Figure 4.12, Bottom Right) no significant correlation was found with the induced value (r^2=0.05). On average, spherical aberration was unchanged by the incision, but its behaviour for individual subjects is important to be remarked. The trend found (r^2=0.29) indicates that the incision generates an increase of spherical aberration (Figure 4.12, Top Right) if the pre-surgery value is under 0.058 μm and a decrease if it is a larger value.

Corneal aberrations induced by cataract surgery have been studied before. With the same incision size, Guirao found that the main changes occurred in non symmetrical aberrations (astigmatism, coma and trefoil) [Guirao et al. 2004]. He also studied the orientation of these aberrations with respect the incision location, finding that the position of the incision determines the astigmatism and trefoil pattern. In this study, our focus was in the magnitudes of the aberration rather than in their locations. Because of this fact, we evaluated coma and trefoil as the root mean square of its two third order components, and did not find any correlation between induced and pre-surgery trefoil. Therefore, the induction of this third order aberration must be mainly due to the incision location. This study is therefore in agreement with that of Guirao. On the other hand we found a relationship in between pre-surgical and induced coma. Eyes with higher amounts of pre-surgical coma are more likely to experience a higher change in this aberration, causing either an increase or decrease in its amount. Better control of the surgical effects on this aberration may help for the implementation of new customized lenses aimed at correcting this aberration [Tabernero et al. 2007].

With respect to spherical aberration, intraocular lens designs based on pre-surgery parameters [Holladay et al. 2002] would be affected by important changes in this aberration induced by cataract surgery and the positive effects of these designs may be reduced. Similar to previous studies, we did not find any change on average [Guirao et al. 2004, Negishi et al. 2010]. When looking individually at the patients, a change in spherical aberration was found. Furthermore, the change caused by the surgery seems to be related on its pre-surgical value. This result was also recently reported by Negishi for a 6mm pupil [Negishi et al. 2010]. It is understandable that non symmetric aberrations would be affected by the incision which is also an asymmetrical change. It is however surprising that spherical aberration, which is radially symmetric, has been altered. This may be caused by changes in corneal biomechanics which are still not well understood. However, this result can improve the benefits of aspheric customization shown by Packer when a selection of the IOL is performed taking into account previous measurements of corneal spherical aberration [Packer et al. 2009].

Chapter 5

CUSTOMIZED IOL POWER CALCULATIONS BY MEANS OF RAY TRACING

After showing the suitability of presurgery anterior corneal topographies to represent the postoperative corneal spherical equivalent, in this chapter we analyzed the new optical procedure we presented in section 3.2.3.1 to determine the optimum power of intraocular lenses (IOLs). The IOL power for 19 normal eyes has been determined and compared with standard predictions. The impact of the chromatic and anterior corneal aberrations on the power predictions has been studied.

5.1. Subjects and experimental procedure

To illustrate the capabilities of the procedure, we determined the optimum IOL power for 19 healthy subjects covering a wide range of refractive states (-1.0±3.6D of average refractive error with a range from -8.5D until +4D). The purpose was to demonstrate the complete IOL power computational procedure as well as to compare the results obtained with those provided by standard IOL power calculations procedures. Consequently, these subjects had not undergone surgery.

The complete set of measurements needed for the prediction was first carried out. Three corneal topographies were recorded for every eye to study the possible variability and its impact on the IOL power calculation. Axial length and anterior chamber depth were measured with an optical biometer (IOL Master; Carl Zeiss Meditec, Jena, Germany). The predictions obtained by different standard formulas were calculated for comparison. In particular, the IOL power predicted by the Haigis [Haigis, 2004], Hoffer Q [Hoffer, 1993], Holladay [Holladay et al. 1988] and SRK/T [Retzlaff et al. 1990] formulas were determined, by using optimized IOL constants for the corresponding IOL model considered for the study (an aspheric monofocal IOL, Tecnis ZA9003, Abbott Medical Optics, Santa, Ana, CA, USA).

Three personalized eye models were built for each subject considering the three anterior corneal topographies recorded. From these models, the final IOL power was determined with our procedure to be the mode of the three results, due to the fact that IOL powers were selected in 0.5D steps. Consequently, IOL power retrieved by each paraxial formula was also rounded according to that. Variability in the calculations due to different topographies was also studied with respect to isolated anterior corneal aberrations computed separately.

5.2. Comparison with standard IOL power calculations

The results of the comparison between current IOL power calculations for normal patients and those retrieved by our customized procedure are presented in this section. Different metrics have been considered for this comparison, as the average IOL power over the population obtained by each method as well as differences between the IOL power predicted by our procedure and the different formulas. This was done since the final refraction was unknown because subjects did not undergo surgery and to avoid the bias due to the residual error calculation, that is modulated by the selected method for its calculation. These differences are presented also in average and as a function of different parameters as the preoperative refractive error and the amount of anterior corneal aberrations.

5.2.1. Average IOL power differences

The average, standard deviation and median IOL power over the population are shown in Table 5.1. All procedures yielded similar average values. In order to explore the relation between the results of ray tracing and the other approaches, the IOL power resulting for each paraxial formula is plotted as a function of the IOL power calculated by our procedure in Figure 5.1. There is a good correlation between the results predicted by standard formulas and our method, although it is possible to observe some differences, especially for higher and lower IOL powers.

	Predicted IOL power (D)	
Method	Mean ± SD	Median
Custom IOL power	19.69±4.96	21.25
Haigis	20.19±4.73	21.75
Hoffer Q	19.81±4.91	21.25
Holladay I	19.92±4.66	21.25
SRK/T	19.92±4.56	21.25

Table 5.1. Predicted IOL power over the population

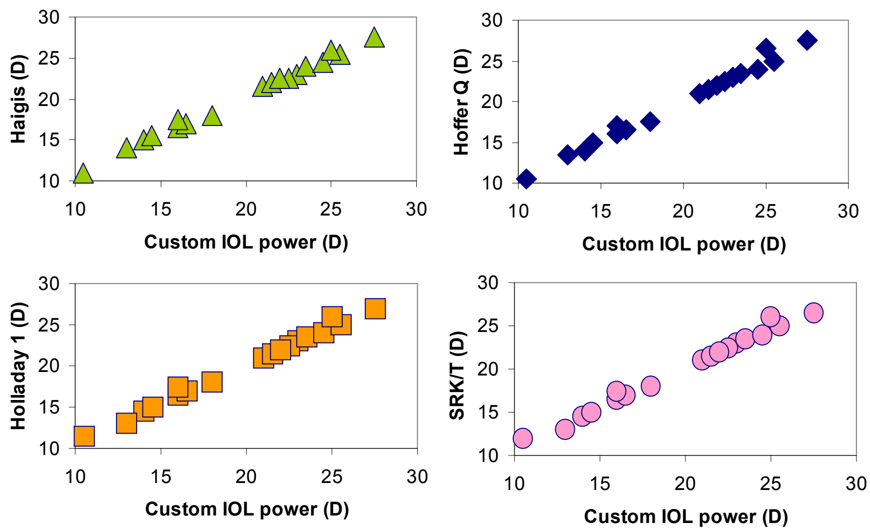

Figure 5.1. Scatter diagram showing the IOL power predicted by different paraxial formulas as a function of the result of our customized procedure.

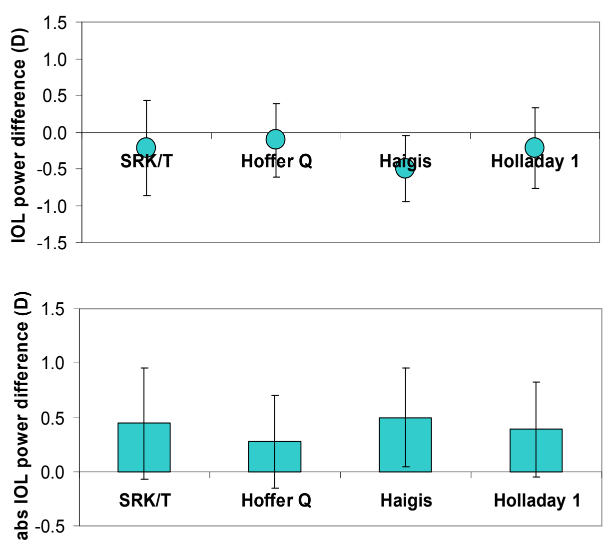

Figure 5.2. (Top) Average difference between the IOL power calculated by our procedure and different existing formulas for all the subjects included in the study and (Bottom) absolute difference between our procedure and standard formulas.

The average differences for all the subjects between the IOL power predicted by ray tracing and different standard procedures are shown in Figure 5.2 (top), together with the average absolute difference (Figure 5.2, bottom), in order to account for sign compensations. These figures do not show significant differences on average between the customized procedure and standard calculations. It should be noted that the difference between formulas is also small.

5.2.2. Individual differences as a function of refractive error

Figure 5.3 shows the differences for each subject between the IOL power calculated in the customized eye model and those retrieved by different formulas as a function of the subject's refractive state. For emmetropic eyes, the maximum difference found was 0.5D, which is the step in power for most IOL models available. For these eyes all the formulas provide relatively similar IOL power outcomes, but for myopes and hyperopes the differences increase. From this result we only can state the differences but we do not know the exact power value.

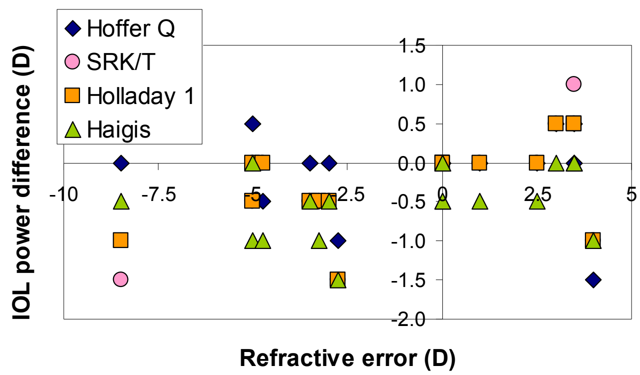

Figure 5.3 Difference between the ray tracing prediction and standard IOL power calculations as a function of subject's refractive state.

Differences also increase between standard formulas with increase in refractive error, establishing also their inaccuracy in those cases. Different solutions has been suggested to increase the accuracy of IOL power calculation considering these formulas, from the selection of the formula which yields the lowest mean absolute error depending on the axial length [Hoffer, 2000 and Aristodemou et al, 2011], the modification of the A constants [Haigis et al. 2009], a myopic targeting for an emmetropic outcome or the transformation of axial length measurements to improve refractive outcome in extreme eyes without sacrificing the outcome in normal eyes [Norrby et al. 2003]. However, the regression and paraxial nature remains leading to outliers. In order to emphasize this finding, Figures 5.4 and 5.5 show the particular case of ammetropic extremes. As an example, in Figure 5.4, the area under the radial MTF as a function of IOL power for the most myopic patient (-8.5D) is shown. In this case, the maximum corresponds to a power of 10.5D, which is the IOL power chosen by the ray tracing procedure. The different standard formulas predict different IOL power, ranging 10.5D for the Hoffer Q formula, to 12.0 D for the SRK/T formula. The corresponding point-spread functions (PSFs) computed in the eye model for the different IOL powers are also displayed, just as an indication of the optical quality with different IOL powers evaluated. The AXL of this particular subject was 25.50 mm. According to previous studies, the Holladay 1 performed better for an axial length range between 23.50 and 26.00 mm, although the SRK/T and Hoffer Q yielded comparable refractive outcomes [Aristodemou et at, 2011]. The differences between the IOL powers calculated with various formulas is indeed an evidence of the inconsistency of the current state of art for IOL power calculation and the need of a robust procedure. A surgeon having this subject as a patient would have problems to select the IOL power to implant due to the dispersion in the prediction yielded by different formulas and the indication of the literature, which does not point any particular formula as having a higher accuracy.

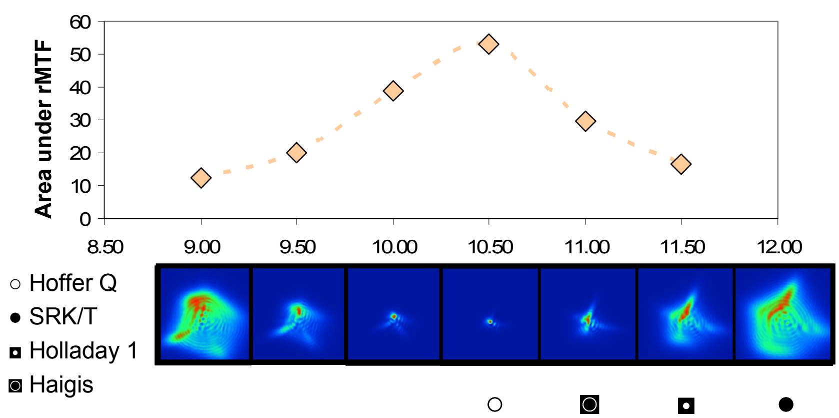

Figure 5.4 Most myopic (-8.5D) patient's overview. Top. Area under the radial MTF for a wide range of IOL powers. Bottom: PSF for each IOL power. Symbols indicate the IOL power yielded by different standard calculations.

Figure 5.5 presents similar information for the most hyperopic eye of the study (+4D). In this case, the maximum for the area under the radial MTF is lower than in the previous myopic subject due to higher amount of anterior corneal aberrations (higher order root mean squared (RMS) was 0.21μm compared to 0.10μm for the previous eye, both calculated at 4mm pupil). Due to the discrete sampling in IOL powers, the maximum is found between 24.5D and 25D, so the IOL power chosen for this patient was 25D. The closest prediction for the regression formulas is 1D higher for three of them and 1.5D higher for the Hoffer Q formula.

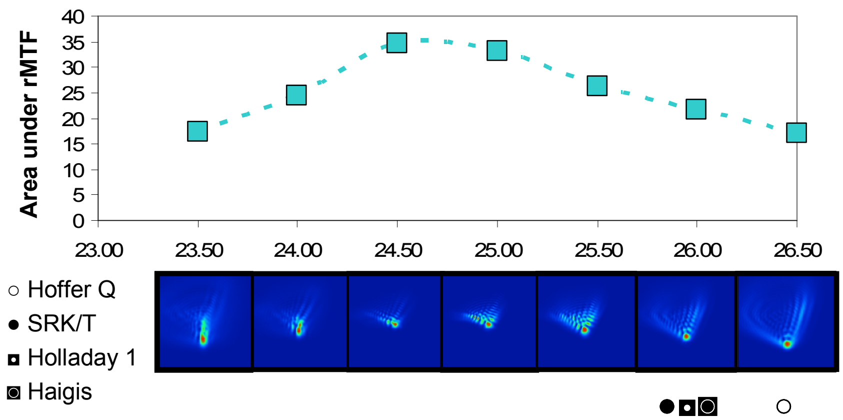

Figure 5.5 Most hyperopic (+4.0D) patient's overview. Top. Area under the radial MTF for a wide range of IOL powers. Bottom: PSF for each IOL power. Symbols indicated the IOL power yielded by different standard calculations.

5.2.3. Individual differences as a function of anterior corneal aberrations

The differences between the IOL power predicted by the model for each patient and those calculated by the different formulas are plotted in Figure 5.6 versus the corneal aberrations RMS for a 4mm pupil. For these eyes, there is no a clear trend relating the differences between IOL power predictions and anterior corneal aberrations.

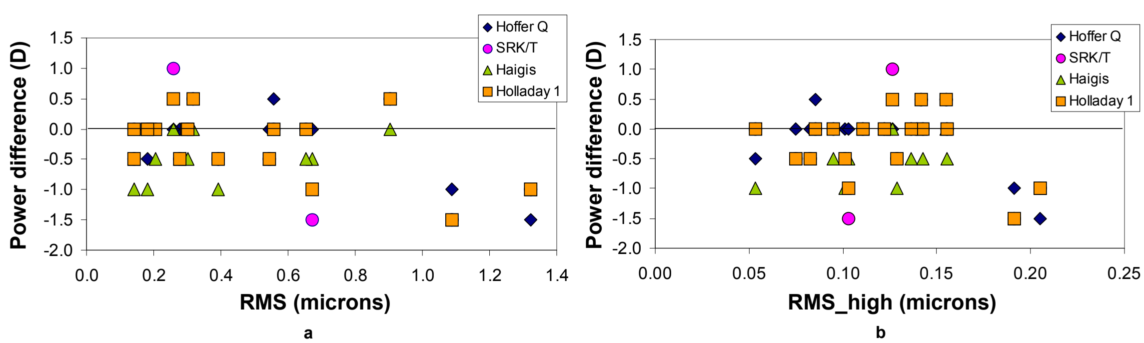

Figure 5.6 IOL power differences between the customized ray tracing procedure and standard formulas versus (a) corneal RMS and (b) corneal higher order RMS calculated for 4mm pupil.

In older subjects the average pupil for photopic conditions is about 3.5 mm while in mesopic conditions is around 5 mm [De Loewenfeld, 1979]. For those pupil sizes and especially at 5 mm, aberrations play a role in optical performance, so paraxial optics should not be used. In this study, we decided to use 4mm as pupil size since it´s realistic for cataract patients when considering the previously reported pupil sizes. However, we didn´t find a correlation between the difference with standard paraxial formulas and our predictions. This may be due to the fact that we included normal eyes that were not highly aberrated. To show the importance of the aberrations in IOL power prediction, we selected one subject and we calculated the IOL power with our procedure considering the natural corneal aberrations and with two, three, four and five times the amount of these corneal aberrations, obtained as a re-scale of the original Zernike terms (Fig. 5.7). The optimum value of IOL power becomes different as higher is the amount of corneal aberrations. Obviously, these changes would not affect the regression formulas due to their paraxial nature. The amount of aberrations is an example that might be high but not unusual in real eyes. For example, those eyes that had undergone standard LASIK surgery present increased amounts of corneal aberrations. For them, even the highest level of aberrations used in the example is plausible.

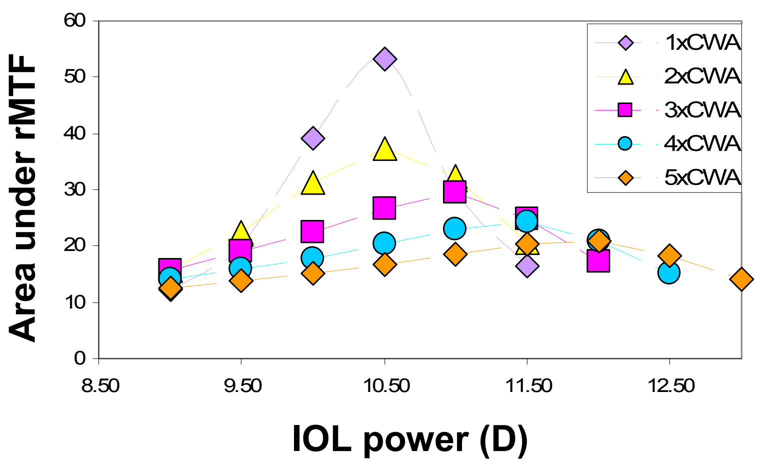

CWA	RMS_high
original	0.0973
x2	0.1946
x3	0.2919
x4	0.3892
x5	0.4865

Figure 5.7 Area under the radial MTF calculated with our customized procedure as a function of the IOL power for different amounts of corneal aberrations (CWA) referred to 4mm pupil. Their impact on IOL power calculation is studied by increasing the original aberration pattern up to 5 times.

5.3. Combined effect of corneal aberrations and polychromatic calculation

In addition to monochromatic aberrations, polychromatic behaviour is also considered in our model. To our knowledge, there is no other IOL power calculation method incorporating this aspect, which may be important for a realistic simulation of the optical quality of the eye. In this direction, recently, the visual impact of correcting spherical and chromatic aberrations was evaluated [Artal et al. 2010]. It has been also shown that chromatic aberration in pseudophakic eyes is mainly due to IOL material [Zhao and Mainster 2007]. In order to emphasize the importance of the combined effect between monochromatic and chromatic aberrations in IOL power calculations we had performed the IOL power prediction with our ray tracing procedure in different conditions. For that comparison, we considered four virtual IOL materials, with having the same index at d-light (587.6 nm), and different Abbe numbers, ranging from 17 up to 77. The impact of pure chromatic aberration can be seen in Figure 5.8. That figure contains the results that the ray tracing procedure yielded in white light and monochromatic conditions (540 nm) when a particular subject is implanted with four virtual IOL models having the same geometrical properties but different materials, with the dispersion properties previously described. Because the aim was to show the impact of chromatic aberration, corneal aberrations were corrected in all the calculations showed at Figure 5.8. As expected, there is less difference between both calculations for that material having highest Abbe number, leading to the same calculated IOL power. In fact, chromatic aberration starts to play a role only for very dispersive, non realistic IOL matherials, since available IOLs present Abbe numbers between 35 and 60 [Zhao and Mainster 2007].

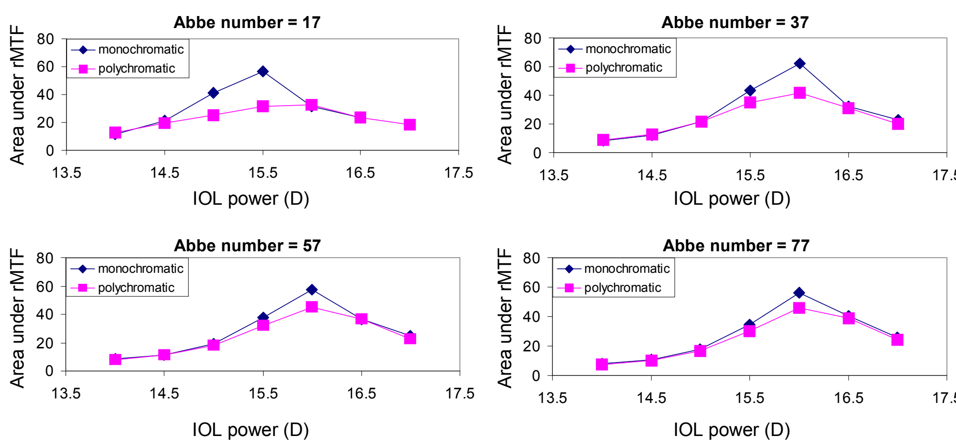

Figure 5.8 Area under the radial MTF calculated with the customized procedure, correcting corneal aberrations, as a function of the IOL power with different IOL materials. Therefore, in this plot we show the pure chromatic aberration effect due to the IOL material's dispersion.

The scenario is different when corneal aberrations are added to the model and considered in the IOL power prediction (Figure 5.9). It is important to note that the calculation retrieves in this case lower MTF values than in Figure 5.8, due to the consideration of corneal aberrations. These affected the monochromatic calculation, which yielded a different IOL power than the polychromatic procedure for lower although realistic IOL's Abbe numbers (37). Then, it can be concluded that the impact of chromatic aberration is modulated also by monochromatic aberrations. It is important to note that current IOL power calculations do not incorporate dispersion effects and for that reason cannot differentiate between IOL materials.

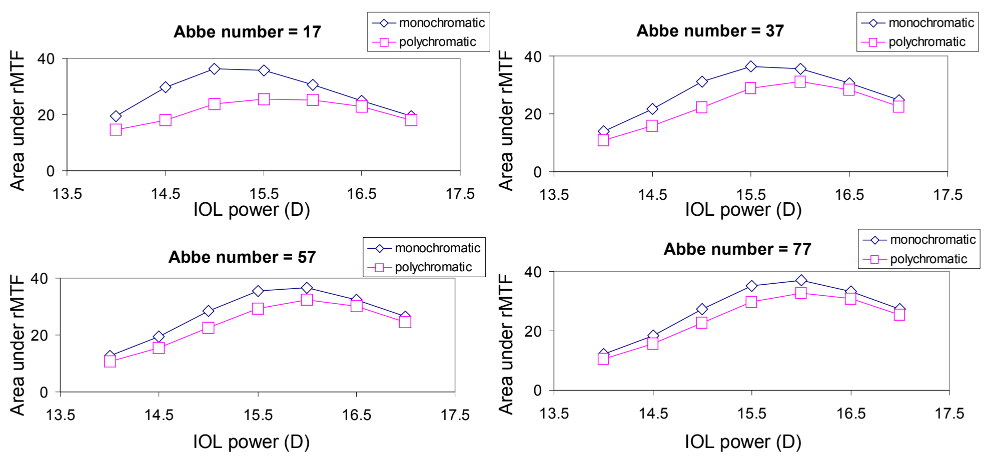

Figure 5.9 Area under the radial MTF calculated with our customized procedure, including corneal aberrations, as a function of the IOL power with different IOL materials. Therefore, in this plot we show the combined effect between chromatic aberration due to the IOL material dispersion and corneal aberrations.

5.4. Sources of error in the procedure

The introduction of the different biometric parameters in the ray-tracing prediction can be a limit of its accuracy because the inherent errors involved to those measurements. Norrby [Norrby, 2008] quantified the sources of error in IOL power calculations, finding that the most limiting parameter is the IOL placement prediction, followed by the actual determination of the postoperative refraction and the different biometric parameters considered in the calculation. In this section we analyzed the impact of two of the parameters involved in the procedure: on one hand we study the influence of introducing a different ACD prediction in our ray tracing prediction. On the other hand, the impact of corneal topography in the procedure, due to the fact that we are calculating the IOL power as the mode of the result retrieved by three different eye models per subject, coming from three different corneal topographies.

5.4.1. ACD prediction

Because the position of the IOL after surgery should be predicted in order to calculate the IOL power to implant, different approaches may be considered. The most desirable would be to have a fully theoretical model which predicts the IOL position after surgery based on patient's anatomical data and IOL mechanical properties. On the other hand, an empirical procedure may also be considered, by relating preoperative anatomical data with the postoperative IOL placement in patients that had undergone a surgery. On the limit of pragmatism, it is also possible to adjust the IOL position in order to be able to predict the postoperative refractive error in those patients. In our approach, the first empirical approach was selected. The actual IOL location after surgery is based on a relationship between the natural lens position (pre-surgery) and the measured IOL position. This relationship was found in a previous study involving patients that underwent surgery. Therefore, this is the only input of the model that is based on non fully customized data, although the lack of optimization should be noted. We decided on using that semi-empirical procedure, due to the lack of data that will lead to fully understand the mechanism which underlies in the final IOL position, that is essential to generate a more theoretical model.

Because we are using an exact ray tracing procedure, the effective lens position as used in paraxial formulas cannot be introduced here. Previous studies with either the thick lens theory or ray tracing have faced the same problem. Olsen [Olsen, 2004] and Norrby [Norrby et al. 2005] have developed elaborated actual lens position predictions based on multiple biometric parameters. These or another actual lens position can be introduced in the customized ray tracing procedure that we are presenting in this paper in order to evaluate their accuracy.

To evaluate the impact of a different IOL placement prediction on the ray tracing procedure, we repeat the calculations for the population included in the study by using an ACD prediction recently presented [Norrby et al. 2010]. We decided to use this prediction because it has been developed for the same IOL model we are using here and it includes axial length and anterior chamber depth, which are parameters we measured in the present study. Figure 5.10a shows the relationship between both ACD predictions for all the population of the study (r^2=0.63). The average difference between both predictions was 0.11±0.15 mm, resulting our prediction in a deeper IOL placement on average than that developed by Norrby et al. There is a subject that seems the responsible of that trend. Indeed, when this subject is removed the correlation is weaker, although still significant (r^2=0.49). Furthermore, the average difference between both predictions is also similar (0.12±0.13 mm). It is also well accepted that the ACD prediction is highly correlated with axial length. However, we did not include this parameter in our prediction. In order to explore the impact of axial length in the IOL position prediction, we represent in Figure 5.10b the difference between ours and Norrby's approach, which includes the AXL as predictor, as a function of eye's axial length. There is, in fact, a linear correlation between the difference and AXL, although there was some dispersion, leading to a weak correlation between both parameters (r^2=0.27). Further studies will reveal the method achieving the highest accuracy for the IOL power procedure, although we still believe that a fully theoretical customized procedure for IOL placement is the best approach in order to complete the eye modelling for IOL power calculations.

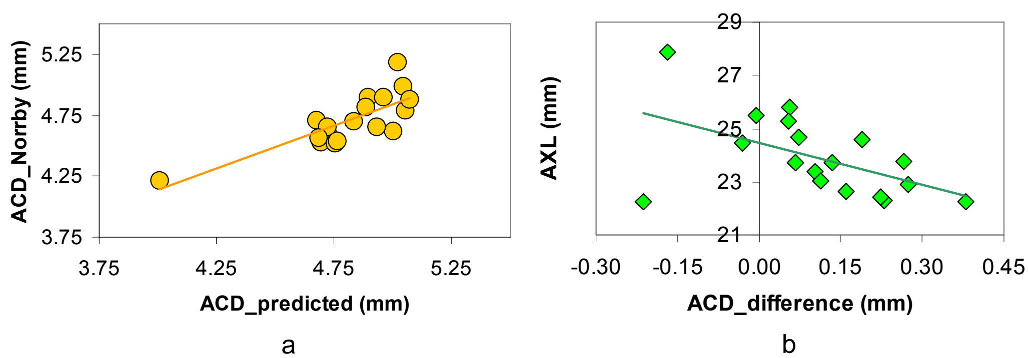

Figure 5.10 (a) ACD prediction used in this work versus the Norrby's prediction [Norrby et al. 2010] for all the study population and (b) difference between both ACD predictions as a function of the axial length.

To explore the impact of these differences in the IOL power prediction, we applied the same ray tracing procedure, by generating three customized eye models corresponding to three different corneal topographies per subject, being the selected IOL power the mode of them. Then, the only difference between previous and these results is purely the IOL placement prediction, considered in this case as Norrby et al [Norrby et al. 2010]. Figure 5.11 shows the IOL power difference between the ray tracing prediction considering our ACD prediction and Norrby's as a function of the ACD difference. As expected, a deeper IOL placement will lead to a higher predicted IOL power, although there is a range where different ACD placement does not translate to a difference between both predictions. This is due to the fact that we are considering an IOL model with 0.5D steps. However, we did not find an ACD difference value wherein there is a clear step into the higher or lower IOL power. This might be related to the fact that the IOL power selection is based on the mode of the results related to three different corneal topographies, making more complex the results interpretation.

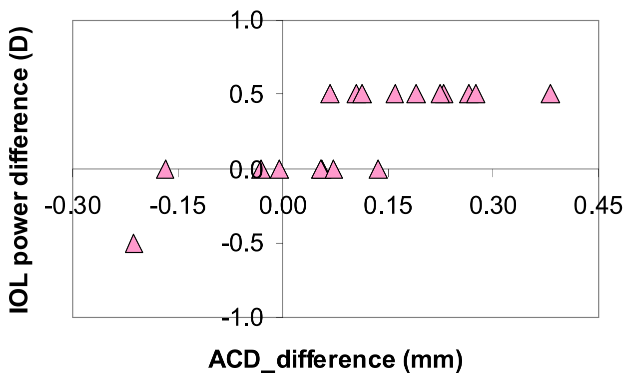

Figure 5.11 IOL power difference between ray tracing considering our ACD prediction and that presented by Norrby et al as a function of the difference between ACD predictions. In both cases, the Norrby prediction is considered as a reference. Therefore, both the IOL power and ACD differences are our approach minus Norrby's.

Although there are differences in the ACD placement, the maximum discrepancy between ray tracing approaches is 0.5D, which is the IOL power step and the variability in the procedure, as we show in Figure 5.11. In addition, the average IOL power with the Norrby's ACD prediction was 19.44±4.84D with a median of 21D, the lowest of all the methods considered in the study, including the ray tracing approach with the ACD prediction herein presented, as can be seen at Table 5.1. However, as we had pointed out, we do not have subject's final refraction results, because they did not undergo cataract surgery. Therefore we can only establish differences between procedures. Further clinical studies will show the most accurate procedure for ACD placement to predict IOL power by ray tracing, although the point of this comparison was also to show the plasticity of the procedure to adopt different ACD predictions.

5.4.2. Corneal topography errors

The IOL power determined was the mode of the values calculated for each of the three topographies recorded for each patient. The maximum spread between results within one single eye was 0.5D. In order to investigate the reason for this difference, subjects were divided in two groups: those with no deviation in the IOL power calculation prediction between topographies and those with a 0.5D change among topographies. Figure 5.12a shows the averaged standard deviation for anterior corneal aberrations RMS (without considering defocus) and anterior corneal astigmatism RMS for both groups. For the group with dispersion, the standard deviation between topographies was higher especially due to corneal astigmatism. Figure 5.12b shows for both groups, the averaged standard deviation for higher order RMS and different third order aberrations as well as spherical aberration. It can be concluded that these factors are not the cause of the spread in IOL power predictions within eyes, as similar values are shown for both groups. Higher order RMS standard deviation was higher for the group with 0.5D dispersion due to coma and trefoil.

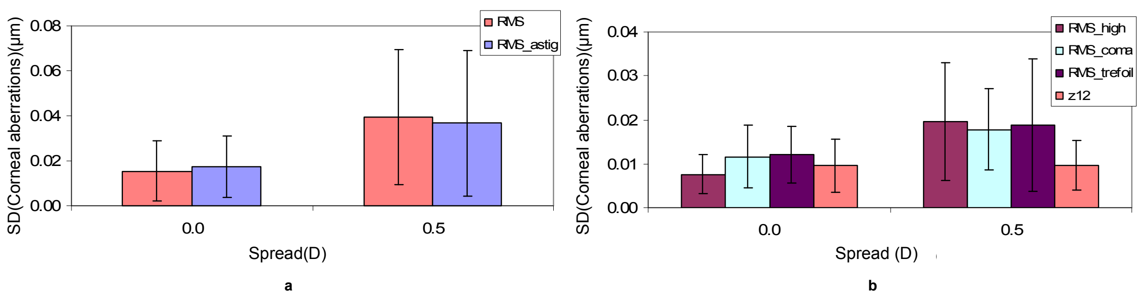

Figure 5.12. Standard deviation for different corneal aberrations (a, RMS and astigmatism, and b, higher order RMS, third order coma, trefoil and spherical aberration) for both, the group of subjects with no difference in computed IOL power through the 3 corneal topographies considered and those with 0.5D difference.

In conclusion, the variability between topographies showed a maximum difference of 0.5D between power predictions. This variability could be avoided by a prior evaluation of those corneal topographies. Therefore, only those topographies within an astigmatism standard deviation smaller than 0.05 microns should be considered for the IOL power prediction.

Another possible limitation to the procedure is the introduction of a fixed equivalent refractive index to account the power of the posterior corneal. Although there are instruments measuring the posterior corneal surface, we believe that the current model incorporating anterior corneal aberrations provides enough important and valid information without increasing the amount of experimental errors in the procedure. Then, the extension of the procedure to consider the posterior corneal is possible, however it would be subject of further research. In addition, the modification of the calculated equivalent refractive index for post-LASIK patients will be described in chapter 7 of the present thesis.

It is important to note that we are using presurgery anterior corneal topographies for calculating IOL power. It has been shown in the previous chapter that cataract surgery induces and modifies corneal aberrations. Although this is the case for higher order aberrations as well as sphere and cylinder, we have shown that the circle of least confusion is unchanged by cataract surgery. Because we are actually calculating the IOL power minimizing this parameter, we can conclude that our procedure is not affected by the changes that surgery imposes in anterior cornea.

Chapter 6

IOL POWER CALCULATION BY USING CUSTOMIZED RAY TRACING IN NORMAL CATARACT PATIENTS

Different aspects related to the customized ray tracing procedure were discussed in the previous chapter. Although the results were in agreement with those in the previous literature, the validity of the procedure was not fully established, due to the fact that post-surgery refraction data were not available because subjects did not actually undergo surgery. Therefore, in this chapter the validity of the procedure in normal cataract patients will be shown as well as its real limitations from a set of cataract patients who were enrolled in a clinical study.

6.1. Patients and protocol

Eighteen normal cataract patients were examined before and after cataract surgery between 2008 and 2009 in the Ophthalmology Service at the "Virgen de la Arrixaca" hospital (El Palmar, Murcia, Spain). All patients included were cataract patients with otherwise healthy eyes, with normal biometric parameters. The research followed the tenets of the Declaration of Helsinki, and all participants provided written consent.

Corneal topography and biometry measurements (axial length and anterior chamber depth) were performed prior the surgery. The instruments used were a Placido based corneal topographer (Atlas; Carl Zeiss Meditec, Dublin CA), an optical biometer (IOL Master; Carl Zeiss Meditec, Jena, Germany) and a conventional ultrasonic system (OcuScan RxP, Alcon, Forth Worth, Texas, USA). Due to the degree of the cataract in some of the patients, optical measurements were not possible and therefore, axial length was measured with the ultrasonic device in the contact method.

All cataract surgeries were performed by the same surgeon (José María Marín) using a small incision technique following the implantation of an aspheric monofocal IOL (Tecnis ZA9003, Abbott Medical Optics, Santa, Ana, CA, USA). The IOL power implanted was selected by the surgeon according to his standard practice. Postoperative measurements were taken one month following the surgery. The same measurements taken preoperatively were performed postoperatively in addition to an accurate subjective refraction based on objective measurements. As a summary, three wavefront aberration measurements are recorded from each patient, using a purpose-designed Hartmann-Shack sensor [Prieto et al, 2000]. From the mean, the objective refraction (sphere and astigmatism) was determined. These values were used as the starting point for the final subjective refraction. From this refraction, the spherical equivalent (SE) was calculated and translated optically to the IOL plane. In each case, this value was added to the IOL power that was implanted, leading to the determination of the optimum IOL power for each patient.

6.2. Custom IOL power prediction validation

The IOL power prediction for each patient was performed by using the customized ray tracing procedure described in section 3.2.3.1. that was build from biometric measurements previously described. For each patient, the procedure is repeated 4 times with 4 different measured topographies. The final IOL power given by the method is the mode of the four predictions.

This procedure can be performed with and without the introduction of corneal aberrations, as was mentioned when the complete ray tracing prediction was described. In the first case, the complete set of elevations retrieved by the corneal topographer is introduced in the model. The IOL power calculated using this procedure is called “custom+CWA” (Figure 6.1). In the second case, only the spherical equivalent power of the cornea is the input. The result of this calculation is called “custom-CWA”. We calculated the IOL power with the ray tracing procedure in both cases for all patients included in the clinical study. We termed the difference between these predictions as corneal wavefront influence (CWI).

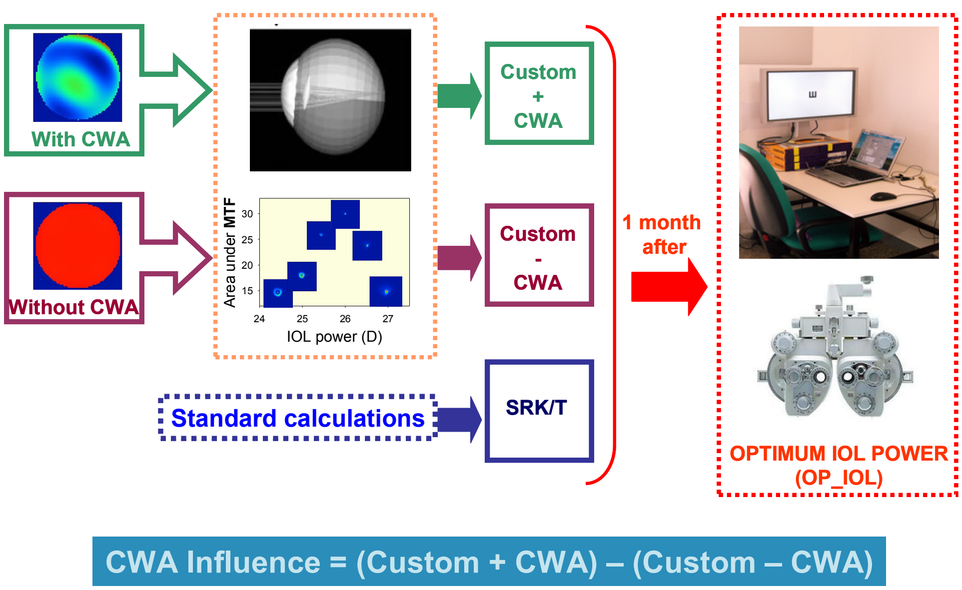

Figure 6.1 Procedure description and CWI definition.

For normal patients, the SRK/T prediction [Retzlaff et al. 1990] was also calculated for comparison purposes.

All IOL power predictions were subtracted from the optimum IOL power determined after the surgery for each patient. In addition, the difference between IOL powers was transformed back to the spectacle plane in order to calculate the residual spherical equivalent error predicted by all procedures. The two sample (paired) t-test was used to evaluate the statistical significance of the difference between mean and mean absolute residual errors, while the consistency in the prediction was tested by means of the f-test for variances.

Figures 6.2a and 6.2b show the average residual spherical equivalent and mean absolute spherical equivalent error retrieved by all the predictions. Although the mean arithmetic residual spherical equivalent was statistically significantly different between the SRK/T and both ray tracing predictions ($p<0.05$), the mean absolute error showed no statistical differences.

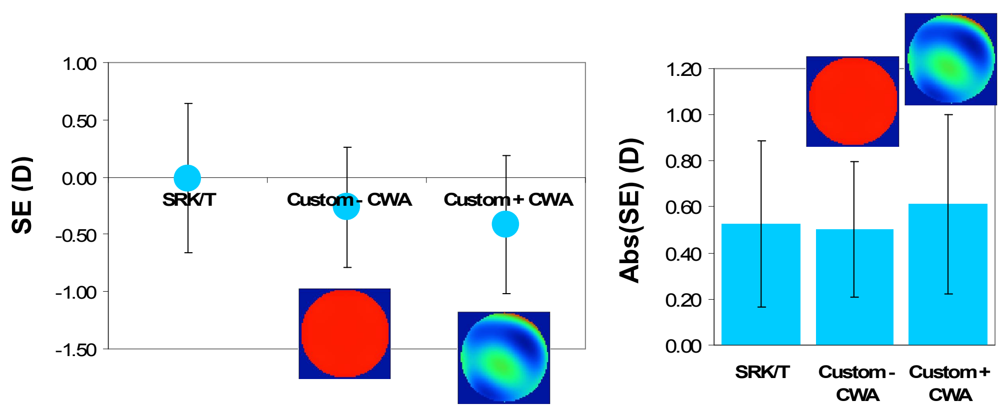

Figure 6.2 (a) Mean spherical equivalent refractive error for the normal cataract population included in the study achieved by the SRK/T and our procedure with (Custom+CWA) and without (Custom-CWA) corneal aberrations (b) mean absolute spherical equivalent refractive error

All the procedures showed the same consistency in the calculation because there were not statistically significant differences in variances. Therefore, the accuracy of the SRK/T and both ray tracing predictions can be considered as similar. This verifies the accuracy of the procedure as the SRK/T formulas has been shown to have similar levels of accuracy to other paraxial formulas for normal patients [Hoffer, 2011b and

Aristodemou et al. 2011]. We classify normal patients to be those having close to average axial lengths. The average axial length of the normal population we considered in our study was 23.7±0.8mm. Then, their classification as average eyes is fully justified.

It is important to note that the ray tracing prediction is based only on the direct optical treatment of patient´s data. Paraxial formulas optimize the A constant in order to keep the average prediction error close to zero, as can be seen in Figure 6.2a for the SRK/T formula. The lack of A constant in the ray tracing approach makes it more sensitive to measurement errors [Norrby, 2008]. In the ray tracing procedure, the average residual error was statistically significant different than the SRK/T, but not the mean absolute error as well as the variance. The fact that the mean spherical equivalent error is greater for the ray tracing procedure is a reflex of the optimization for the A constant used in the SRK/T prediction. There are not fudged parameters in the ray tracing procedure that can compensate for experimental errors. On the other hand, the consistency of both procedures is similar because the variance is not statistically different.

Therefore the similarity in the predictive results for both methods is in fact a validation of the ray tracing procedure. In other words, ray tracing can be used in order to calculate the optimum IOL power for a specific lens and an individual patient. Future developments on the procedures related to the introduction of the posterior cornea to avoid the use of an equivalent refractive index as well as an improved IOL placement prediction algorithm may improve the outcomes of the ray tracing prediction.

6.3. Effect of the amount of corneal aberrations in the IOL power prediction

Corneal aberrations were also calculated for each topography measurement by means of ray tracing in a separate model following the procedure described in section 3.2.2 and averaged for each patient. In this case, the focal is set to minimize the root-mean-square spot size at the image plane for a 4mm pupil, the same pupil for which corneal aberrations are calculated.

The difference between ray tracing predictions due to corneal aberrations, corneal aberration influence (CWI), as previously defined, is plotted versus its amount in Figure 6.3. Corneal aberrations are represented as the root mean square of all 3rd-order and above wavefront aberrations (RMS_high). There was a slight correlation between both parameters (r^2=0.58). It is important to note that the maximum difference between ray tracing predictions was 0.5D, which was also the power increment for IOL model considered in this study.

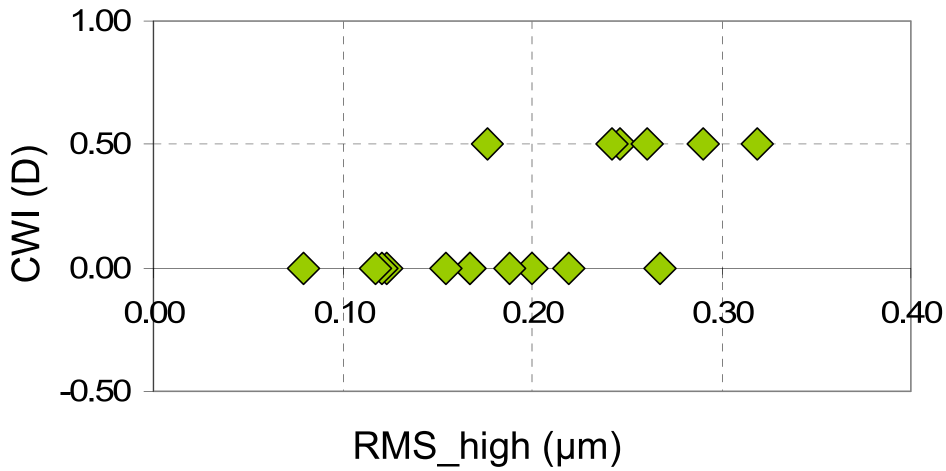

Figure 6.3 Corneal aberrations influence (CWI) in the ray tracing prediction, defined as the difference between the ray tracing prediction with corneal aberrations and without them, as a function of the corneal higher order aberrations for the normal cataract population.

The impact of corneal aberration on the calculation was limited for normal patients primarily because the amount of corneal aberrations was also limited for those patients. In fact, the ray tracing prediction incorporating corneal aberrations yielded a slightly higher error than the ray tracing procedure that does not consider corneal aberrations (figures 6.2a and 6.2b). Because the impact of corneal aberrations on the calculation was small, their consideration introduces noise, reducing the stability of the prediction.

Future studies of this procedure may lead to improvements in the results for normal patients by reducing the limitations of the current study. The approximation related to the equivalent refractive index may be considered one of these limitations [Fam and Lim, 2007]. Although the value chosen for the model is equivalent to that predicted by physiological measurements [Dubbelman et al. 2006], a fully customized model can be developed if the posterior corneal surface is also considered, although the impact of introducing further experimental measurements should be evaluated. In addition, the IOL placement prediction remains a challenge and is particularly important for hyperopic eyes [Olsen, 2007]. Improvements in the accuracy of the inputs to the model will lead to further diminish the errors in the IOL power prediction. It is one belief that when these inaccuracies are reduced, the impact of both corneal and IOL aberrations will be evident even for normal patients.

Chapter 7

IOL POWER CALCULATION BY USING CUSTOMIZED RAY TRACING IN POST-LASIK CATARACT PATIENTS

In this chapter, we apply the ray tracing method to post-LASIK patients. The first section evaluates the accuracy of ray tracing for calculating IOL power in this population with respect to current procedures. This accuracy is also related to the amount of corneal aberrations that these patients present and especially, to corneal spherical aberration. The second section studies the impact of the equivalent refractive index in the ray tracing procedure. The last section is a clinical application of the conclusions yielded by the ray tracing procedure: corneal spherical aberration is considered together with current paraxial approaches to generate different regression formulas for myopic post-LASIK patients. This approach could be easily introduced in the clinical practice as an intermediate step until customized ray tracing procedures are of general use.

7.1. Accuracy of ray tracing versus conventional calculations

The objective of the customized ray tracing for IOL power calculations is to have a robust procedure valid for all kind of patients and all type of IOLs. In the previous chapter, the method was validated for normal cataract patients, where IOL power calculations are well known by their average accuracy. In this chapter we show the higher accuracy of the procedure for post-LASIK patients comparing the results of a clinical study with the current state of art in IOL power calculations for this population.

7.1.1. Patients and protocol

Ten post-LASIK cataract patients (2 hyperopic and 8 myopic) were examined before and after cataract surgery between 2008 and 2010 in the Ophthalmology Service at the "Virgen de la Arrixaca" hospital (El Palmar, Murcia, Spain). All patients included were cataract patients with otherwise healthy eyes. The research followed the tenets of the Declaration of Helsinki, and all participants provided written consent. All biometric pre-cataract surgery measurements were performed following the same protocol as described in the previous chapter. The IOL model used was an aspheric mofocal (Tecnis ZA9003, Abbott Medical Optics, Santa, Ana, CA, USA). The power of the implanted IOL was selected by the surgeon according to his standard practice. Postoperative measurements were taken 1 month following the surgery. The same type of measurements described as in the previous chapter were performed postoperatively. From the refraction data, the spherical equivalent was calculated and translated optically to the IOL plane. This value was added to the IOL power implanted leading to the determination of the optimum IOL power for each patient.

7.1.2. Custom IOL power prediction validation

IOL power predictions were performed by using the customized ray tracing procedure described in section 3.2.3.1., being in this case the IOL power selected by the procedure the mode of the result of four different personalized models build from four corneal topographies recorded by patient. This procedure is be performed with and without the introduction of corneal aberrations. In the first case, the complete set of elevations retrieved by the corneal topographer is introduced in the model. The IOL power calculated using this procedure is called “custom+CWA”. In the second case, only the spherical equivalent power of the cornea is the input. The result of this calculation is called “custom-CWA”, following the same nomenclature as in the previous chapter.

Different IOL power predictions were calculated for comparison. The simple SRK/T [Retzlaff et al. 1990] (referred as SRK/T in figures) was included for all subjects. In addition, the double-K [Aramberri, 2003] SRK/T method was used for eyes that had myopic LASIK and the SRK/T with Masket method for eyes that had hyperopic LASIK [Masket and Masket, 2006] (this combined method referred to as double-K/Masket in the figures). These were selected because they are reported to be the most accurate methods for IOL power calculation after refractive using the data that were available in this study [Masket and Masket, 2006 and Wang et al. 2010]. To generate the double-K prediction, the corneal power before LASIK surgery was used in all cases in which this value was available. In cases in which it was not, 43.86 D was used as the preoperative corneal power [Wang et al. 2010]. For myopic eyes, the correction of post-LASIK corneal power was performed as suggested by Savini [Savini et al. 2006]. For eyes that had hyperopic LASIK, the IOL power was calculated with the SRK/T formula modified by the Masket method [Masket and Masket, 2006] which considers the surgically induced change in the manifest refraction after LASIK.

All paraxial and ray tracing predictions were subtracted from the optimum IOL power calculated after the surgery for each patient. In addition, the difference between IOL powers was transformed back to the spectacle plane in order to calculate the residual spherical equivalent error predicted by each procedure. The two sample (paired) t-test was used to evaluate the statistical significance of the difference between mean and mean absolute residual errors, while the consistency in the prediction was tested by means of the f-test for variances.

Figures 7.1a and 7.1b compare the average residual spherical equivalent and average absolute spherical equivalent error for all the predictions. Although the mean residual error retrieved by the Double K/Masket and ray tracing procedure incorporating corneal aberrations was not statistically significantly different ($p>0.05$), the Double K/Masket method showed a greater variance than the ray tracing procedure ($p<0.05$). In the case of the mean absolute spherical equivalent error, Double K/Masket procedures and the ray tracing procedure without considering corneal aberrations did not retrieve statistically significantly different results. On the other hand, when corneal aberrations are considered in the ray tracing prediction, the mean absolute spherical error is statistically significant better than the Double K/Masket ($p<0.05$). Therefore, the accuracy of the ray tracing prediction incorporating corneal aberrations was higher than the Double K/Masket method with corrected corneal power, while the ray tracing procedure that does not consider aberrations produced results in a similar level of the accuracy to both considered formulas.

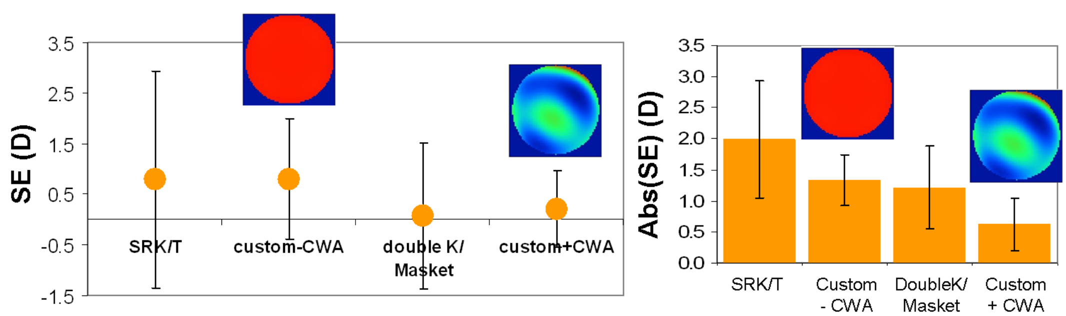

Figure 7.1. (a) Mean spherical equivalent refractive error for the post-Lasik cataract population included in the study achieved by the SRK/T, Double K/Masket and our procedure with (Custom+CWA) and without (Custom-CWA) corneal aberrations (b) mean absolute spherical equivalent refractive error

When considering the accuracy of the ray tracing prediction for these post-LASIK patients, in comparison with the current state of art, it is worthwhile to note that despite both methods predict on average a zero spherical equivalent, the standard deviation is higher for the corrected Double K/Masket method (0.8D versus 1.5D), fact reflected also by the significantly greater variance (0.6D versus 2.1D) ($p<0.05$). The difference is also evident in the mean absolute spherical equivalent error, where the Double K/Masket formula resulted in 1.2±0.7D versus the ray tracing which showed 0.6±0.4D. It can be therefore concluded that the ray tracing approach is more accurate and more predictable than the current state of art in IOL power calculations in eyes that have had LASIK for myopia or hyperopia. This result therefore confirms the validity of the procedure as a global method that may be used for IOL power calculations in both normal and post-LASIK patients, when results from this and the previous chapter are combined.

7.1.3. Effect of the amount of corneal aberrations in the IOL power prediction. Impact of corneal spherical aberration

We named the difference between the ray tracing prediction with and without considering anterior corneal aberration as corneal wavefront influence (CWI). Figure 7.2 shows this parameter versus the amount of corneal aberrations for each patient. For post-LASIK patients the degree to which corneal aberrations influences optimal IOL power depends on the amount of corneal aberrations, reaching up to 3D, with a correlation (r^2=0.59) similar to that found in normal patients (r^2=0.58). But since, the amount of corneal aberrations in these patients is much higher than in normals, the implication is a more significant impact when they are considered. The range of values for corneal RMS was approximately doubled for these patients with respect the normal population. In fact, if the same amount of aberrations is considered for post-LASIK patients than for normal cataract patients (up to 0.3 μm), the differences between both ray tracing predictions for post-LASIK patients are similar to those for normals. Thus, the main difference between the impact of corneal aberrations in both populations is due to the increased amount of aberrations in post-LASIK patients. And this point is of special relevancy since current IOL power calculation procedures are based on paraxial optics and therefore cannot account for corneal or IOL aberrations. Therefore, when increased amounts of aberrations are present, the ray tracing procedure is more accurate and predictable.

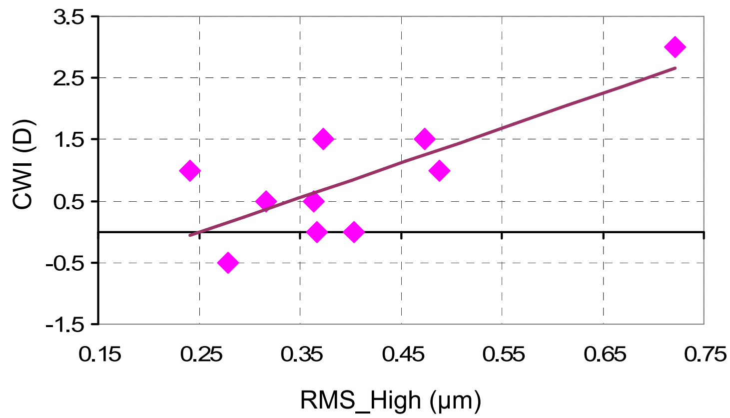

Figure 7.2. Corneal wavefront aberrations influence (CWI) in the ray tracing prediction as a function of the corneal higher order aberrations for the post-Lasik cataract population.

Figure 7.3 shows the difference between ray tracing predictions versus corneal spherical aberration. The CWI parameter presents a better correlation with corneal spherical aberration (r^2=0.82) than with all higher order corneal aberrations (r^2=0.59). Therefore, the larger corneal spherical aberration in post-LASIK patients is probably responsible for the increased accuracy of the ray tracing procedure with respect to the rest of IOL power predictions.

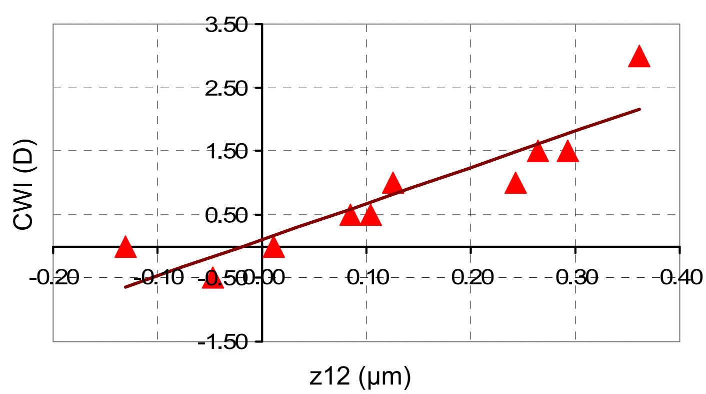

Figure 7.3. Corneal aberrations influence (CWI) in the ray tracing prediction as a function of the corneal spherical aberration for the post-Lasik cataract population.

An increase with respect normals in corneal spherical aberration for LASIK patients who had undergone standard procedures has been widely reported [Moreno-Barriuso et al. 2001, Benito et al. 2009, Kohnen et al. 2005]: eyes of patients that have had standard myopic corneal surgery show increased values of positive spherical aberration while those that have had hyperopic LASIK present negative corneal spherical aberration. The post-LASIK patients included in our study also showed this trend. The patients in figure 7.3 with negative spherical aberration were those that had undergone hyperopic LASIK surgery. It is not surprising that taking into consideration the large values of spherical aberration in these patients improved the IOL power predictions. A combination of nonparaxial optical calculations and consideration of the actual aberrations in the cornea and the IOL produced better results.

Several empirical approaches have been developed to improve IOL power prediction in post-LASIK patients. Masket presented a method where the refractive error corrected by the LASIK surgery was incorporated to correct the IOL power yielded by current formulas [Masket and Masket, 2006]. Yoon et al evaluated the sources of the spherical aberration induced by standard LASIK surgery [Yoon et al. 2005]. They found that the spherical aberration induction is directly related to the correction applied. These two results when considered together are supporting our findings. Accordingly for IOL power calculation, corneal spherical aberration provides a theoretical explanation for the hyperopic shift found in myopic post-LASIK patients. Moreover, customized ray tracing uses only on data collected prior to cataract surgery and does not relies on the patient's history, which is not always available. Thus, the consideration of current patient's data is an added advantage of the ray tracing versus the current approaches for IOL power calculation in post-LASIK patients.

The impact of corneal topography in IOL power calculation has been previously studied. Preussner et al introduced personalized corneal eccentricities in a non paraxial ray tracing procedure, calculated from anterior corneal topography, showing its influence in the calculation, especially for post-LASIK patients [Preussner et al. 2005]. However, the impact of higher order aberrations was not objectively established, because they were not included in the calculation, although a visual impression was generated in order to judge subjectively their impact. In our procedure we objectively include all anterior corneal aberrations in the calculation because the IOL power is selected based on the maximization of the optical quality of the eye with the implanted IOL. In addition, we considered the impact of corneal HOAs, relating its amount with the improvement in the calculation due to its introduction. At this point, it is interesting to reevaluate normal cataract patients. Although Figure 7.3 plots the results in post-LASIK eyes, it shows the impact of corneal spherical aberration for a wide range of values. The mean corneal spherical aberration for a 6.0 mm aperture is 0.27 ± 0.02 μm [Holladay et al. 2002]; this rescales to 0.05 μm for a 4.0 mm pupil. According to the regression provided by the results in Figure 7.3, the impact of considering corneal spherical aberration in IOL power calculation for normal patients was 0.39 D at the IOL plane, which translates to 0.30 D at the spectacle plane [Feiz et al, 2001] This value might be easily be influenced by errors related to the rest of the input variables because, for example, the refraction process itself has a standard deviation of 0.39 D [Norrby, 2008]. As we previously discussed, this difference may be relevant when the errors related to the rest of the biometric input parameters are further reduced. When this is achieved, corneal aberrations will play a role in IOL power calculation, even for lower amounts.

With respect to the procedure, the same limitations can be applied for post-LASIK and normals patients.

7.2. Modified equivalent refractive index for IOL power calculations in myopic post-LASIK patients

Despite residual spherical equivalent was found as zero with the customized ray tracing prediction when myopic and hyperopic post-LASIK patients are evaluated together, a slight positive residual value is found for myopic post-LASIK patients as well as slight negative for hyperopic post-LASIKs when evaluated separately, leading to a slight hyperopic error for myopic post-LASIK patients and slight myopic residual refraction for patients with a prior hyperopic refractive surgery.

One potential responsible for this systematic error may be the equivalent refractive index. In fact, the impact of that approximated equivalent refractive index of the cornea should be theoretically larger for post-LASIK patients. The modification in ERI for post-LASIK patients may be partially explained because of the asymmetric modification between anterior and posterior corneal due to the refractive surgery [Masket and Masket, 2006]. As an example, table 1 presents the ERI calculated prior and after LASIK surgery from literature data [Perez-Escudero et al. 2009]. The ERI used in the customized ray tracing procedure (1.330) is overestimated, leading to a higher total corneal power than real that underestimates the IOL power in myopic post-LASIK eyes.

	Ra	Rp	Rp/Ra	corneal thickness	ERI
pre	7.70	6.38	0.83	572	**1.329**
post	8.52	6.37	0.75	493	**1.323**

Table 7.1 ERI pre and post-LASIK from literature data [Perez-Escudero et al. 2009]

In this section we study the impact of the ERI calculated by different methods in the customized ray tracing procedure for IOL power prediction in myopic post-LASIK patients.

7.2.1. Patients and procedures

We retrospectively reviewed twenty five eyes of twenty five myopic post-LASIK cataract patients who were examined before and after cataract surgery between 2008 and 2009 in the Baylor College of Medicine (Houston, Texas, USA). This additional group extended the number of post-LASIK patients we had previously available. The mean age was 59±10 years (range 44 to 77 years) and the myopic correction -5.59±2.93D (range -12.00 to -2.00D). All patients included were cataract patients with otherwise healthy eyes. The research followed the tenets of the Declaration of Helsinki, and all participants provided written consent. Pre-LASIK history was available for all the patients included in the study: corrected refraction as well as pre-LASIK biometry and keratometry, performed with a low coherence interferometer (IOL Master; Carl Zeiss Meditec, Jena, Germany). Corneal topography, measured with a placido based corneal topographer (Atlas; Carl Zeiss Meditec, Dublin CA) and biometry measurements (axial length and anterior chamber depth) were performed prior the cataract surgery, and will be further refer as post-LASIK data.

All cataract surgeries were performed by the same surgeon (Douglas D. Koch) using a small incision technique following the implantation of an aspheric monofocal IOL (Alcon, SN60WF). The IOL power implanted was selected by the surgeon according to his standard practice. Postoperative measurements were taken 1 month following the surgery. The same preoperative measurements were performed postoperatively in addition to a subjective refraction. From this refraction, the spherical equivalent was calculated and translated optically to the IOL plane. This value was added to the IOL power implanted leading to the determination of the optimum IOL power for each patient.

7.2.2. ERI calculation methods from anterior corneal data and eye models

ERI was calculated by paraxial optics from the post-LASIK total corneal power. The latter was obtained by using the Gaussian formula corresponding to the power (P) of the coupling of two refractive surfaces with isolated powers (P1) and (P2) separated by a distance d in an inner medium of index n, as represented in equation 7.1.

$$P = P_1 + P_2 – (d/n)*P_1*P_2 \qquad [7.1]$$

In this particular case, P represents the post-LASIK total corneal power, while P_1 and P_2 are related to the anterior and posterior post-LASIK corneal powers. D is the central corneal thickness and n the corneal refractive index.

Anterior and posterior corneal powers (P_i with i=1,2) are calculated by approximating them to a spherical surface, as resembles Eq 7.2:

$$P_i=(n_A-n_B)/r_i \qquad [7.2]$$

where r_i is the corresponding surface radius and n_B and n_A the refractive indexes corresponding to the media prior and after the spherical surface respectively.

Post-LASIK anterior corneal radius was calculated in every case by ray tracing at 4mm pupil through the corneal elevation map corresponding to the anterior corneal topography measured prior the cataract surgery (Figure 7.4). The focal length of this corneal surface was set in order to minimize the root-mean-square spot size at the image plane. This focal distance yielded by ray tracing served to calculate the anterior corneal radius by using paraxial optics.

Posterior corneal radius was not measured in the study. Then, two approaches were considered, assuming in both cases physiological values [Dubbelman et al. 2006] and that the posterior cornea was not affected by LASIK surgery [Zhang et al. 2010, Perez-Escudero et al. 2009]. On one approach, pre-LASIK anterior corneal values were used to calculate the posterior corneal radius by means of a physiological fixed ratio of 0.838 [Dubbelman et al. 2006]. In addition, post-LASIK corneal thickness was estimated by subtracting from an average physiological corneal thickness of 579 μm [Dubbelman et al. 2006] the ablation depth calculated from the Munnerlyn formula [Munnerlyn et al. 1988] that accounts for the refraction corrected by LASIK surgery. In the second and alternative approach for estimating posterior corneal radius, only post-LASIK data were used and the posterior corneal radius was assumed constant through the population and equal to 6.53mm [Dubbelman et al. 2006]. In this case, corneal thickness was calculated from the average in normal population (579 μm) by subtracting the ablation depth calculated from the change of corneal radius due to the LASIK:

$$\Delta=r^2/2*(1/r_1-1/7.79) \qquad [7.3]$$

where Δ is the change in corneal thickness due to the LASIK surgery, r is the radius of ablation zone, considered here as 3mm, r_1 the calculated post-LASIK corneal radius and 7.79mm the pre-LASIK radius got from average physiological values [Dubbelman et al. 2006], that was also considered as fixed for all patients.

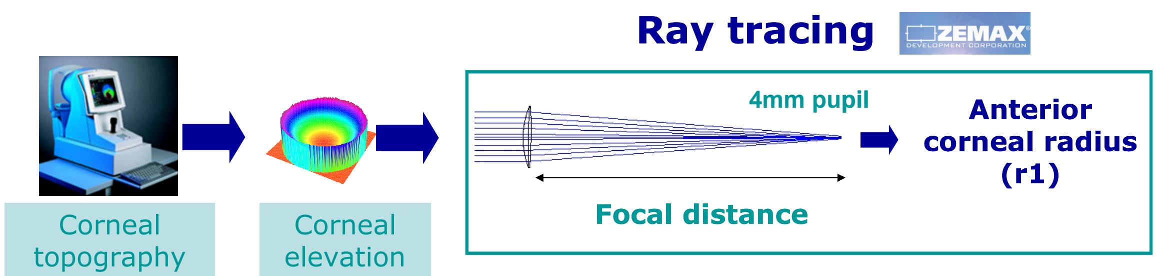

Figure 7.4 Diagram illustrating the procedure followed to determine post-LASIK anterior corneal radius.

In all the cases, ERI was calculated by making Eq 7.1, that is, total post-LASIK corneal power from both surfaces, equal to Eq 7.2, which is the power of the anterior corneal surface and getting the ERI as result. The procedure is schematically shown at figure 7.5. where r_1 radius is the post-LASIK anterior corneal surface, P is the post-LASIK total corneal power, n_B is 1 and n_A is the calcuated ERI value, as stated in equation 7.2. Because two different approaches are considered to account for posterior corneal power, for each patient, two different ERI are calculated using either pre-LASIK data or only post-LASIK data. The first yields a partially custom value of the ERI due to the fact that pre-LASIK subject data are used to calculate the posterior corneal radius. However, the second approach considers the posterior corneal radius fixed for the whole population, and therefore, the level of customization in the calculated ERI should be lower.

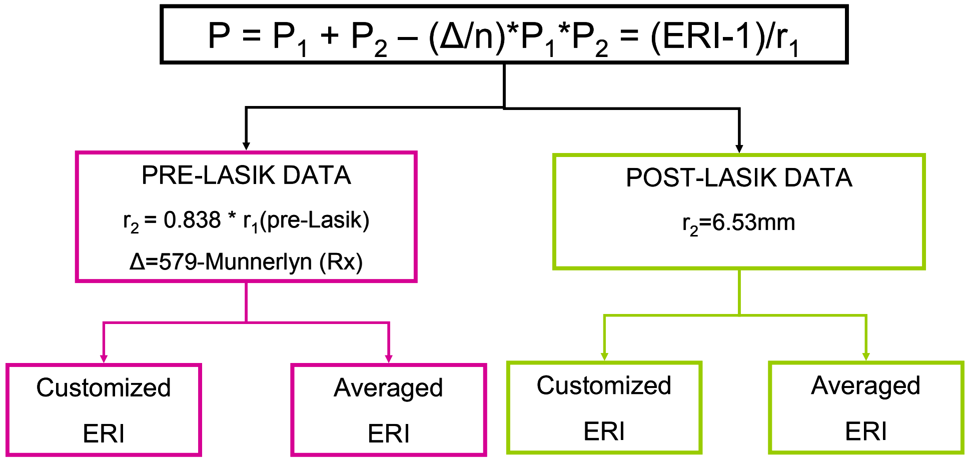

Figure 7.5 Schematic diagram showing the approaches for ERI calculation.

Table 7.2 shows the average ERI calculated by using both procedures, thus, incorporating pre-LASIK or with the only consideration of post-LASIK data. Both procedures retrieved similar results in this population, presenting also a similar dispersion. We have therefore demonstrated that the ERI in post-LASIK patients is indeed different to that for normal patients, that we estimated as 1.330.

	Customized ERI	**Averaged ERI**
POST-LASIK DATA	ranging from 1.314 to 1.331	1.325±0.004
PRE-LASIK DATA	ranging from1.316 to 1.329	1.324±0.003

Table 7.2 ERI values calculated with different procedures in average and range for all the patients included

Savini found a correlation between the ERI and the attempted correction by LASIK performing a paraxial treatment as we used here, although with some major differences [Savini et al. 2007]. Figure 7.6 shows the ERI in our population for both proposed methods versus de refraction corrected by LASIK. In both cases there is a relationship between the corrected sphere and the ERI. This was stronger for ERI calculated with pre-LASIK values (r^2=0.70) than for ERI using only post-LASIK parameters and average values (r^2=0.53) Thus, the partial customization related to the posterior cornea at the total power calculation with pre-LASIK data improves that correlation. However, the impact of that extra level of customization at the ERI calculation on the accuracy of IOL power prediction should be established, due to the fact that need of pre-LASIK data may limit the feasibility of the procedure to those patients that have this data available.

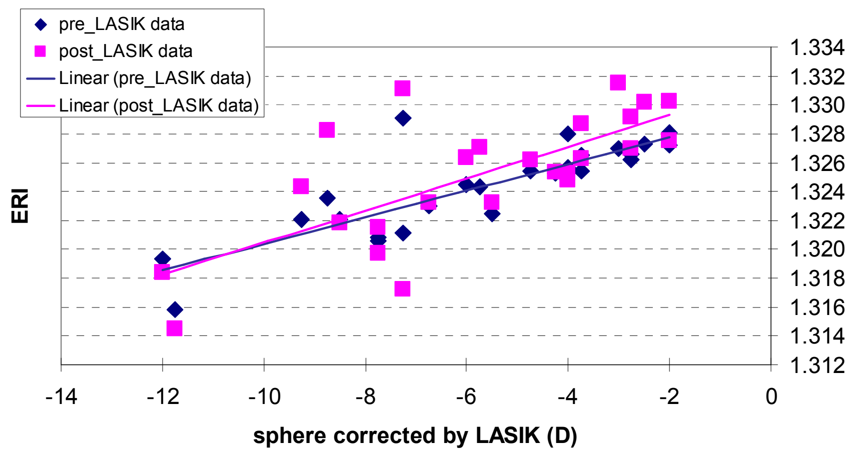

Figure 7.6 Scatter plots showing the ERI calculated with pre-LASIK and post-LASIK data versus the amount of change in refraction by the LASIK procedure.

7.2.3. ERI impact in IOL power calculation procedures

Five IOL power predictions were generated per patient using the customized ray tracing procedure considering five different ERI: the average for normals (1.330) and those individually calculated using pre-LASIK and post-LASIK data as well as the average through the population for both procedures. In this case, we incorporated a different formula to predict the IOL position [Norrby et al. 2010] due to the lack of data in our own procedure for the IOL model used in the study. In addition, the IOL power prediction according to the Haigis L formula [Haigis, 2008] has been calculated for each patient for comparison.

In order to calculate the IOL power error for each procedure, the IOL power prediction was subtracted from the optimum IOL power per patient. That was calculated from the implanted IOL power and the residual refraction once translated into the IOL plane. The paired t-test was used to evaluate the statistical significance of the difference between mean and mean absolute IOL power error with respect to the Haigis-L, while the consistency in the prediction was tested by means of the f-test for variances.

The mean and mean absolute IOL power difference between the optimum IOL power and the predictions related to each procedure previously described are shown in figure 7.7. Figure 7.8 shows the percentage of eyes within a certain IOL power error for each procedure.

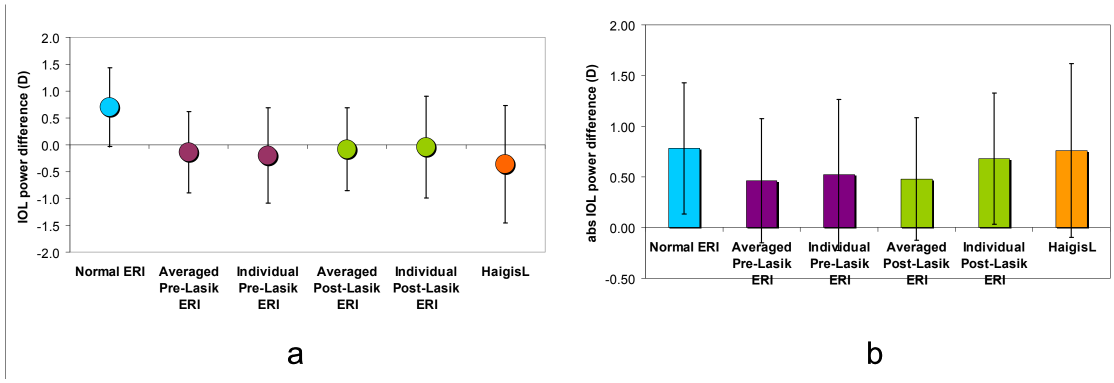

Figure 7.7 (a) Mean residual error and (b) mean absolute IOl power error for each procedure. Error bars represent one standard deviation (SD).

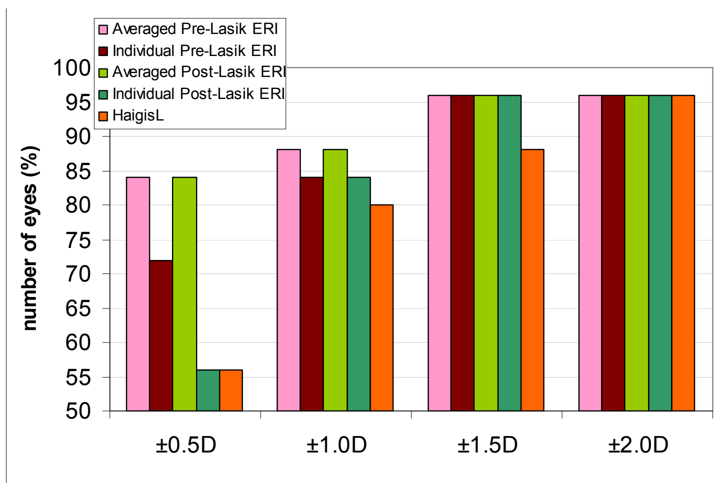

Figure 7.8 Percentage of eyes within a determined absolute IOL power error.

The average positive IOL power difference in the ray tracing procedure when the ERI for normals is used is omitted for all the calculated ERI (Figure 7.7). In addition, when the individual ERI calculated from pre-LASIK data is used, the ray tracing procedure yields a larger number of eyes within 0.5D than when individual ERI from post-LASIK and physiological values are used, although it did not result in a more precise IOL power calculation than the use of an average ERI.

It is important to note that in the ray tracing procedure, there are no fudged parameters that can be optimized in order to improve outcomes, because all the distances included in the model are real [Norrby, 2008]. Then, the impact of measurement errors is crucial since can reduce the benefit of the exact calculation or of the introduction of anterior corneal aberrations. We did not find any improvement in the IOL power calculation when the individualized ERI is considered with respect the average over the population. Along the same line, IOL power predictions considering pre-LASIK data to calculate ERI were not more accurate than those based in post-LASIK data and physiological values. This indicates of the impact that experimental errors have in the whole procedure and further validate the decision to not introduce posterior corneal data, whose impact in the eye's optical performance is smaller due to the reduced change in refractive index between cornea and aqueus humor in comparison to the change between air and cornea that occurs in anterior corneal surface. This is also our point to consider a paraxial approach to model the power of the posterior cornea to calculate the ERI that we introduced in the ray tracing procedure.

Tables 7.3 and 7.4 showed the mean and mean absolute IOL power error, as well as their statistical significance with respect the Haigis L formula. At this respect, the variance corresponding to the mean IOL power error with the ray tracing prediction incorporating averaged ERI from pre or post-LASIK data was statistically significantly better than the corresponding difference calculated with the Haigis L formula ($p<0.05$). In the case of the mean absolute IOL power error, both the average and the variance were statistically significantly better than the Haigis L when the ray tracing prediction incorporating average ERI from post-LASIK data is considered.

	ERI Normals	Averaged pre_Lasik ERI	Individual pre_Lasik ERI	Averaged post_Lasik ERI	Individual post_Lasik ERI	HaigisL
average	0.70	-0.14	-0.20	-0.08	-0.04	-0.36
SD	0.74	0.76	0.89	0.77	0.95	1.09
variance	0.54*	0.57*	0.79	0.60*	0.89	1.20

Table 7.3 Mean IOL power error, standard deviation and variance for all the ray tracing approaches with the different ERI as well as the Haigis-L (*Significantly different from Haigis L (P<0.05))

	ERI Normals	Averaged pre_Lasik ERI	Individual pre_Lasik ERI	Averaged post_Lasik ERI	Individual post_Lasik ERI	HaigisL
average	0.78	0.46*	0.52	0.48*	0.68	0.76
SD	0.65	0.61	0.74	0.60	0.64	0.86
variance	0.42	0.37	0.55	0.36*	0.41	0.73

Table 7.4 Mean absolute IOL power error, standard deviation and variance for all the ray tracing approaches with the different ERI as well as the Haigis-L (*Significantly different from Haigis L (P<0.05))

These results showed that ray tracing is an accurate and predictable procedure for IOL power calculation in myopic post-LASIK patients by including only anterior corneal data and an ERI calculated by paraxial optics, whose customization does not increased precision to the calculation. Results of the ray tracing prediction with this averaged ERI are statistically significantly better than the current state of art in IOL power calculations for myopic post-LASIK patients, represented by the Haigis-L formula. Further development in posterior corneal description may lead to a fully customized eye model that could improve IOL power calculations. The ideal scenario for complete customization would be to consider exact ray tracing through all the surfaces, resembling with more fidelity the eye. Although it is important to note that the results without its introduction are more accurate and predictable than the current state of art in IOL power calculations for myopic patients.

7.3. IOL power regressions considering corneal aberrations for myopic post-LASIK patients

We have shown during this work that ray tracing is a robust procedure for IOL power calculations, that improves the predictability of current IOL power calculation methods especially in post-LASIK patients. In spite of its increased accuracy and robustness, the lack of a fully automated procedure makes it nowadays unfeasible in clinical practice. This work helped to identify the parameters that achieve the greater accuracy of the procedure, that in the case of post-LASIK patients is corneal spherical aberration. Therefore, and in an attempt to create an alternative procedure that can be immediately applied in clinical practice while ray tracing is properly implemented for the clinical environment and may benefit from the information provided by this work, we propose a new modification of standard IOL power calculation formulas using only standard post-

LASIK data and corneal spherical aberration. For that purpose, we describe the method and apply this modification to a set of post-LASIK cases using Haigis [Haigis, 2004], Hoffer Q [Hoffer, 1993], Holladay 1 [Holladay et al. 1988] and the SRK/T [Retzlaff et al. 1990] formulas.

7.3.1. Study group and data

We retrospectively evaluated the data of 29 patients that had previously undergone myopic LASIK and had subsequently developed a cataract. Some of these patients were those evaluated in the previous section. Prior to cataract surgery, the patients' biometry with IOL Master (Carl Zeiss Meditec, Jena) was measured, including axial length, anterior chamber depth and corneal power. A corneal topographer (Atlas; Carl Zeiss Meditec, Dublin CA) was also used in order to measure the topography of the anterior cornea of each eye.

Corneal spherical aberration for a 4mm pupil was calculated from corneal elevations by means of the procedure described in section 3.2.2. Although pre-LASIK data were available, they were not used in this study.

The surgeon selected the IOL power to be implanted. It was recorded as well as the stable residual refraction following surgery for each patient. The IOL power that would have provided emmetropic outcome was calculated for each subject by adding the residual refraction post-op translated from the spectacle plane to the IOL plane to the implanted IOL power. Table 7.5 shows the mean, standard deviation and range of values for the axial length, corneal power, spherical aberration and emmetropic IOL power for the population evaluated.

	Mean ± SD	Range
AXL (mm)	26.11±1.49	23.34 to 28.96
K (D)	40.00 ±2.89	33.68 to 46.41
z12 (μm)	0.16 ±0.09	0.02 to 0.31
Emmetropic IOL power (D)	19.96 ±2.51	14.58 to 26.05

Table 7.5 Patient demographics

7.3.2. New fitted formulas

IOL power using Haigis [Haigis, 2004], Hoffer Q [Hoffer, 1993], Holladay 1 [Holladay et al. 1988] and the SRK/T [Retzlaff et al. 1990] formulas were calculated for each subject based on pre-cataract data. It is important to note that corneal power was not corrected and therefore, the IOL power calculation was performed as for normal patients.

For each original formula, a new regression formula was generated by fitting the results obtained with the standard formula and the corneal spherical aberration to the optimum IOL power calculated post-surgery for all subjects included in the study. Therefore, four new formulas were defined using Equation 7.4

$$\text{Standard+z12} = a{*}\text{Standard} + b{*}z12 + c \qquad [7.4]$$

where Standard+z12 is the new formula fitted from the IOL power calculated with the corresponding standard formula (Standard) and corneal spherical aberration (z12). The standard error value for each coefficient (a and b) was also calculated, and from these, the t-observed value was retrieved for each regression coefficient to identify their statistical significance.

New formula	t(z12)
Haigis+z12 = 1.11 + 0.99*Haigis + 3.79*z12	2.08
HofferQ+z12 = 2.06 + 0.94*HofferQ + 4.67*z12	2.56
Holladay1+z12 = 2.79 + 0.89*Holladay1 + 9.70*z12	4.51
SRK/T+z12 = 1.70 + 0.96*SRK/T + 9.80*z12	4.50

Table 7.6. New developed formulas based respectively on standard Haigis, HofferQ, Holladay1 and SRK/T, and corneal spherical aberration. The t-observed value for the regression coefficient corresponding to spherical aberration is also shown for each case.

Table 7.6 shows the new regression formulas fitted for the 29 eyes evaluated in the study. T-observed values for the slopes corresponding to the spherical aberration terms are also included for each of the new regression. Considering that the t-critical is 2.06 for a two tailed Student's t-distribution with 26 degrees of freedom and a significance level of 0.05 and the fact that all the t-observed values for slopes weighting corneal spherical aberration values were higher than this t-critical, the inclusion of spherical aberration was statistically significant in all cases, meaning that spherical aberration is a parameter that is needed to fit standard formulas to the IOL power resulting in emmetropia for myopic post-LASIK patients.

Figure 7.9 (left) shows the mean IOL power error for both the standard formula and the new fitted version including spherical aberration for all the paraxial formulas considered in this study. Figure 7.9 (right) shows the mean absolute IOL power error for both the standard formula and the new fitted version including spherical aberration for each paraxial formula. In order to calculate the IOL power error, predicted IOL power was subtracted from the IOL power resulting in emmetropia. Therefore, a positive difference means that the formula is underestimating the IOL power, leading to a hyperopic refraction error.

As expected, all the standard formulas yielded a positive mean IOL power error, related to the reported hyperopic surprise found with these formulas for myopic post-LASIK patients. In the case of the newly developed regression formulas, the average error is negligible in all the cases, due to the fitting process. It is important to note that for the mean absolute IOL power error, the improvement, defined as the difference between the mean absolute IOL power error before and after the fitting, depends on the formula, ranging from 0.83D for the Haigis+z12 formula to 1.67D for the SRK/T+z12 formula. Additionally, the net value of the mean absolute IOL power error for the new regression formula depends on the level of accuracy of the original standard formula on which it is based. Therefore, the best results are related with the fitting considering spherical aberration to the Haigis and the HofferQ because of the fact that these formulas initially had the smallest prediction error prior the fitting.

In addition, there is a reduction in the standard deviation when spherical aberration is considered in comparison with the standard calculation for all the considered formulas.

This reflects the importance of corneal spherical aberration for IOL power calculation in post-LASIK patients.

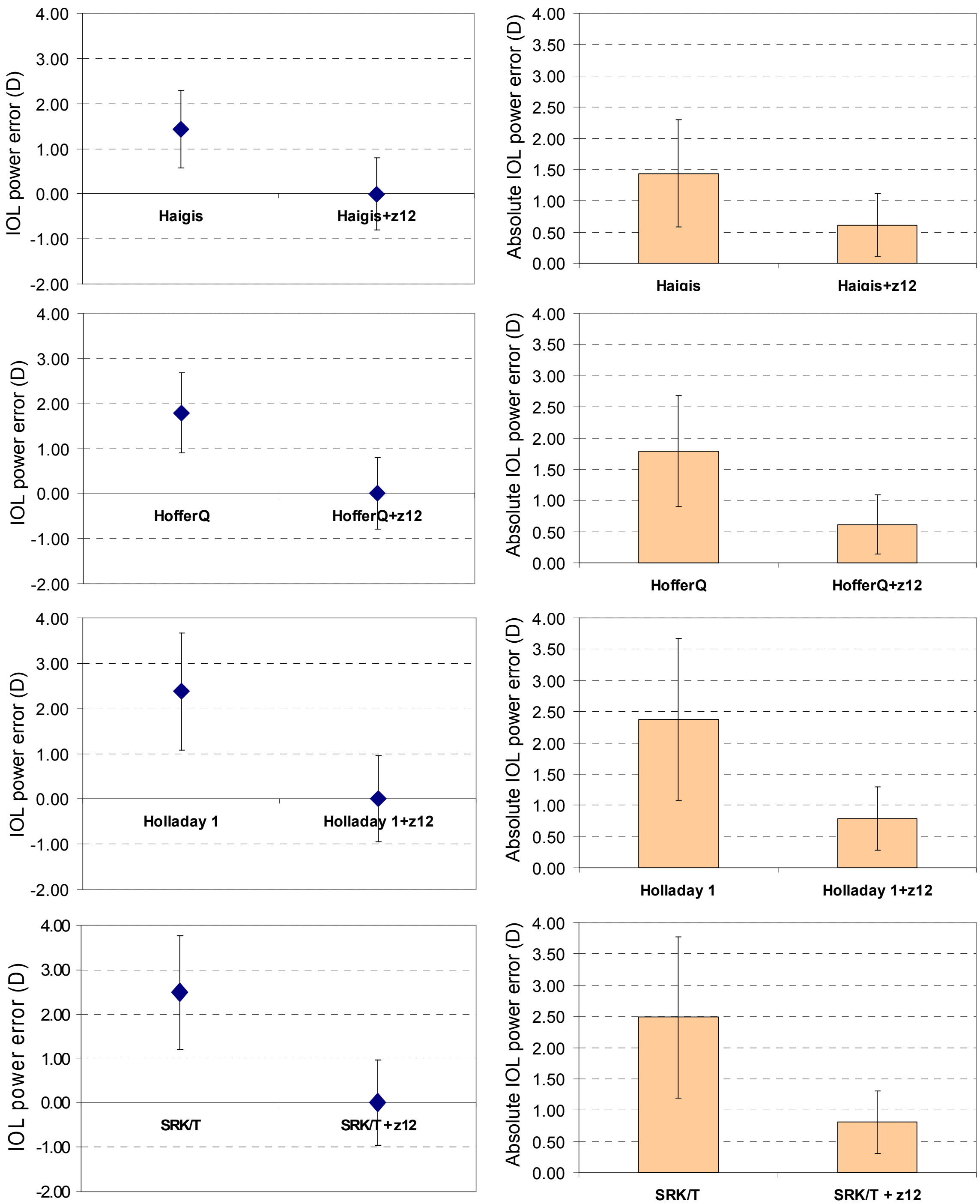

Figure 7.9 Mean IOL power error (left) and mean absolute IOL power error (right) for the 29 eyes considered in the study compared both for the standard and new fitted formula considering corneal spherical aberration.

Because of formulas' regression nature, constants which weight the different parameters included can be modified or personalized for the IOL model used or for the surgeon, similar to the A constant in current formulas. One limitation of this study is the number of patients included in the analysis. The more patients included in the generation of new formulas, the more accurate they will be. In addition, formulas like those we present here for myopic post-LASIK patients can be developed for hyperopic post-LASIK patients. They might be separate formulas because the amount and sign of the spherical aberration induced by the refractive surgery is different, but these patients could also benefit from the application of this principle.

In order to compare the results of the new method with those provided by current procedures, IOL power predictions were generated as well with the Haigis-L [Haigis, 2008] for all cases. The paired t-test was used to evaluate the statistical significance of the difference between the newly developed formulas and the results provided by the Haigis-L, while the consistency in the prediction was tested by means of the f-test for variances.

Table 7.7 shows the average IOL power prediction error and average absolute IOL power prediction error with their respective standard deviation for all the new regression formulas incorporating corneal spherical aberration as well as for the Haigis-L. Although standard deviation is smaller for some of the new fitted formulas, these differences are not statistically significant. In fact, the new regression based on the Haigis formula was the most accurate within the new fit regressions, in the limit of the statistical significance with respect the Haigis-L ($p=0.05$) for the mean IOL power error.

Additionally we defined the maximum range of error for each particular formula as the sum in absolute value between the most positive and most negative IOL power error over all the subjects. Figure 7.10 shows that value for all the formulas considered in this study. The range of error is smaller for the new fitted formulas including spherical aberration than for the Haigis-L, with the maximum difference being 0.56D.

	Power error (D)	SD	Abs Power error (D)	SD
Haigis L	-0.22	0.86	0.66	0.58
Haigis+z12	0.00	0.80	0.61	0.50
HofferQ+z12	0.00	0.79	0.62	0.48
Holladay 1 + z12	0.00	0.95	0.79	0.51
SRK/T + z12	0.00	0.97	0.81	0.50

Table 7.7 Mean IOL power errors and mean absolute IOL power errors for all the methods considered in the study.

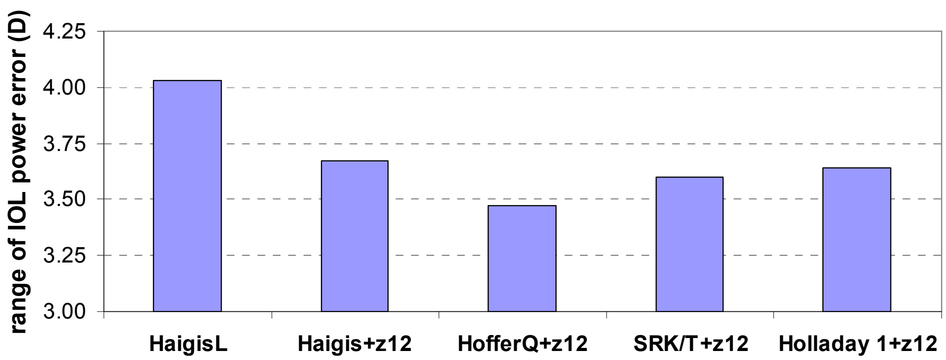

Figure 7.10 Range of IOL power error, defined as the sum in absolute value of the most positive and most negative IOL power error, compared for all the methods considered in the study.

The percentages of eyes within a specific range of IOL power error can be seen in Figure 7.11. The Haigis+z12 and HofferQ+z12 have a greater amount of eyes with lower IOL power prediction error than the Holladay 1+z12 and the SRK/T+z12 for all the ranges, except ±2D, where SRK/T+z12 was the only formula achieving 100% of eyes within that range. When the results for Haigis+z12 and HofferQ+z12 are compared with the current state of art, its performance is similar for the number of patients that would achieve ±0.5D. The scenario is different for ±1.0D and ±1.5D, where both HofferQ+z12 and Haigis+z12 showed a superior performance, reaching up to 97% and 93% respectively in comparison with the 86% achieved by the HaigisL.

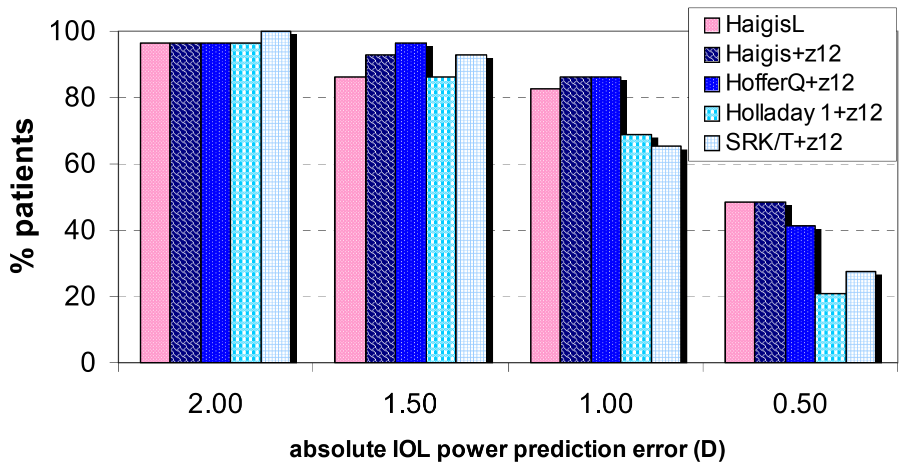

Figure 7.11 Percentage of eyes within a certain absolute IOL power prediction error for all different calculation procedures considered in the study.

In conclusion, the introduction of corneal spherical aberration increases the accuracy of IOL power prediction for myopic post-LASIK patients with the use of standard formulas and without any pre-LASIK data. However, when these results are compared to those provided by ray tracing, shown at Figure 7.8, it is possible to note the increased accuracy of the customized procedure that yields the 84% of eyes within 0.5D of IOL power error. Therefore, although the introduction of corneal spherical aberration in paraxial formulas increased their accuracy, it is still below of that provided by the customized ray tracing procedure.

Chapter 8

Conclusions

1. We have developed a complete customized predictive procedure that allows for calculating the optimum IOL power for a specific lens and individual patient. This procedure is based on a series of clinical biometric measurement of the eye and on polychromatic ray tracing calculations.

2. We have studied the induction of corneal aberrations due to cataract surgery, as well as their temporal evolution. Anterior corneal topographies measured prior to the cataract surgery can be used in order to predict IOL power in the customized ray tracing procedure, because the corneal spherical equivalent has been found stable before and after cataract surgery.

3. The polychromatic treatment combined with the introduction of monochromatic corneal aberrations is relevant for IOLs with low Abbe number. The accuracy of the ray tracing procedure is limited by the quality of the inputs, especially of the anterior corneal topographies.

4. Ray tracing and conventional formulas retrieve the same accuracy in normal average patients. The introduction of corneal aberrations does not translate into a lower IOL power prediction error. However, the difference between regular regression formulas and ray tracing is larger as higher is the ametropia prior the cataract surgery.

5. The introduction of anterior corneal aberrations is important in the ray tracing procedure for post-LASIK patients. The accuracy of the ray tracing procedure including corneal aberrations is higher than the current state of art in IOL power calculations especially due to corneal spherical aberration.

6. Polychromatic ray tracing through customized eyes models can be considered as a robust method for IOL power calculation, valid for normal and myopic and hyperopic post-LASIK patients.

7. The accuracy of the ray tracing procedure for myopic post-LASIK patients can be improved when the equivalent refractive index is modified with respect that used for normal patients. This equivalent refractive index can be calculated from paraxial optics, postoperative measurements and average physiological values.

8. The incorporation of anterior corneal spherical aberration increases the accuracy of current IOL power calculation procedures for post-LASIK patients. A simple regression formula that considers both anterior corneal spherical aberration and the result of paraxial formulas as applied for normal patients yields smaller range of error than the current state of art. However, the accuracy of this regressive approach is below the customized ray tracing procedure.

BIBLIOGRAPHY

[Ali and Little, 2011] Ali N and Little BC, "Causes of cataract surgery malpractice claims in England 1995–2008". Br J Ophthalmol 2011;95: 490-492.

[Altmann et al. 2005] Altmann GE, Nichamin LD, Lane SS and Pepose JS, "Optical performance of 3 intraocular lens designs in the presence of decentration".J Cataract Refract Surg. 2005;31:574-585.

[Apple and Sims, 1996] Apple D and Sims J, "Harold Ridley and the Invention of the Intraocular Lens" Surv Ophthalmol 1996;40:279-292.

[Applegate et al. 2003] Applegate RA, Marsack JD , Ramos R and Sarver EJ, "Interaction between aberrations to improve or reduce visual performance" J Cataract Refract Surg 2003; 29:1487–1495.

[Applegate et al. 2009] Applegate RA, Thibos LN, Twa MD and Sarver EJ, "Importance of fixation, pupil center, and reference axis in ocular wavefront sensing, videokeratography, and retinal image quality" J Cataract Refract Surg. 2009;35:139–152.

[Aramberri, 2003] Aramberri J, "Intraocular lens power calculation after corneal refractive surgery: double-K method", J Cataract Refract Surg. 2003; 29, 2063-2068.

[Aristodemou et al. 2011] Aristodemou P, Cartwright NEK, Sparrow JM and Johnston RL, Intraocular lens formula constant optimization and partial coherence interferometry biometry: Refractive outcomes in 8108 eyes after cataract surgery, J Cataract Refract Surg 2011; 37:50–62.

[Artal et al. 1995] Artal P, Marcos S, Navarro R, Miranda I and Ferro M, "Through focus image quality of eyes implanted with monofocal and multifocal intraocular lenses," Optical Engineering 1995;34: 772-779.

[Artal et al. 2002] Artal P, Berrio E, Guirao A and Piers P "Contribution of the cornea and internal surfaces to the change of ocular aberrations with age" J. Opt. Soc. Am. A 2002; 19: 137-143.

[Artal et al. 2006] Artal P, Benito A and Tabernero J, "The human eye is an example of robust optical design" J. Vis 2006; 6; 1-7.

[Artal and Tabernero, 2008] Artal P and Tabernero J, "The eye's aplanatic answer". Nature Photonics 2008;2: 586-589.

[Artal, 2009] Artal P, “History of IOLs that correct spherical aberration”, J Cataract Refract Surg. 2009;35:962–964.

[Artal et al. 2010] Artal P, Manzanera S, Piers P and Weeber H, "Visual effect of the combined correction of spherical and longitudinal chromatic aberrations". Opt. Express 2010; 18: 1637-1648.

[Artal et al. 2011] Artal P, Benito A, Perez GM, Alcon E, De Casas A et al, “An Objective Scatter Index Based on Double-Pass Retinal Images of a Point Source to Classify Cataracts” PLoS 2011; ONE 6(2): e16823.

[Atchison and Smith, 2000] Atchison DA and Smith G. “Optics of the human eye”. Ed. Elsevier (2000).

[Atchinson and Smith, 2005] Atchison DA and Smith G, “Chromatic dispersions of the ocular media of human eyes”. J Opt Soc Am A Opt Image Sci Vis 2005;22:29-37.

[Barbero et al. 2002] Barbero S, Marcos S, Merayo-Lloves J and Moreno-Barriuso E, "A validation of the estimation of corneal aberrations from videokeratography: test on keratoconus eyes," J Refract Surg 2002;18: 267-270.

[Bauer et al. 2011] Bauer NJC, de Vries NE, Webers CAB, Hendrikse F and Nuijts RMMA, “Astigmatism management in cataract surgery with the AcrySof toric intraocular lens”, J Cataract Refract Surg 2008; 34:1483–1488.

[Bellucci et al. 2005] Bellucci R, Scialdone A, Buratto L, Morselli S, Chierego C, Criscuoli A, Moretti G and Piers P, “Visual acuity and contrast sensitivity comparison between Tecnis and AcrySof SA60AT intraocular lenses: A multicenter randomized study” J Cataract Refract Surg. 2005; 31: 712-717.

[Benito et al. 2009] Benito A, Redondo M and Artal P, “Laser in situ keratomileusis disrupts the aberration compensation mechanism of the human eye” Am J Ophthalmol. 2009;147: 424-431.

[Binkhorst, 1979] Binkhorst RD, “Intraocular lens power calculation” Int Ophthalmol Clin 1979;19: 237– 252.

[Born and Wolf, 1989] Born M and Wolf E, “Principles of Optics”. New York: Pergamon, 1989.

[Byrne, 1995] Byrne SF, “A-Scan Axial Eye Length Measurements: A Handbook for IOL Calculations”. Mars Hill, NC:. Grove Park Publishers (1995).

[Campbell, 1997] Campbell C, “Reconstruction of the Corneal Shape with the MasterVue Corneal Topography System”. Opt. Vis. Sci.1997; 74: 899-905.

[Cánovas and Artal, 2011] Cánovas C and Artal P, "Customized eye models for determining optimized intraocular lenses power," Biomed. Opt. Express 2011;2: 1649-1662.

[Castejon-Monchon et al. 2002] Castejon-Monchon JF, Lopez-Gil N, Benito A and Artal P, “Ocular wavefront aberration statistics in normal young population”, Vision Res 2002; 42:1611-1617.

[Chen, 1989] Chen H, “Causes of cataract”, BMJ 1989; 298: 1470-1471.

[Chylack et al. 1993] Chylack LT, Wolfe JK, Singer DM, Leske MC, Bullimore MA, Bailey IL , Friend J , Carthy MC and Wu SY, “The Lens Opacities Classification System III. The Longitudinal Study of Cataract Study Group" Arch Ophthalmol 1993 111: 831–836.

[Colenbrander, 1973] Colenbrander MC, “Calculation of the power of an iris-clip lens for distant vision” Br J Ophthalmol 1973;57: 735–740.

[Cumming et al. 2001] Cumming JS, Slade SG and Chayet A, “Clinical evaluation of the model AT-45 silicone accommodative intraocular lens: results of feasibility and the initial phase of a food and drug administration clinical trial” Ophthalmology 2001;108:2005–2008.

[De Loewenfeld, 1979] De Loewenfeld, “Pupillary changes related to age”, in Topics in Neuro-Opthalmology, T. HS, ed. (Williams & Wilkins, Baltimore, 1979), pp. 124-150.

[Dubbelman et al. 2001] Dubbelman, M, van der Heijde GL and Weeber HA, “The thickness of the aging human lens obtained from corrected Scheimpflug images”. Optom. Vis. Sci. 2001:78; 411–416.

[Dubbelman et al. 2002] Dubbelman M, Weeber HA, van der Heijde GL and Volker-Dieben HJ, “Radius and asphericity of the posterior corneal surface determined by corrected Scheimpflug photography”. Acta Ophthalmol. Scand. 2002; 80: 379–383.

[Dubbelman et al. 2004] Dubbelman M, van der Heijde GL and Weeber HA, “Change in shape of the aging human crystalline lens with accommodation”. Vision Res. 2004;45: 117–132.

[Dubbelman et al. 2006] Dubbelman M, Sicam VA and Van der Heijde GL, “The shape of the anterior and posterior surface of the aging human cornea”, Vision Res. 2006;46: 993-1001.

[Duncan et al. 1997] Duncan DD, Shukla OB, West SK and Schein OD, “New objective classification system for nuclear opacification”. J Opt Soc Am A 1997;14: 1197–1204.

[Dupps, 2010] W. Dupps, “Intraocular lens calculations: Call for more deterministic models” J Cataract Refract Surg 2010; 36: 1447-1448.

[Escudero-Sanz and Navarro, 1999] Escudero-Sanz I and Navarro R, “Off-axis aberrations of a wide-angle schematic eye model,” Journal of the Optical Society of America A, Vol. 1999;16: 1881-1891.

[Fam and Lim, 2007] Fam H and Lim K, “Validity of the keratometric index: Large population-based study” J Cataract Refract Surg. 2007; 33, 686-691.

[Freeman and Pesudovs, 2005] Freeman G and Pesudovs K, “The impact of cataract severity on measurement acquisition with the IOLMaster”, Acta Ophthalmol. Scand. 2005: 83: 439–442.

[Feil et al. 1994] Feil SH, Crandall AS and Olson RJ, “Astigmatic decay following small incision, self-sealing cataract surgery” J Cataract Refract Surg. 1994; 20; 40-43.

[Feiz et al. 2001] Feiz V, Mannis MJ, Garcia Ferrer F, Kandavel G, Darlington JK, Kim E, Caspar J, Wang J-I and Wang W, “Intraocular lens power calculation after laser in situ keratomileusis for myopia and hyperopia: a standardized approach” Cornea 2001; 20:792–797.

[Fercher et al. 1988] Fercher AF, Mengedoht K and Werner W, “Eye-length measurement by interferometry with partially coherent light,” Optics Letters 1988;13: 186-188.

[Fyodorov and Kolinko, 1967] Fyodorov SN and Kolinko AI. “Estimation of optical power of the intraocular lens”, Vestnik Oftalmologic (Moscow) 1967;4:27.

[Fyodorov et al. 1975] Fyodorov SN, Galin MA and Linksz A, “Calculation of the optical power of intraocular lenses” Invest Ophthalmol 1975;14: 625– 628.

[Gimbel and Sun, 2001] Gimbel HV and Sun R, “Accuracy and predictability of intraocular lens power calculation after laser in situ keratomileusis” J Cataract Refract Surg 2001; 27, 571-576.

[Glasser et al. 1998] Glasser A and Campbell MCW, “Presbyopia and the optical changes in the human crystalline lens with age” Vision Research 1998; 38: 209-229.

[Glasser and Campbell, 1999] Glasser A and Campbell MC, “Biometric, optical and physical changes in the isolated human crystalline lens with age in relation to presbyopia” Vision Res 1999;39:1991–2015.

[Glasser, 2008] Glasser A, “Restoration of accommodation: surgical options for correction of presbyopia” Clin Exp Optom 2008; 91: 3: 279–295.

[Goodman, 1996] Goodman JW, “Introduction to Fourier Optics” New York: McGraw-Hill, (1996)

[Guirao et al. 2000] Guirao A, Redondo M and Artal P, “Optical aberrations of the human cornea as a function of the age”, Journal of the Optical Society of America A, 2000;17: 1697-1702.

[Guirao and Artal, 2000] Guirao A and Artal P, “Corneal wave aberration from videokeratography: accuracy and limitations of the procedure”, J Opt Soc Am A 2000;17, 955-965.

[Guirao et al. 2002] Guirao A, Redondo M, Geraghty E, Piers P, Norrby S and Artal P, “Corneal optical aberrations and retinal image quality in patients in whom monofocal intraocular lenses were implanted” Arch. Ophthalmol. 2002;120: 1143-1151.

[Guirao et al. 2004] Guirao A, Tejedor J and Artal P, “Corneal aberrations before and after small-incision cataract surgery” Invest Ophthalmol Vis Sci. 2004; 45:4312-4319.

[Guyton et al. 1990] Guyton DL, Uozato H and Wisnicki HJ, “Rapid determination of intraocular lens tilt and decentration through the undilated pupil”, Ophthalmology 1990; 97: 1259-1253

[Haigis et al. 2000] Haigis W, Lege B, Miller N and Schneider B, “Comparison of immersion ultrasound biometry and partial coherence interferometry to intraocular lens power calculation according to Haigis”, Graefe’s Arch Clin Exp Ophthalmol 2000;238:765–773

[Haigis, 2004] Haigis W, “The Haigis formula”. In “Intraocular Lens power calculations”, Shammas J, ed. (Slack Incorporated, 2004).

[Haigis, 2008] Haigis W, “Intraocular lens calculation after refractive surgery for myopia: Haigis-L formula” J Cataract Refract Surg 2008; 34, 1658-1663.

[Haigis, 2009] Haigis W, “Intraocular lens calculation in extreme myopia” J Cataract Refract Surg. 2009;35: 906-911

[Haigis, 2011] Haigis W, “Axial length: Laser interferometry. Basics of the IOL Master”. In “IOL power”, Hoffer KJ, ed. (Slack Incorporated , 2011), pp.63-66.

[Hamed et al. 2002] Hamed AM, Wang L, Misra M and Koch DD, “A comparative analysis of five methods of determining corneal refractive power in eyes that have undergone myopic laser in situ keratomileusis” Ophthalmology 2002; 109, 651-658.

[Hayashi et al. 2009] Hayashi K, Yoshida M and Hayashi H, “Postoperative corneal shape changes: microincision versus small-incision coaxial cataract surgery” J Cataract Refract Surg. 2009; 35(2); 233-239.

[Helmholtz, 1925] Helmholtz HH von,. “Helmholtz’s Treatise on Physiological Optics”, Vol 1. New York: Optical Society of America (1925).

[Hill, 2008] Hill W. “Expected effects of surgically induced astigmatism on AcrySof toric intraocular lens results”, J Cataract Refract Surg 2008; 34: 364-367.

[Hitzenberger, 1991] Hitzenberger CK, “Optical measurement of the axial eye length by laser Doppler interferometry:. Invest Ophthalmol Vis Sci 1991;2:616–624.

[Hoffer, 1984] Hoofer KJ, “The effect of axial length in posterior chamber lenses and posterior capsule position”, Current Concepts in Ophthalmic Surg. 1984;1:20.22

[Hoffer, 1993] Hoffer KJ, “The Hoffer Q formula: a comparison of theoretic and regression formulas”, J Cataract Refract Surg 1993; 19: 700-712. Erratum in: “The Hoffer Q formula: a comparison of theoretic and regression formula” J Cataract Refract Surg 1994;20:677. Erratum in: “The Hoffer Q formula: a comparison of theoretic and regression formula”, J Cataract Refract Surg 2007;33:2-3.

[Hoffer, 1995] Hoffer KJ, “Intraocular lens power calculation for eyes after refractive keratotomy”, J Refract Surg. 1995;11: 490-493.

[Hoffer, 2000] Hoffer KJ, “Clinical results using the Holladay 2 intraocular lens power formula”. J Cataract Refract Surg 2000; 26:1233–1237.

[Hoffer, 2011a] Hoffer KJ, “Formulas and programs: Formula history and basis”. In “IOL power”, Hoffer KJ, ed. (Slack Incorporated , 2011), pp.137-142

[Hoffer, 2011b] Hoffer KJ, “Formulas and programs: Regression and Theoretic formulas”. In “IOL power”, Hoffer KJ, ed. (Slack Incorporated , 2011), pp.143-148.

[Hoffman et al, 2011] Hoffman PC, Auel S and Hutz WW, “Results in higher power toric intraocular lens implantation”. J Cataract Refract Surg 2011; 37:1411-1418.

[Holladay et al. 1988] Holladay JT, Prager TC, Chandler TY, Musgrove KH, Lewis JW and Ruiz RS, “A three-part system for refining intraocular lens power calculations”, J Cataract Refract Surg. 1988;14:17-24.

[Holladay, 1989] Holladay JT, “Consultations in refractive surgery” Refract Corneal Surg 1989; 5, 203.

[Holladay et al. 2002] Holladay JT, Piers PA, Koranyi G, van der Mooren M and Norrby NE, “A new intraocular lens design to reduce spherical aberration of pseudophakic eyes”. J Refract Surg. 2002; 18; 683-691.

[Kohnen et al. 1995] Kohnen T, Dick B and Jacobi KW, “Comparison of the induced astigmatism after temporal clear corneal tunnel incisions of different sizes”. J Cataract Refract Surg. 1995; 21; 417-424.

[Kohnen et al. 2005] Kohnen T, Mahmoud K and Bühren J, “Comparison of corneal higher-order aberrations induced by myopic and hyperopic LASIK”, Ophthalmology 2005;112: 1692-1698.

[Kooijman, 1983] Kooijman AC, “Light distribution on the retina of a wide-angle theoretical eye,” Journal of the Optical Society of America 1983; 73: 1544-1550.

[Le Grand and El Hague, 1980] Le Grand Y and El Hage SG, “Physiological Optics”, (Springer-Verlach, 1980).

[Lichtinger et al. 2011] Lichtinger A, Sandstedt CA, Schwartz DM and Chayet AS, “Correction of Astigmatism After Cataract Surgery Using the Light Adjustable Lens: A 1-Year Follow-Up Pilot Study” J Refract Surg. 2011;17:1-4.

[Lim et al. 2005] Lim MCC, Hoh S-T, Foster PJ, et al. “Use of optical coherence tomography to assess variations in macular retinal thickness in myopia”. Invest Ophthalmol Vis Sci 2005; 46:974-978.

[Liou and Brennan, 1997] Liou H-L and Brennan NA, “Anatomically accurate, finite model eye for optical modeling”, Journal of the Optical Society of America A 1997;14: 1684-1695.

[Mahajan, 1998] Mahajan VN, “Optical Imaging and Aberrations. Part I: Ray Geometrical Optics”. Bellingham: SPIE (1998).

[Marcos et al. 2007] Marcos S, Rosales P, Llorente L and Jiménez-Alfaro I, “Change in corneal aberrations after cataract surgery with 2 types of aspherical intraocular lenses” J Cataract Refract Surg. 2007;33; 217-226.

[Masket and Tennen, 1996] Masket S and Tennen DG, “Astigmatic stabilization of 3.0 mm temporal clear corneal cataract incisions”. J Cataract Refract Surg. 1996; 22; 1451-1455.

[Masket and Masket, 2006] Masket S and Masket SE, “Simple regression formula for intraocular lens power adjustment in eyes requiring cataract surgery after excimer laser photoablation”, J Cataract Refract Surg. 2006;32, 430-434.

[Masket et al. 2009] Masket S, Wang L and Belani S, “Induced astigmatism with 2.2- and 3.0-mm coaxial phacoemulsification incisions” J Refract Surg. 2009; 25;21-24.

[Mckay, 1998] Mckay T, “A clinical guide to the Humphrey Corneal Topography System”, Humphrey System (1998)

[McLeod et al. 2007] McLeod SD, Vargas LG, Portney V and Ting A, “Synchrony dual-optic accommodating intraocular lens Part 1: Optical and biomechanical principles and design considerations” J Cataract Refract Surg 2007; 33:37–46.

[Menapace at al. 2007] Menapace R, Findl O, Kriechbaum K and Leydolt-Koeppl C, “Accommodating intraocular lenses: a critical review of present and future concepts”. Graefes Arch Clin Exp Ophthalmol. 2007;245:473-489.

[Merriam et al. 2003] Merriam JC, Zheng L, Merriam JE, Zaider M and Lindström B, “The effect of incisions for cataract on corneal curvature”. Ophthalmology. 2003;110; 1807-1813.

[Mester et al. 2003] Mester U, Dillinger P and Anterist N, “Impact of a modified optic design on visual function: clinical comparative study”. J Cataract Refract Surg. 2003; 29; 652-660.

[Mester et al. 2009] Mester U, Sauer T and Kaymak H, “Decentration and tilt of a single-piece aspheric intraocular lens compared with the lens position in young phakic eyes”, J Cataract Refract Surg. 2009; 35; 485-490.

[Moreno-Barriuso et al. 2001] Moreno-Barriuso E, Lloves JM, Marcos S, Navarro R, Llorente L and Barbero S. “Ocular aberrations before and after myopic corneal refractive surgery: LASIK-induced changes measured with laser ray tracing”, Invest Ophthalmol Vis Sci. 2001;42: 1396-403.

[Mrochen et al 2001] Mrochen M, Kaemmerer M, Mierdel P and Seiler T, “Increased higher-order optical aberrations after laser refractive surgery: a problem of subclinical decentration” J Cataract Refract Surg 2001;27:362–369.

[Munnerlyn et al. 1988] Munnerlyn CR, Koons Sj and Marshall J, “Photorefractive keratectomy: a technique for laser refractive surgery”. J Cataract Refract Surg. 1988;14:46-52.

[Mutlu at al. 1998] Mutlu FM, Bilge AH, Altinsoy HI and Yumusak E, “The role of capsulotomy and intraocular lens type on tilt and decentration of polymethylmethacrylate and foldable acrylic lenses” Ophthalmologica. 1998;212:359-363.

[Nakazawa and Ohtsuki, 1984] Nakazawa M and Ohtsuki K, “Apparent accommodation in pseudophakic eyes after implantation of posterior chamber lenses: optical analysis” Invest Ophthalmol Vis Sci 1984;25:1458–1460.

[Navarro et al. 1985] Navarro R., Santamaria J. and Bescos J, “Accommodation dependent model of the human eye with aspherics,” Journal of the Optical Society of America A 1985;2:1273-1281.

[Navarro et al. 1993] Navarro R, Ferro M., Artal P and Miranda I, “Modulation transfer functions of eyes implanted with intraocular lenses,” Applied Optics 1993; 32: 6359-6367.

[Negishi et al. 2010] Negishi K, Kodama C, Yamaguchi T, Torii H, Saiki M, Dogru M, Ohnuma K and Tsubota K, “Predictability of ocular spherical aberration after cataract surgery determined using preoperative corneal spherical aberration”. J Cataract Refract Surg. 2010; 36(5); 756-761.

[Noll, 1976] Noll R.J, “Zernike polinomials and atmospheric turbulence,” Journal of the Optical Society of America 1976; 66: 207-211.

[Norrby, 1995a] Norrby S, “Standardized methods for assessing the imaging quality of intraocular lenses,” Applied Optics 1995;34: 7327-7333.

[Norrby, 1995b] Norrby S, “The lens haptic plane (LHP) a fixed reference for IOL implant power calculation”. Eur J Implant Refract Surg 1995; 7:202–209.

[Norrby et al. 2003] Norrby S, Lydahl E, Koranyi G and Taube M, “Reduction of trend errors in power calculation by linear transformation of measured axial lengths”, J Cataract Refract Surg.2003;29, 100-105.

[Norrby, 2004] Norrby S, “Using the lens haptic plane concept and thick-lens ray tracing to calculate intraocular lens power” J Cataract Refract Surg. 2004;30: 1000-1005.

[Norrby, 2005] Norrby S, “The Dubbelman eye model analysed by ray tracing through aspheric surfaces” Ophthalmic Physiol Opt. 2005;25: 153-161.

[Norrby et al. 2005] Norrby S, Lydahl E, Koranyi G and Taube M, “Clinical application of the lens haptic plane concept with transformed axial lengths”, J Cataract Refract Surg 2005; 31: 1338–1344.

[Norrby, 2008] Norrby S, “Sources of error in intraocular lens power calculation” J Cataract Refract Surg. 2008;34: 368-376.

[Norrby et al. 2010] Norrby S, Findl O, Hirnschall N, Nishi Y and Bergman R, “Modeling the Pseudo-Phakic Eye for the Purpose of Sphero-Cylindrical IOL Power Calculation”, presented at ARVO annual meeting, Fort Lauderdale (FL), 2-6 May, 2010.

[Norrby, 2011] Norrby S, “Special circumstances: Influence of spherical aberration on IOL power calculation”. In “IOL power”, Hoffer KJ, ed. (Slack Incorporated , 2011), pp.207-210.

[Olsen, 1986] Olsen T, “On the calculation of power from curvature of the cornea”, British Journal of Ophthalmology 1986; 70: 152-154.

[Olsen, 1988] Olsen T, “Pre- and postoperative refraction after cataract extraction with implantation of standard power IOL”. Br J Ophthalmol 1988; 72: 231–235.

[Olsen and Nielsen, 1989] Olsen T and Nielsen PJ, “Immersion versus contact technique in the measurement of axial length by ultrasound”, Acta Ophthalmologica 1989; 67; 101-102.

[Olsen, 2004] Olsen T, “The Olsen formula”. In “Intraocular Lens power calculations”, Shammas J, ed. (Slack Incorporated, 2004).

[Olsen and Thorwest, 2005] Olsen T and Thorwest M, “Calibration of axial length measurements with the Zeiss IOL Master”, J Cataract Refract Surg 2005;31: 1345-1350.

[Olsen, 2006] Olsen T, “Prediction of the effective postoperative (intraocular lens) anterior chamber depth”, J Cataract Refract Surg 2006; 32:419–424.

[Olsen, 2007] Olsen T, “Improved accuracy of intraocular lens power calculation with the Zeiss IOL Master”, Acta Ophthalmol. Scand 2007;85, 84-87.

[Olsen, 2007] Olsen T, "Calculation of intraocular lens power: a review," Acta Ophthalmol. Scand 2007;85: 472-485.

[Oshika and Tsuboi, 1995] Oshika T and Tsuboi S. “Astigmatic and refractive stabilization after cataract surgery”. Ophthalmic Surg. 1995; 26; 309-315.

[Oshika et al. 2002] Oshika T, MimuraT, Tanaka S, Amano S, Fukuyama M, Yoshitomi F, Maeda N, Fujikado T, Hirohara Y and Mihashi T, “Apparent accommodation and corneal front aberration in pseudophakic eyes”. Invest Ophthalmol Vis Sci 2002;43:2882–2886.

[Ossma et al. 2007] Ossma IL, Galvis A, Vargas LG, Trager MJ, Vagefi MR and McLeod SD, ”Synchrony dual-optic accommodating intraocular lens. Part 2: pilot clinical evaluation”. J Cataract Refract Surg. 2007; 33; 47-52.

[Packer et al. 2002] Packer M, Fine IH, Hoffman RS and Piers PA, “Prospective randomized trial of an anterior surface modified prolate intraocular lens”. J Refract Surg. 2002; 18(6); 692-696.

[Packer et al. 2009] Packer M, Fine IH and Hoffman RS, “Aspheric intraocular lens selection based on corneal wavefront”. J Refract Surg. 2009; 25; 12-20.

[Perez-Escudero et al. 2009] Perez-Escudero A, Dorronsoro C, Sawides L, Remon L, Merayo-Lloves J and Marcos S, “Minor Influence of Myopic Laser In Situ Keratomileusis on the Posterior Corneal Surface”, Invest Ophthalmol Vis Sci. 2009;50:4146–4154.

[Piers et al. 2007] Piers P, Weeber HA, Artal P and Norrby S, “Theorethical comparison of aberration-correcting customized and aspheric intraocular lenses”. J Refract Surg. 2007;23:374-384.

[Porter et al. 2001] Porter J, Guirao A, Cox IG and Williams DR, “Monochromatic aberrations of the human eye in a large population”. J Opt Soc Am A 2001;18:1793-1803.

[Preussner et al. 2002] . Preussner R, Wahl J, Lahdo H, Dick B and Findl O, "Ray tracing for intraocular lens calculation," J. Cataract. Refract. Surg. 2002;28: 1412-1419.

[Preussner et al. 2005] Preussner PR, Wahl J, and Weitzel D, "Topography-based intraocular lens power selection," J. Cataract. Refract. Surg. 2005;31: 525-533.

[Preussner et al. 2008] Preussner PR, Olsen T, Hoffmann P and Findl O, "Intraocular lens calculation accuracy limits in normal eyes," J. Cataract. Refract. Surg.2008;34: 802-808.

[Prieto et al. 2000] Prieto PM, Vargas-Mart┌ ın F, Goelz S, Artal P. “Analysis of the performance of the Hartmann-Shack sensor in the human eye”. J Opt Soc Am A 2000; 17:1388–1398

[Retzlaff, 1980] Retzlaff J, “A new intraocular lens calculation formula”, Am Intraocular Implant Soc 1980;6: 23-27.

[Retzlaff et al. 1990] Retzlaff JA, Sanders DR and Kraff MC, “Development of the SRK/T intraocular lens implant power calculation formula”, J Cataract Refract Surg. 1990;16, 333-340. Erratum in: Development of the SRK/T intraocular lens implant power calculation formula. J Cataract Refract Surg. 1990;16:528.

[Rosales and Marcos, 2007] Rosales P and Marcos S, “Customized computer models of eyes with intraocular lenses”, Opt Express 2007;15:2204-2218.

[Salmon, 1999] Salmon T, “Corneal contribution to the wavefront aberration of the eye”, dissertation.

[Sanders and Kraff, 1980] Sanders DR and Kraff MC, “Improvement of intraocular lens power calculation using empirical data”. J Am Intraocul Implant Soc 1980; 6: 263–267.

[Sanders et al. 1988] Sanders DR, Retzlaff J and Kraff MC, “Comparison of the SRK II formula and other second-generation formulas. J Cataract Refract Surg 1988;14: 136–141.

[Sandstedt et al. 2006] Sandstedt CA, Chang SH, Grubbs RB and Schwartz DM, “Light-adjustable lens: customizing correction for multifocality and higher-order aberrations”, Trans Am Ophthalmol Soc 2006;104:29-39.

[Savini et al. 2006] Savini G, Barboni P and Zanini M, “Intraocular lens power calculation after myopic refractive surgery: theoretical comparison of different methods”. Ophthalmology. 2006;113:1271-1282.

[Savini et al. 2007] Savini G, Barboni P and Zanini M, “Correlation Between Attempted Correction and Keratometric Refractive Index of the Cornea After Myopic Excimer Laser Surgery”, J Refract Surg. 2007;23:461-466.

[Schelenz and Kammann, 1989] Schelenz J and Kammann J, “Comparison of contact and immersion techniques for axial length measurement and implant power calculation”, J Cataract Refract Surg 1989;15: 425-428.

[Schrader, 2004] Schrader WE, “Traditional cataract treatment and the healers perspective: dialogue with western science and technology in Nigeria, West Africa,” Annals of African Medicine 2004;3:153-158.

[Schwartz, 2003] Schwartz DM, ”Light adjustable lens”. Trans Am Ophthalmology Soc 2003;101: 417-436.

[Schwartz, 2004] Schwartz DM, ”Light adjustable lens: Development of in vitro nomograms”. Trans Am Ophthalmology Soc 2004;102: 67-74.

[Schwiegerling et al. 1995] Schwiegerling J, Greivenkamp JE and Miller JM, "Representation of videokeratoscopic height data with Zernike polynomials," J Opt Soc Am A 1995;12: 2105-2113.

[Shammas, 1982] Shammas JH, “The fudged formula for intraocular lens power calculations”, American Intra-Ocular Implant Society Journal, 1982;8:350-352.

[Shammas, 1984] Shammas HJ, “A comparison of immersion and contact techniques for axial length measurements”, American Intra-Ocular Implant Society Journal 1984;10: 444-447.

[Shammas et al. 2003] Shammas HJ, Shammas MC, Garabet A, Kim JH, Shammas A and LaBree L, “Correcting the corneal power measurements for intraocular lens power calculations after myopic laser in situ keratomileusis” Am J Ophthalmol. 2003; 136, 426-432.

[Shammas, 2004] Shammas HJ, ‘Intraocular Lens power calculations’, ed. (Slack Incorporated, 2004).

[Shepherd, 1989] Shepherd JR, “Induced astigmatism in small incision cataract surgery”. J Cataract Refract Surg. 1989;15;85-88.

[Sheng et al. 2004] Sheng H, Bottjer CA and Bullimore MA, “Ocular Component Measurement Using the Zeiss IOLMaster”, *Optometry and Vision Science* 2004;81:27-34.

[Smith, 1990] Smith WJ, “Modern optical engineering: The design of optical systems ”, MacGraw-Hill Inc (1990).

[Speicher, 2001] Speicher L, “Intra-ocular lens calculation status after corneal refractive surgery”, Current Opinion in Ophthalmology 2001, 12:17–29.

[Srivannaboon et al. 2008] Srivannaboon S, Rakpanichmanee T, Cheng AC and Fam HB, “Estimation of posterior corneal power for IOL calculation after myopic LASIK”, J Refract Surg. 2008;24:946-951.

[Tabernero et al. 2006(a)] Tabernero J, Benito A, Nourrit V and Artal P, “Instrument for measuring the misalignments of ocular surfaces”, Opt. Exp. 2006;14:10945-10956.

[Tabernero et al. 2006(b)] Tabernero J, Piers P, Benito A, Redondo M and Artal P, “Predicting the optical performance of eyes implanted with IOLs to correct spherical aberration”, Invest Ophthalmol Vis Sci., 2006;47: 4651-4658.

[Tabernero et al. 2007] Tabernero J, Piers Pand Artal P, “Intraocular lens to correct corneal coma”, Opt. Lett. 2007; 32: 406-408.

[Thibos et al. 1997] Thibos LN, Wheeler W and Horner D, “Power vectors: An application of Fourier analysis to the description and statistical analysis of refractive error”. Optom Vis Sci 1997; 74:367-375.

[Thibos et al. 2000] Thibos LN, Applegate RA, Schwiegerling JT, Webb R and VSIA Standards Taskforce Members, “Standards for Reporting the Optical Aberrations of Eyes,” Journal of Refractive Surgery 2000;18: S652-S660.

[Thibos et al. 2004] Thibos LN, Hong X, Bradley A and Appelgate R, “Accuracy and precision of objective refraction from wavefront aberrations”. J. Vis, 2004; 4; 329-351.

[Tong et al. 2008] Tong N, He JC, Lu F, Wang Q, Qu J and Zhao YE, “Changes in corneal wavefront aberrations in microincision and small-incision cataract surgery”. J Cataract Refract Surg. 2008; 34(12); 2085-2090.

[van der Heijde, 1976] van der Heijde GL, “The optical correction of unilateral aphakia” Trans Sect Ophthalmol Am Acad Ophthalmol Otolaryngol. 1976;81:80-88.

[van Meeteren, 1974] A. van Meeteren, "Calculations of the optical modulation transfer function of the human eye for white light", Optica Acta 1974;21: 395-412.

[Vivino et al. 1993] Vivino MA, Chintalagiri S, Trus B and Datiles M, "Development of a Scheimpflug slit lamp camera system for quantitative densitometric analysis". Eye 1997;7: 791–798.

[von Mohrenfels et al. 2010] von Mohrenfels CW, Salgado J, Khoramnia R, Maier M and Lohmann CP, "Clinical results with the light adjustable intraocular lens after cataract surgery". J Refract Surg. 2010;26:314-320.

[Walter et al. 2006] Walter KA, Gagnon MR, Hoopes PC Jr and Dickinson PJ, "Accurate intraocular lens power calculation after laser in situ keratomileusis, bypassing corneal power" J Cataract Refract Surg 2006; 32, 425-429.

[Wang and Koch, 2005] Wang L and Koch DD, "Effect of decentration of wavefront-corrected intraocular lenses on the higher-order aberrations of the eye". Arch Ophthalmol. 2005;123:1226-1230.

[Wang et al. 2010] Wang L, Hill WE and Koch DD, "Evaluation of intraocular lens power prediction methods using the American Society of Cataract and Refractive Surgeons Post-Keratorefractive Intraocular Lens Power Calculator" J Cataract Refract Surg 2010;36: 1466-1473.

[Weeber and Piers, 2012] Weeber H and Piers P, "Theorethical performance of intraocular lenses correcting both spherical and chromatic aberration", J Refract Surg. 2012;28:48-52.

[Welford, 1986] Welford TW, "Aberrations of Optical Systems". Bristol: Adam Hilger (1986).

[Yang et al. 2002] Yang Y, Keith T and Burns SA, "Pupil location under mesopic, photopic and pharmacologically dilated conditions", Invest Ophthalmol Vis Sci. 2002;43:2508-2512.

[Yoon and Williams, 2002] Yoon G and Williams DR, "Visual performance after correcting the monochromatic and chromatic aberrations of the eye. J Opt Soc Am A Opt Image Sci Vis. 2002;19(2):266-275.

[Yoon et al. 2005] Yoon G, Macrae S, Williams DR and Cox IG, “Causes of spherical aberration induced by laser refractive surgery”. J Cataract Refract Surg. 2005;31: 127-135.

[Zhang and Wang, 2010] Zhang L and Wang Y, “The shape of posterior corneal surface in normal. post-LASIK, and post-epi-LASIK eyes”, Invest Ophthalmol Vis Sci. 2010;51:3468-3475.

[Zhao and Mainster, 2007] Zhao H and Mainster MA, “The effect of chromatic dispersion on pseudophakic optical performance”, Br J Ophthalmol.2007;91:1225-1229.

ACKNOLEDGEMENTS / AGRADECIMIENTOS

Like the beginning of thesis, the last section will be written in a mixture between English and Spanish, because this is like my heart is also now, between two different lands, although the language of one of them is not especially English but Nederlands…

Let me start in Spanish. En Murcia realicé la mayor parte del trabajo. Para no romper la tradición propia de las tesis, la primera persona a la que debo mencionar en este apartado es a Pablo Artal. Pero no es simplemente por tradición. De pequeña me enseñaron que es de bien nacido el ser bien agradecido y a Pablo le debo todo lo que soy como investigadora. Desde aquella beca de verano de 2004 en el Laboratorio de Óptica de la Universidad de Murcia, él me enseño a sentir curiosidad por los fenómenos ópticos que ocurren en el ojo y así me introdujo en este apasionante mundo de la óptica, que se ha convertido en parte esencial de mi vida. Pablo es pues el espejo en el que mirarse y espero algún día poder convertirme en alguien de quien se pueda sentir orgulloso.

El primer día de aquella beca de verano de 2004 conocí a una chica de Librilla con la que conecté al primer instante. Ella, Encarna es mi mejor amiga dentro del laboratorio y con ella he pasado los momentos más divertidos que recuerdo de mi paso por el LOUM. Hasta tal punto llegamos a conectar que llegamos a hacernos indistinguibles. Aun en ARVO, compañeros de otros laboratorios me preguntan por Carmen y por nuestro crucero por Las Bahamas… También ella me ayudo muchísimo durante la tesis con su seriedad habitual en el trabajo y su infinita experiencia clínica, así como Eloy, ambos ópticos-optometristas que me enseñaron lo que era una esfera o un cilindro inducido. Imposible no echar de menos esas grandiosas y larguísimas discusiones acerca de los signos de la esférica con Eloy! Gracias por vuestro apoyo y como no olvidar que a vosotros os debo parte de las medidas clínicas de esta tesis. En este punto debo también recordar a Salome Abenza y José María Marin, ambos oftalmólogos del Hospital Virgen de La Arrixaca. Ellos fueron quienes nos suministraron pacientes y como no, los operaron, así que sin ellos nada de la parte clínica contenida en esta tesis hubiera sido posible.

Volvamos al laboratorio… Silvestre, no me puedo olvidar de tu paciencia y meticulosidad en el laboratorio. Pocas veces se conoce a alguien tan excepcional como

tu. Gracias por tu ayuda y paciencia. Alejandro, Alejo, que esta ya en su tierra, aunque lejos de su Astrid… Largas horas en el laboratorio con el sistema de OA, que aunque no aparece en esta tesis, ocupo también parte de mi tiempo. Lo siento, Alejandro, pero como habrás visto he utilizado ese verde asqueroso que no me dejabas poner en las graficas de las medidas que hacíamos juntos… Christina, siento los días que te hacemos pasar en el lab de medidas interminables en el simulador binocular. Espero que no me guardes mucho rencor, aunque siempre puedo practicar mi pobre holandés contigo para ver si coincide con alguna palabra en alemán. Pero si lo que quiero es practicar holandés, Bart es la persona adecuada, aunque como su español ahora es perfecto, la verdad es que me da un poco de pereza…No me puedo olvidar tampoco de Joshua, que siempre me ha dado muy buenos y sabios consejos, así como Pedro. Y Juanma, que decir de Juanma… a pesar de su apariencia en principio un poco dura, es una de las mejores personas del laboratorio. Si algún día he necesitado algo, Juanma sin dilación ni duda me lo ha dado, de la forma más generosa posible. Y hablando de alguien generoso, se me viene a la cabeza Esther. Ella es un alma libre, que no se preocupa de si misma, porque los demás son lo más importante. Y así lo demuestra día a día. Antonio y Guillermo han sido también grandes compañeros siempre diligentes y excelentes profesionales.

Es bien sabido que los últimos serán los primeros y por ello Juan ocupa este lugar. Gracias Juan por tu ayuda durante todo este tiempo. De ti herede Zemax y por ello, a ti te debo una parte especial dentro de los agradecimientos de esta tesis. Si al principio hablaba de Pablo como espejo en el que mirarse, Juan también puede considerarse como tal.

He repasado uno a uno a todos los miembros del laboratorio, pues son individualmente excelentes personas, pero es también de ley decir que juntos forman un equipo científico de calidad poco común. Si es importante el conocimiento, la colaboración es esencial para que ese conocimiento fluya y eso se ha reflejado durante esta y todas y cada una de las tesis y los trabajos que han resultado del laboratorio. Así pues debo agraceder a todos y cada uno de los miembros del laboratorio que de forma directa o indirecta han colaborado y han sido parte de este trabajo. Gracias a todos, amigos, y espero que esta no sea la ultima vez que trabajamos juntos.

I have to change now language and come back to English. If the LOUM staff has been essential contributor in this thesis, I cannot forget AMO people. I still remember the first time I met Patricia and Henk in one of their visits to the LOUM. Future is totally unpredictable, so I would never imagine that I would end up in Groningen with them. However, I strongly believe that this, in addition with having done my PhD in the LOUM is one of the best decisions I have never taken. If the LOUM team is an example of collaboration and good environment, Groningen cannot be described in a different way. Also, if Pablo is the mirror in which every optical scientist should look at, Patricia is also an incredible example to follow. Her successful career is completely amazing and this is something easy to understand whenever you talk to her. She always has a smart idea that can turn out in a success. Thanks Patricia for your help and your patience reviewing the language of each of the articles I wrote since I am in Groningen and of this long manuscript as well. I would never finish this thesis in the schedule I did without your help and support. You trusted in me and brought me here and I also would like you to be proud of my future career of which you are and will be a key part. I also mentioned before Henk. He is peace, analysis and accuracy. I also would like to reach part of his level of knowledge in the future and do it without the need of talking to myself, something that should be really disturbing for him, because I do it in Spanish in our room… And if someone schijnt in Groningen, here is Marrie. His philosophy ("keep it simple") is one of the most worthwhile lessons I have never learnt. He helped me with the statistical analysis included in this thesis and with the development of the last chapters. Therefore, thanks for this and for everything else. Thanks Luuk for your friendship and help in Nederlands. We started together in AMO and your support, especially at the beginning was essential for me. And Kaccie, I cannot forget you (dat kan niet!). Thanks for your support, reminding to me every single day that I had to finish this thesis. Finally thanks to the rest of the R&D people in Groningen, Sieger, Ageeth, John, Michelle and to the rest of people in the Groningen site, for making me fell at home, because now Groningen is my home.

I would not like to finish these acknowledgements without mentioning my family. And for that I have to change again to Spanish.

Si hay alguien a quien quiero en este mundo ese es mi padre. El me enseñó que la constancia y el respeto son la base del éxito. El es mi ejemplo en la vida pues ha sabido llevar una familia adelante sin una protesta ni reproche. Sin embargo, siempre me dijo

que a la persona a la que mas tengo que querer no es a él mismo, si no a mi madre. Y así lo hago. Solo hay una cosa que hace que mi traslado a Groningen no sea perfecto, y eso es que ellos no están aquí. Ellos me dieron lo más grande, la vida. Se sacrificaron por mí y me dieron todo lo que ahora tengo, por eso no tengo ni tendré palabras para agradecerles lo que han hecho por mí. Por eso les pago con lo único que puedo, con un amor incondicional e inmenso. Mi corazón tiene amor para alguien mas, con quien mi lista de agradecimientos termina. Como dije antes, los últimos serán los primeros, y David es el último de esa lista. Sin David no hubiese venido aquí. Mi gratitud infinita por haber emprendido esta aventura dejándolo todo en España sin ninguna duda para venir a una tierra hostil para el, en la que aun le cuesta comunicarse. No estoy segura de si sabe cuanto le agradezco esto, pero como a mis padres, lo único que puedo hacer es pagárselo con mi más profundo amor y mi eterna gratitud. Gracias Pupy, por soportarme todas las batallitas que te cuento y perdona por todas las horas que debería haberte dedicado y le he dado a esta tesis. Espero que con el fin de este trabajo empiece el resto de nuestra vida.

Curriculum Vitae

CARMEN CÁNOVAS VIDAL

Born September 23, 1982 in Spain
Home address: Klinkerstraat 25
9732 ML Groningen
The Netherlands
Phone: (+31) 0626 526257

AMO Groningen B.V.
Van Swietenlaan 5
Groningen 9728 NX, The Netherlands
Ph: +31505296611 Fax: +31505276824
Carmen.Canovas@amo.abbott.com

ACADEMIC DEGREES

In preparation: **PhD in Optical Sciences** 2005-expected 2012
Research field: visual optics, LOUM, Spain
Advisor: Prof. Pablo Artal

Licenciate degree in Optics 2005-2007
Research field: visual optics, LOUM, Spain
Licenciate thesis: "Customized modeling in pseudophakic eyes"
Advisor: Prof. Pablo Artal

BSc+MSc in physics
2000-2005
Focus studies: Optical physics, LOUM, Spain and Applied Physics, Physics department, Murcia University, Spain.

EMPLOYMENT

Optical Scientist position Jan 2010- present
in AMO Gronigen B.V.

Predoctoral student position 2005- Jan 2010
in visual optics at LOUM, Spain

RESEARCH EXPERIENCE AND ACHIEVEMENTS

- Development of a ray tracing optical model to calculate the optimum power for a specific IOL and individual patient in cataract surgery. Organization and analysis of a clinical testing of this procedure both in normal and patients who had undergone Lasik.
- Studying of corneal refraction and aberration evolution after cataract surgery.
- Development of a hybrid adaptive optics simulator combining both a deformable mirror and a liquid crystal phase modulator. Investigation of the impact of different ocular aberrations and/or diffractive or refractive phase profiles in visual performance by means of the experimental set up and its comparison with computational simulations.

- Process and follow up in clinical studies involving different IOLs.

- Active participation in IOL design work and development and testing of software for toric IOL power calculation.

- Design and test of an ocular wavefront sensor for measuring aberrations in real time including a MatLab software which retrieve the wavefront using Fourier methods and comparison with centroiding and other wavefront analysis methods. This work was performed in collaboration with Erez Ribak in Technion (Haifa, Israel) in the Sharp-Eye research and training network.

SCHOLARSHIPS OBTAINED FOR RESEARCH AND TRAVEL

ARVO international travel grant	2009
Sharp-Eye research network	2005

EDUCATIONAL MEETINGS

9TH Summer School on Adaptive Optics 2008
Organized by Center for Adaptive Optics, University of California, Santa Cruz

Summer School for Visual Optics 2007
Organized by Visual Science Committee, Spanish Optical Society

Advanced Summer School for Optics 2004
Organized by LOUM.

PAPERS

6 peer reviewed articles

- C Cánovas, S. Abenza, E. Alcon, EA. Villegas, JM. Marin, and P Artal, "**Impact of corneal aberrations on IOL power calculation**" (accepted for Publication in JCRS).

- P Artal, C Schwarz, C Cánovas, A Mira-Agudelo, "**Night myopia studied with an adaptive optics visual analyzer**" (accepted for Publication in PLOS one).

- C Cánovas, and P Artal, "**Customized eye models for determining optimized intraocular lenses power**". Biomed. Opt. Express 2, 1649-1662 (2011).

- C. Cánovas, P. M. Prieto, S. Manzanera, A. Mira and P. Artal, **"Hybrid adaptive optics visual simulator**", Opt Express. 16(11):7748-55 (2008).

- S. Manzanera, C. Cánovas, P. M. Prieto and P. Artal, "**A wavelength tunable wavefront sensor for the human eye**", **Opt. Express**, 16, 7748-7755 (2008).

- C. Cánovas and E. N. Ribak, "**Comparison of Hartmann analysis methods**", **Appl. Optics**, 46, 1830-1835 (2007).

3 manuscripts in preparation

- C Cánovas, M van der Mooren, P Piers, L Wang, DD Koch, and P Artal, "Effect of the equivalent refractive index on IOL power prediction by ray tracing in myopic post-LASIK patients"
- C Cánovas, M van der Mooren, P Piers, L Wang, DD Koch, and P Artal, "Corneal spherical aberration regression formulas for myopic post-LASIK patients"
- C. Cánovas, EA Villegas, E Alcon, E Rubio, JM Marin and P Artal, "Prediction in corneal aberrations changes after small incision cataract surgery"

CONFERENCE CONTRIBUTIONS

2012

- C Cánovas, P Piers and JT Holladay, "**Comparison between cylinder IOL power calculations: fixed ratio vs complete calculation**", oral presentation at ESCRS, Milan, September 2012.

- C Cánovas, T de Jong, H Weeber, H Zhao, N Jansonius and P Piers, "**Impact of under and overcompensation on astigmatism correction**", oral presentation at ESCRS, Milan, September 2012.

- C Cánovas, T de Jong, H Weeber, N Jansonius and P Piers, "**Head stabilization impact on aberration induction with an adaptive optics visual simulator**", poster presentation at ARVO, Ft. Lauderdale, FL, May 2012.

- C Schwarz, C Cánovas, S Manzanera, P Prieto, H Weeber, P Piers and P Artal "**Depth of focus with induced coma at different orientations**", oral presentation at ARVO, Ft. Lauderdale, FL, May 2012.

- P Piers, S Manzanera, C Schwarz, C Cánovas, P Prieto, H Weeber*, and P Artal, "**Visual acuity with scaled natural and modified aberrations**", oral presentation at ARVO, Ft. Lauderdale, FL, May 2012.

- M. van der Mooren, C. Cánovas , O. Findl and P. Piers**, "Ocular spherical aberration prediction",** poster presentation at ARVO, Ft. Lauderdale, FL, May 2012.

- C. Cánovas, M. van der Mooren, P. Piers, L. Wang, D. Koch and P. Artal "**Ray tracing prediction of IOL power in myopic post-LASIK patients: Effect of the Equivalent Refractive Index`**", oral presentation at ASCRS, Chicago, April 2012.

- C Cánovas, P Piers and JT Holladay, "**Comparison between cylinder IOL power calculations: fixed ratio vs complete calculation**", poster presentation at ASCRS, Chicago, April 2012.

2011

- C. Cánovas, M. van der Mooren, P. Piers, L. Wang, D. Koch and P. Artal **"Ray Tracing prediction of Intraocular Lenses Power in myopic post-Lasik patients: Effect of the Equivalent Refractive Index**" poster presentation at ARVO, Ft. Lauderdale, FL, May 2011.

- P. Artal, C. Schwarz, C. Cánovas and A. Mira-Agudelo, “**Night Myopia Explored With An Adaptive Optics Visual Simulator”**, oral presentation at ARVO, Ft. Lauderdale, FL, May 2011.

2010

- C. Cánovas, S. Manzanera, P. M. Prieto and P. Artal, **“Hybrid adaptive optics visual simulator**”, presentation at SPIE BiOS, San Francisco, January 2010.

- C. Cánovas and P. Artal, **“Customized modeling as a tool for IOL power calculations”**, presentation at EOS meeting, Stockholm, August 2010.

- C. Cánovas and P. Artal, **“Spherical aberration and IOL power calculations”**, presentation at IOL Power Club, Venice, August 2010.

- C. Cánovas, S. Abenza, J.M. Marin and P. Artal, **“Impact of corneal aberrations on IOL power calculations”**, presentation at ESCRS, Paris, September 2010.

2009

- C. Cánovas, S. Manzanera, P. M. Prieto and P. Artal, **“Dual adaptive optics visual simulator: combining a deformable mirror and a spatial modulator**”, presentation at Reunión Nacional de Óptica, Spain, September 2009.

2008

- C. Cánovas, S. Abenza, E. A. Villegas, J. M. Marin and P. Artal, **“Ray-tracing Prediction of Intraocular Lenses Power: Effect Of Corneal Aberrations”**, poster presentation at ARVO, Ft. Lauderdale, FL, May 2009.

- S. Manzanera, P.M. Prieto, C. Cánovas, H. Weeber, P. Piers and P. Artal, **“Predicting Visual Estimates of Depth Of Focus From Optical Data”**, poster presentation at ARVO, Ft. Lauderdale, FL, May 2009.

- E. Alcon, C. Cánovas, E.A. Villegas, J.M. Marin, E. Rubio and P. Artal, **“Wave-aberrations In Light Adjustable Intraocular Lenses”**, oral presentation at ARVO, Ft. Lauderdale, FL, May 2009.

- E. A. Villegas, E. Rubio, E. Alcon, C. Cánovas, S. Manzanera, J.M. Marin and P. Artal, **“Refractive Efficacy Of Light Adjustable Intraocular Lenses”**, poster presentation at ARVO, Ft. Lauderdale, FL, May 2009.

- P. Artal, E. Villegas, E. Alcon, C. Cánovas, E. Rubio and J. Marin, **“Refraction accuracy of light adjustable intraocular lenses”** , oral presentation at ASCRS, San Francisco, April 2009.

2008

- C. Cánovas, J. Tabernero and P. Artal, **“Customized ray-tracing modelling for optimized IOL power calculations”**, oral presentation at ESCRS, Berlin, September 2008.

- C. Cánovas ,E. Villegas, E. Alcon, E. Rubio, J. Marin and P. Artal**, “Temporal changes of corneal refraction and aberrations after cataract”**, oral presentation al ESCRS, Berlin, September 2008.

- P. Artal, E. Villegas, E. Alcon, C. Cánovas, E. Rubio and J. Marin, **“Refraction and wavefront aberrations in patients implanted with the light adjustable lens”**, oral presentation al ESCRS, Berlin, September 2008.

- P.A. Piers, S. Manzanera, H. Weeber, A. Mira, C. Cánovas and P. Artal, **“Depth of Focus for Different Aberration Patterns Using an Adaptive-Optics Vision Simulator”**, oral presentation at ARVO, Ft. Lauderdale, FL, April 2008.

2007

- E.N. Ribak, Y. Carmon, A. Talmi, O. Glazer and C. Cánovas, **“Hartmann Fourier Analysis for Sensing and Correction”**, oral presentation at Adaptive Optics: Análisis and Methods (AO), Vancuver, June 2007.
- C. Cánovas, J. Tabernero and P. Artal, **“Optimized power predicted by customized modelling”**, poster presentation at ARVO, Ft. Lauderdale, FL, May 2007.
- C. Cánovas, S. Manzanera and P. Artal, “**Fiber Interferometer to estimate cone spacing”**, oral presentation at Red de Óptica Visual, Murcia, March 2007.

2006

- Y Carmon, A Talmi, C Cánovas and E N Ribak, **“Comparative study of Hartmann-Shack reconstruction methods”**, oral presentation at Conference on Visual Optics in Mopani Camp (South Africa), August 2006.
- C. Cánovas and E. Ribak, **“Fast Fourier Demodulation”**, oral presentation at Sharp Eye Meeting, Murcia, March 2006.

PATENT APPLICATIONS

3 submitted patent applications.

- “Customized intraocular lens power calculation system and method”, US 2012/0044454 A1
- “Apparatus system and method for intraocular lens power calculation using a regression formula incorporating corneal spherical aberration”.

OTHER SKILLS

Languages
Spanish (native), English (fluent), Dutch (initial).

Computer skills
Advanced user of MS-Office and analysis software (sigmaplot).
Programming in Fortran, MatLab and optical design software (Zemax).